ALMA MATER STUDIORUM
UNIVERSITÀ DI BOLOGNA

DOTTORATO DI RICERCA IN

SCIENZE E TECNOLOGIE DELLA SALUTE

Ciclo 38

Settore Concorsuale: 09/G2 Bioingegneria

Settore Scientifico Disciplinare: ING-IND/34 – Bioingegneria Industriale

DEVELOPMENT OF A STOCHASTIC APPROACH TO ESTIMATE SUBOPTIMAL CONTROL IN AN ADULT POPULATION

Presentata da: Alex Bersani

Coordinatore Dottorato
Igor Diemberger

Supervisore
Marco Viceconti

Co-Supervisori
Giorgio Davico
Walter Maetzler

Esame finale anno 2026

Abstract

Humans are capable of extraordinary things thanks to the muscles, degrees of freedom and the central nervous system. Understanding how the brain selects motor control strategies in healthy and clinical populations is paramount to advancing our knowledge and better treat neuromuscular diseases.

Historically, neuromuscular modelling approaches can be categorised into three groups: i) the reductionist approach, which splits the nervous and musculoskeletal systems, ii) the explicit modelling of the coupling nervous-musculoskeletal systems, and iii) the stochastic approach, which implement the uncontrolled manifold theory to explore the space of plausible neural solutions.

Myobolica belongs to the latter, as it employs Bayesian statistics and a Markov Chain Monte Carlo algorithm to predict numerous plausible muscle control strategies. Unlike existing methods, Myobolica incorporates physiological constraints to ensure realistic solutions.

To evaluate its performance, public datasets were used. Myobolica successfully simulated lower limb and shoulder biomechanics, showing a good correlation with experimental joint loads (R^2 = 0.92, RMSE = 0.3 BW and R^2=0.6, RMSE=0.73 BW, respectively). Following, Myobolica was also applied to simulate four patients with Parkinson's disease. This explorative assessment suggests its potential for deepening disease mechanisms and predicting progression.

Before Myobolica can be used to address specific clinical needs, it is paramount to perform a robust validation. A preparatory sensitivity analysis – key part of the validation – on 48 simulations have been discussed to plan an optimal strategy for this future development. In parallel, some effective methods to perform such analysis and communicate obtained results were evaluated.

List of the Main Abbreviations

Central Nervous System:	CNS
Musculoskeletal:	MSK
Electromyography:	EMG
Markov Chain Monte Carlo:	MCMC
Joint Contact Force:	JCF
BodyWeight:	BW
Gleno-Humeral Joint Force:	GJF
Gleno-Humeral:	GH
Probability Distribution Function:	PDF
Rate of Force Development.	RFD
Rate of Torque Development:	RTD
Maximal Voluntary Isometric Contraction:	MVIC
Root Mean Square Error:	RMSE
Parkinson's Disease:	PD
Hoehn & Yahr:	H&Y

Table of Contents

Thesis overview

This section provides an overview of the thesis structure and outlines the content of each chapter. The document comprises seven chapters, with the goal of conducting the reader through the comprehension of the human motor control and the state-of-the-art computational approaches used to interpret its underlying principles. Following, a novel computational approach, developed throughout this project, will be deepened.

In Chapter 1, “Motor control and sub-optimal motor control: a brief introduction”, an introduction of the human motor control is presented: what we do intend for “motor control”, the main motor control theories, the importance of deeply understand motor control. Parallelly, this section provides a brief overview of the key variations in the motor control in clinical populations, as documented in current scientific literature.

Chapter 2, “Modeling human suboptimal control: a review”, presents a literature review published in the Journal of Applied Biomechanics. The review provides an outline of the approaches to model neuromuscular control, splitting the narrative into three main approaches: “reductionist approach”, “stochastic approach”, and approaches that explicit model the controller-actuator coupling.

Chapter 3, “Exploring muscle recruitment by Bayesian methods during motions”, presents a study published on the journal Chaos, Solitons & Fractals. It delves into the mathematical foundations of the toolbox Myobolica, the core of this project, explaining the Bayesian inverse problem (for the muscle dynamics) and how to use it to effectively predict muscle forces.

Chapter 4, “Myobolica: a stochastic approach to estimate physiological muscle control variability”, presents a study published in IEEE Transactions on Neural Systems and Rehabilitation Engineering. Here, the toolbox Myobolica, previously described in its mathematical concepts, is applied in a first case study, to simulate lower limb biomechanics and compare the predicted results to available experimental data. A dedicated section outlines the methodology used to calculate the main parameter’s values.

Chapter 5, “Stochastic modelling of muscle control during shoulder abduction”, presents a study published in Journal of Biomechanics. It presents the application of the toolbox Myobolica to simulate upper limb biomechanics, focusing on shoulder abduction. Additionally, it introduces an approach to improve the physiological accuracy of results predicted by Myobolica, based on experimental electromyography data.

In Chapter 6, “Explorative assessment of the knee joint load variability in four patients with Parkinson’s disease”, an exploration analysis on the knee joint force variability is investigated using the toolbox Myobolica. Specifically, it simulates the locomotion of four patients with varying clinical presentation of Parkinson’s disease, both under the influence of medication aimed at alleviating motor symptoms and in its absence.

Chapter 7, “Toward future developments of Myobolica”, presents some preparatory activities for a future validation of the toolbox Myobolica. In particular, it illustrates a preliminary uncertainty quantification designed to evaluate various methods for presenting and interpreting the obtained

results. This is followed by a concise overview of potential future applications of Myobolica in clinical contexts or as a means to enhance other modelling approaches.

To conclude, after the Bibliography section, the candidate's scientific production is listed.

Motor control and sub-optimal motor control: a brief introduction

The human musculoskeletal system is capable of extraordinary things. Humans can perform a variety of tasks and movements, from the coarser and simpler, such as walking or moving a chair, to extremely fine motions such as singing or performing in sports. All thanks to the numerous actuators (our muscles), degrees of freedom (allowed motions) and, above all, to the way the central nervous system (CNS) and the brain control every aspect of it. While individuals often exhibit common patterns in performing motor tasks (such as walking, jumping, or singing), there is remarkable variability in both performance and the neuromotor control strategies adopted [1], [2], [3]. Those variations emerging across individuals are influenced by factors such as experience, physical changes, and – notably – the presence of pathologies or disabilities. As a result, some individuals may excel in athletic or motor-intensive activities.

In contrast, others may find even basic tasks, such as walking between two rooms, to be a challenge (for example, individuals with Parkinson's disease or Multiple Sclerosis). Understanding the mechanisms underlying motor control is paramount to advancing our knowledge across disciplines related to human movement and health. Indeed, through research in this area, it is possible to develop more effective assistive devices such as exoskeletons [4], injury prevention strategies [5], optimising movement techniques and improving sport performances [6], [7], [8], or supporting the treatment of neuromusculoskeletal disorders by assisting the design of their targeted rehabilitations and therapies [9], [10]. However, this is not trivial, since scientists still debate how motor control works. Several theories have been proposed to explain the mechanism of motor control, and a consensus is still lacking [11]; different theories address motor control, focusing on various aspects of the neuromotor system. Some such theories are the Equilibrium-point hypothesis [12], which suggests that the CNS alters "thresholds" at which muscles activate, setting the target muscles' lengths and joints' angles that the muscles attempt to return to when activating, the Generalised Motor Program theory [13], which proposes that the CNS memorised abstract movement patterns for similar actions and customises those when performing a specific movement, or the Reflex theory [14], which proposes that all movements are results of simple reflexes chains; besides, there is also the Uncontrolled Manifold Theory [15], which is particularly relevant to this project and theorises that the CNS allows uncontrolled variability in the motor control strategies not directly affecting the task execution. The core aspect that every motor control theory tries to unveil is the problem of motor redundancy, which is how the CNS selects a specific control strategy, as there are more degrees of freedom (i.e., the allowed motions) than muscle actuators [16]; it has been recently re-defined as "motor abundance" by Mark Latash in 2000 [17], to frame it not as a "problem", but as the ability to perform tasks in multiple ways, emphasising how the neuromuscular system bears flexibility and adaptability to injuries and unexpected events.

The number of empirical evidences supporting motor control theories is increasing, driven by the acquisition and analysis of human performance; this includes experimental measurements of the kinematics and the muscle activity [6], [18], with first investigations dating from several decades ago [19]. A key area of investigation involves the comprehension of motor control in impaired individuals (older adults, individuals with neuromuscular disease, injured people, and so on). In fact, the principles of motor control mentioned above also apply to impaired subjects; however, a key challenge lies in the fact that the way the CNS controls muscles to perform a motor task can vary

consistently in these populations [20], [21]. Motor control, seen to be “optimal” in a healthy (unimpaired) population, can stop being optimal and start being “suboptimal” in an impaired population [21]. Alterations in muscle activations are observed in patients with Parkinson’s disease [22], Huntington disease [23], post-stroke [24], and cerebral palsy [25], as well as other muscular deficits [26], [27], [28]. Those alterations lead to subsequent changes in muscle co-contraction patterns [29], contributing to pathologic motor control [23], [30]. The mentioned alteration in the muscle control causes a large number of diseases to impact individuals with motor disabilities (Figure 1). Among all, one could recall signature disabilities such as freezing of gait (temporary inability of the subject to perform the task, even while “thinking” of doing it) which is typical of Parkinson’s disease [31], [32], or muscle spasticity (increase in muscle tone and spasms) that could lead to abnormal walking patterns (i.e., crouch gait) which is typical of pathologies such as cerebral palsy, but the list is much longer and granular. While Latash justifies it as a shift in the priorities considered by the CNS while searching for a motor control pattern to perform a task [21], more evidence are being documented to characterise suboptimal motor control better, to improve targeted treatments for its underlying causes or associated motor disabilities.

Characterisation of suboptimal motor control is frequently performed through the subject’s gait evaluation. Commonly performed clinical tests, such as the 6-minutes Walking Test (6MWT) [33], and clinical scales for neuromuscular pathologies such as the Unified Parkinson’s Disease Rating Scale (UPDRS) for Parkinson’s disease severity evaluation [32] rely on the subject’s walking performance. Overground gait represents the most performed task by humans, and it is widely recognised as stereotypical since it is a repetitive and rhythmic movement performed without explicitly thinking about it. Nonetheless, impaired locomotion limits people's independence, increases fall risk and causes pain and muscle weakness; for this reason, locomotion and gait parameters (such as stride length or gait velocity) are central when studying pathologies that cause motor disabilities and are often highly correlated to their severity and progression. Recent studies documented higher gait variability (i.e., the measure of variability in walking parameters over steps) and a combination of decreased stride (i.e., phase of the gait cycle from one foot ground contact to subsequent ground contact of the same foot) length and increased stride time in subjects with Parkinson’s disease [34], [35], [36] and with Huntington disease [37] (compared to healthy controls). Lower gait velocity is documented in subjects with Huntington disease [37], as well as subjects with multiple sclerosis [38] and chronic obstructive pulmonary disease (COPD) [39], [40] when compared to healthy subjects. Similarly, reduced cadence (i.e., number of steps per unit of time) and longer duration of step phases (stance, swing, and single and double support duration) are reported in subjects with multiple sclerosis [38], [41] when compared to healthy subjects. Limitations in trunk movements control while moving are reported for subjects with multiple sclerosis [41]. In general, disease progression is associated with poorer motor control and reduced mobility [34], [36], [38], [42], low balance and a higher risk of falling [42]. A worsening that is also partly visible in the ageing population [43], [44], [45].

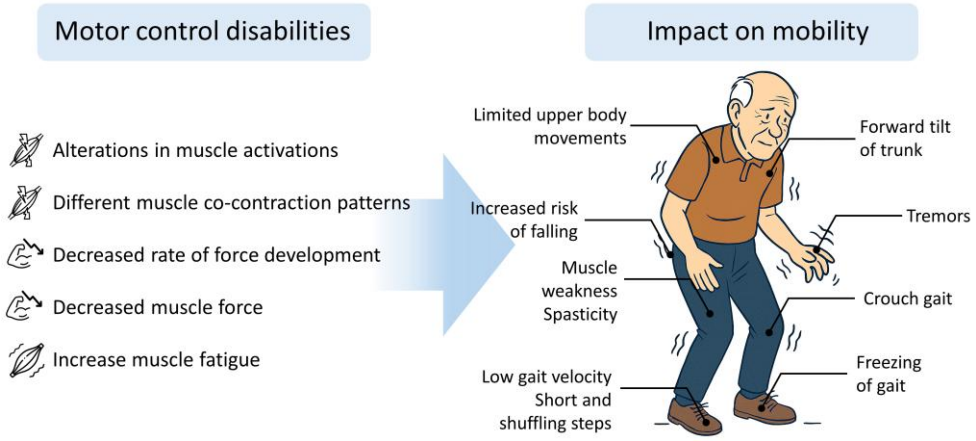

Figure 1. Infographic summary of the most common motor control disabilities and their impact on the subject's mobility. The design of the old person has been generated with the assistance from Microsoft Copilot (Microsoft, 2026).

Understanding motor control and the impact of a surgery or a rehabilitation program on it is important to ensure satisfactory outcomes, especially when the aim is to preserve or restore motor function [46]. The scientific literature widely documents therapeutic strategies rooted in motor control understanding. Those have been applied to support recovery from a pathological state [10], to restore a lost function [47], to improve after a surgical (or not) intervention [48], and to guide motor re-education for restoring balance [9], [49], locomotion [50], or fine manipulation activities [51], [52]. A more comprehensive – and refined – understanding of motor control could allow progress in neurorehabilitation.

Biomechanical models, used to investigate neuromuscular functions, may represent a valuable resource to explain or interpret the principles underlying motor control. In fact, a class of those models, the musculoskeletal models (i.e., models of the muscular and skeletal anatomical systems), can provide insights into parameters of the human body that are commonly non-measurable, such as individual muscle forces or the loading pattern of a joint [53], [54], [55]. Information obtained from musculoskeletal models may be used to acquire knowledge about physiology and physiopathology [56], [57], [58], [59], [60], predict the impact of behaviours or gestures [5], [61], [62], and better plan surgical and clinical interventions [63], [64].

An overview of the computational approaches that have been developed over the years to model neuromuscular control is presented in the next chapter.

Modeling human suboptimal control: a review

Alex Bersani[1,2], Giorgio Davico[1,2], Marco Viceconti[1,2]

[1] Medical Technology Laboratory, IRCCS istituto Ortopedico Rizzoli, Bologna, Italy

[2] Department of industrial Engineering, Alma Mater Studiorum, University of Bologna, Bologna, Italy

Adapted from a publication in:

Journal of Applied Biomechanics

(2023)

https://doi.org/10.1123/jab.2023-0015

The authors wish to thank Journal of Applied Biomechanics for providing the permission to re-use the manuscript titled “Modeling human suboptimal control: a review” in the present PhD thesis

Abstract

This review paper provides an overview of the approaches to model neuromuscular control, focusing on methods to identify nonoptimal control strategies typical of populations with neuromuscular disorders or children. Where possible, the authors tightened the description of the methods to the mechanisms behind the underlying biomechanical and physiological rationale. They start by describing the first and most simplified approach, the reductionist approach, which splits the role of the nervous and musculoskeletal systems. Static optimization and dynamic optimization methods and electromyography-based approaches are summarized to highlight their limitations and understand (the need for) their developments over time. Then, the authors look at the more recent stochastic approach, introduced to explore the space of plausible neural solutions, thus implementing the uncontrolled manifold theory, according to which the central nervous system only controls specific motions and tasks to limit energy consumption while allowing for some degree of adaptability to perturbations. Finally, they explore the literature covering the explicit modeling of the coupling between the nervous system (acting as controller) and the musculoskeletal system (the actuator), which may be employed to overcome the split characterizing the reductionist approach.

Keywords

Muscle control; Optimization methods; Stochastic approach; EMG informed; Feedback control

Introduction

To produce controlled movements, the human central nervous system (CNS) sends excitation signals to the skeletal muscles in the form of motoneurons action potentials, causing their contraction in a timely fashion. Traditionally, neurophysiologists focus on the control unit (the nervous system) rather than on the actuation unit (the musculoskeletal system), while biomechanists do the opposite.

It has been observed experimentally[65], [66] that the nervous system of healthy adult subjects who are performing nonmaximal motor tasks, such as level walking, select those muscle activation patterns that, while ensuring instantaneous equilibrium and the desired kinematics, also minimize certain cost functions (eg, the smallest consumption of metabolic energy). For this reason, this particular control strategy is frequently referred to in the biomechanics literature by the term *optimal control.*[67], [68], [69] Studying the movement of a human body under optimal control only requires detailed modeling of the dynamics of the musculoskeletal system (MSK system), and the neuromuscular control mechanisms can be represented implicitly by imposing such an optimal control.[70]

Unfortunately, most applied biomechanics research focuses on the movement of nonhealthy, and frequently also nonadult, subjects. A child with cerebral palsy or an elder with an artificial total knee replacement surely does not usually walk by adopting an optimal control strategy. But modeling nonoptimal control is a lot more challenging, and it remains one of the open problems in applied biomechanics research.

This review paper summarizes some of the work done so far on this topic. The review is organized in 3 parts:

1. First, we provide some examples of the traditional reductionist approach, with the older neurophysiology literature investigating the neuromuscular control modeling the MSK system

in an oversimplified way and the biomechanics literature investigating human movement assuming optimal control.

2. Then, we will look at the more recent literature exploring neuromuscular control as a combination of multiple cost functions, a stochastic process, and a derivation of the uncontrolled manifold theory.
3. Last, we will look at the most recent literature, which tries to overcome the reductionist split between biomechanics and neurophysiology and explore the possibility of explicitly also modeling the controller which, depending on the different theories, might rely on voluntary control of the involuntary reflex chain on central pattern generators (CPG), or more complex predictor–corrector controllers (Figure 2).

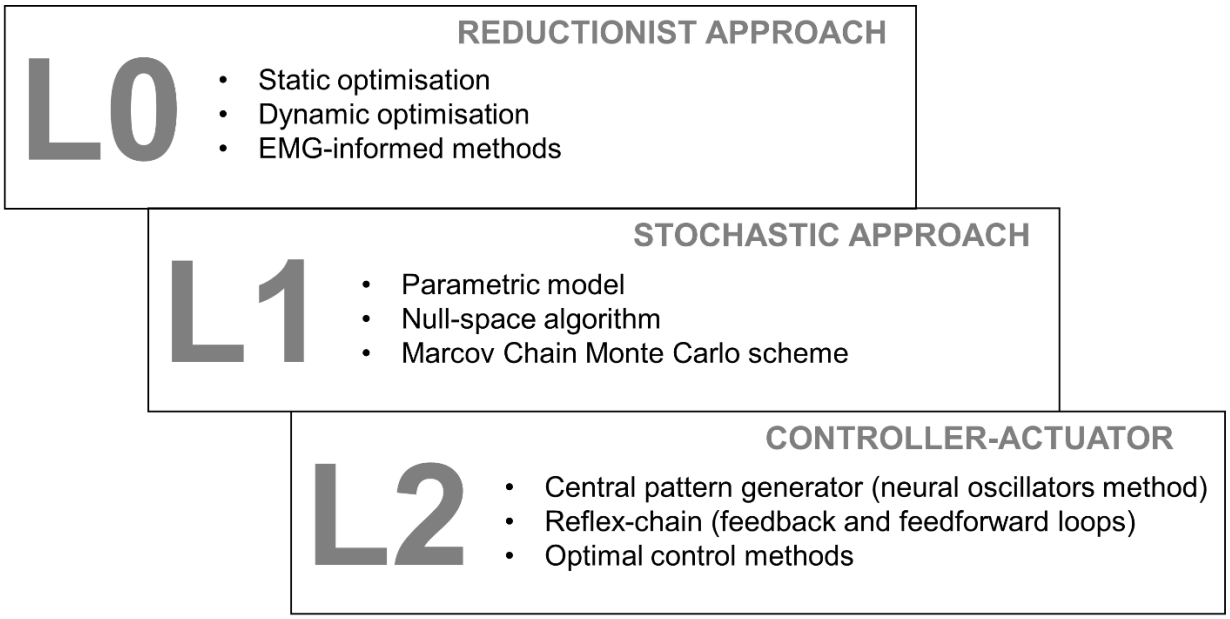

Figure 2. Summary of the 3 approaches developed and adopted over the years to estimate muscle activations and forces using musculoskeletal models. EMG indicates electromyography.

Reductionism in action: separation between controller and actuator

In the mid-60s, biomechanics research dealt with a complex problem: how to unravel the redundancy of the musculoskeletal system, a system with more actuators (the muscles) than degrees of freedom. In other words, if several options (in terms of muscle forces and activations) are available, how can we tell which "strategy" the CNS selects to achieve a specific goal? The so-called muscle redundancy (MR) problem was first introduced by Nikolai Bernstein in 1967.[16] In the decades following, several solutions to the MR problem were proposed, in most cases supported by scientific (physiological) evidence and experimental studies.

Static and Dynamic Optimization Approaches

Under the assumption that the CNS adopts a single strategy (among infinite available) according to an unspecified physiological criterion (e.g., minimization of muscle stresses), an elegant yet

simplistic and reductionist approach was theorized. The MR problem could be described as an optimization problem, where a given cost function (representative of the intended physiological criterion) was to be minimized or maximized. Thus, providing an "optimal" solution to the problem.

In 1973, taking on this concept, Seireg and Arvikar[71] proposed a cost function comprising two weighted terms, one for the individual muscle forces and one for the joint moments (Eq. 1). At each time frame, within a simulation, the cost function was minimized, to provide an "optimal" solution that produced nonnegative muscle forces and guaranteed dynamic equilibrium (joint dynamics):

$$J_1 = \sum_{i=1}^{n} \omega_i \cdot F_i + \sum_{i=1}^{n} \omega_i \cdot M_i \qquad (1)$$

Thus, the MR problem is reduced to a simple equilibrium problem but disregards the link between neural command (brain and CNS) and muscle activation and force generation.

Despite this, the idea rapidly gained momentum. The same approach was employed to study human and animal[72] musculoskeletal biomechanics in several works, to get insights into the role of muscles in various districts of the body, including the masticatory system,[73] the upper limbs (shoulder, elbow and wrist),[74], [75], [76], [77], [78], [79], [80], [81], [82], [83] the spine,[84], [85], [86], [87] and the lower limbs (hip, knee, and ankle).[59], [88], [89], [90], [91], [92], [93], [94], [95] Variations of the linear cost function proposed by Seireg et al. [71] were introduced, for example, which minimized relative muscle forces, discouraging the large muscles in the model from providing the biggest contribution. Formulations not including the second term in (Eq. 1), which is associated with the external joint moments, also began to appear. Of note, the propensity for a linear rather than a nonlinear cost function was primarily due to numerical reasons. Algorithms for efficient and stable solutions were already widely used for linear optimization compared to nonlinear optimization algorithms,[90] with no physiological ground.[95] Traditional approaches (e.g., simplex method) to solve the MR problem via the optimization of linear cost functions may lead to the sole recruitment of a limited (minimal) number of muscles (which is not consistent with electromyography [EMG] recordings).[96], [97] Moreover, to penalize excessive individual muscle forces, nonlinear cost functions were developed where the sum of squared (relative) muscle forces was minimized. The resulting muscle recruitment strategy (and activation patterns) better approximated the experimental EMG data[76], [95] and was associated with a more physiological load sharing between muscles, compared to those obtained with linear cost functions.

This was just the beginning. Advancements in knowledge, pushed by scientific discoveries in various disciplines, shed new light on the mechanisms behind/governing human motion and the principles underpinning the generation of muscle force.[98], [99] Several cost functions were introduced (Table 1), which promised to represent a physiological criterion (e.g., minimization of muscle stresses). Some were more task specific (e.g., to simulate walking or simple locomotor tasks), and others were district specific (e.g., for the upper or lower extremities).

In 1981, Crowninshield and colleagues [90] introduced a new physiological property in the cost function: the muscle physiological cross-sectional area (PCSA), i.e. the cross-sectional area of muscle multiplied for its cosine of fibre pennation angle. More specifically, they divided the force term by the muscle PCSA, defining a cost function that minimised the overall muscle stress (force over surface). Interestingly, increasing the power to 2 [77], [100] or 3 [90], the identified 'optimal' solution was representative of a recruitment strategy that minimises the overall muscle activation or maximises muscle endurance to contraction [101] (typical in prolonged and repetitive activities [90]) respectively. Along the same line, other authors [93] suggested adding some physiological constraints to the optimisation (e.g., to minimise the total mechano-chemical power of muscles with similar

function/role) [93], however, it was noticed that the higher the power in the cost function the lesser the need for additional constraints [76], [97]. An and colleagues [74], on the other hand, preferred to treat muscles as independent from one another (as they are independent in terms of energy stock and blood provision), and looked for a solution that minimised the cost function independently for each muscle. Noteworthy, the cost function suggested by An [74] and a polynomial cost function with a high exponent [97] produce substantially equivalent solutions.

Table 1. Summary of the cost function proposed to solve the muscle redundancy problem as an optimisation problem.

Physiological rationale	Cost function	Specific references
Minimise muscle forces	$\sum_{i=1}^{n} \omega_i \cdot F_i + \sum_{i=1}^{n} w_i \cdot M_i$	Seireg and Arvikar, 1973 [71]
Minimise muscle activations	$\sum_{i=1}^{n} F_i / F_{max,i}$	Pedotti et al., 1978 [95]
Minimise muscle fatigue	$\sum_{i=1}^{n} (F_i)^2$	Pedotti et al., 1978 [95]
Minimise muscle activations More physiological results	$\sum_{i=1}^{n} (F_i / F_{max,i})^2$	Pedotti et al., 1978 [95]
Minimise muscle stresses	$\sum_{i=1}^{n} F_i / PCSA_i$	Crowninshield et al., 1978 [89]
Increased endurance	$\sum_{i=1}^{n} (F_i / PCSA_i)^3$	Crowninshield and Brand, 1981 [90]
Minimise muscle stresses Consider each muscle as individual	$Min\ \sigma \mid {}^{F_i}/_{PCSA_i} \leq \sigma$	An et al., 1984 [74]
Joint stability	$\sum_{i=1}^{n} (F_i - F_s)^2$	Forster et al., 2004 [102]
Minimise joint contact force joint	$\left(\frac{\left\| \vec{F}(\vec{a},\ t) \right\|}{\left\| \vec{F}_{act}(\vec{a}_{act},\ t) \right\|} \right) + \omega_2 R(\vec{a}, t)$	van Veen et al., 2019 [103]
Track experimentally measured joint contact force	$\omega_1 \left(\frac{\left\| \vec{F}_{exp}(t) \right\| - \left\| \vec{F}(\vec{a}, t) \right\|}{\left\| \vec{F}_{exp}(t) \right\|} \right)^2 + \omega_2 R(\vec{a}, t)$	van Veen et al., 2020 [104]

Note: For a more comprehensive list of cost functions, the reader is referred to the appendix of the study of Tsirakos et al[105]. The cost functions are reported in chronological order. PCSA indicates physiological cross-sectional area of a muscle. References are provided for completeness.

Indeed, healthy individuals tend to minimally activate their muscles while performing simple locomotor tasks [90], in an attempt to save energy and/or sustain the activity for long periods of time.

However, the same may not hold true for pathological populations who may present with spastic (permanently contracted) muscles or individuals performing strenuous tasks requiring a different metabolic demand (i.e., to generate a large amount of muscle force/power in a short timeframe) [106]. Furthermore, it is not uncommon in the elderly or in subjects who underwent joint arthroplasty to observe the synchronous activation of both agonist and antagonist muscles in the attempt to stabilise their joints, which is probably related to their self-sense of weakness. Any cost function aiming to favour (metabolic) efficiency discourages co-contractions and cannot be considered representative of any such situation. Additional terms may be required, as suggested in the study of Forster et al. [102].

Extensive research has been conducted to define more suited cost functions able to capture abnormal responses or atypical (not optimal) activation patterns that characterise pathological populations [102], [103]. By minimising or maximising specific internal biomechanical quantities, e.g., joint torques or articular loads, one can induce (therefore mimic) muscle co-contraction or joint overloading and predict contact force profiles that better approximate in vivo data [103]. Nonetheless, discrepancies between predicted muscle activations and EMG data remain.

The source for this can be found in the way muscle dynamics is commonly (not properly) implemented. Classical inverse dynamics (optimisation-based) approaches fail to model the physiological behaviour of a muscle [107]. The MR problem is commonly solved separately at each timeframe, resulting in a solution that respects the physiological constraints at the single time frame but is independent of the previous or following instant. Time history is not accounted for. Static optimisation algorithms may generate muscle activation patterns exhibiting sudden bursts, which are not physiologically plausible. A suggested solution to avoid this unwanted outcome was the Physiological Inverse Approach (PIA) [107] based on a combination of inverse dynamic analysis – the musculoskeletal kinematics is fixed – and dynamic optimisation to estimate muscle forces together with activation and contraction dynamics. An alternative method where continuity in the solution was ensured through time integration (over time windows) were implemented is the Computed Muscle Control (CMC) [108], [109] which combines static optimisation to compute muscle activations and time integration (employing proportional-derivative controllers). However, there is conflicting evidence regarding this method. CMC predictions were found to overestimate the muscle and joint contact forces compared to static optimisation [110], casting some doubts on the reliability of this approach. In addition, ensuring continuity in the solution through time integration – although computationally expensive [111] – was not shown to improve predictions in gait analysis [112].

EMG-informed approaches

In the early 90's, with a series of studies by McGill [113] and McGill and Norman[114] the use of EMG data to inform or drive the models became a reality. Abnormal muscle activation patterns (including, but not limited to, muscle co-contractions) could finally be accounted for, enabling to investigate and study the effect of neuromuscular disorder on human biomechanics (e.g., causes behind gait disorders in cerebral palsy [60], [115], or post-stroke patients [116]).

In an EMG-informed model, muscle activations and forces are predicted through forward-dynamics simulations directly from a limited number of EMG signals recorded in vivo (and properly elaborated), while the multibody dynamics (joint kinematics and kinetics) are computed using an inverse paradigm based on experimental data. For the above reason, the EMG-informed method has also been referred to as *forward-inverse* approach [117]. The EMG signals can further be used to tune

the parameters defining the behaviour of the modelled muscles so that these could reproduce the experimentally derived linear envelopes (surrogate of muscle activations), while generating the required joint torques [118], [119]. This process, conceptualized by Hatze and Herbert [120], is referred to as model calibration and influences the overall predictive accuracy of a model [121].

The relationship between EMG signal and muscle force, which plays a key role in an EMG-driven model, was initially simplified to a linear function (i.e., muscle force was proportional to the excitation level) and later refined by Lloyd and Besier [121], who presented a new model able to describe (i) the second-order filtering with damping response that links EMG signal to muscle excitation and (ii) the non-linear (exponential) activation-to-force relationship [121].

Over the years, the methods were further refined (i.e., the development of an EMG-assisted approach) to enhance the dynamic consistency of EMG-driven models, thus ensuring more physiologically plausible estimates [122]. The cost function now includes three weighted terms governing the model's ability (and of the neural solution) to generate estimates in line with experimental joint moments and EMG data. In the last decades, EMG-informed models have been used for both clinical [60], [115], [123], [124], [125] and sport-related applications [126].

Although presenting some limitations – primarily connected to the nature of the EMG signals and to the methods to acquire these, the EMG-informed approach represented a step forward towards modelling sub-optimal muscle control. While the number of sensors (electrodes) that can be placed on the subjects is limited (typically between 8 and 16) – especially in children, the number of modelled muscles driven by EMG data can be expanded. Muscles sharing the same innervation (same motoneuron) show similar excitation patterns [127]. In addition, synergy-based methods now enable the reconstruction of missing EMG signals from primitives and weights extracted from normative datasets combined with those (few) collected on the patient himself [58], [128]. For more details on synergy-based methods, the reader is referred to [129]. Complementary information may be extracted from signals recorded with an array and/or matrices of electrodes (instead of bipolar or fine-wire electrodes) [130]. High-density EMG traces (HD-EMG), processed and decomposed [130], [131], [132], provide insights on the motor neurons firing (rate) and activity and may be employed to drive or inform MSK models [131], [133], [134].

Indeed, the development and use of EMG-informed approaches contributed to shifting the paradigm from searching for the optimal solution to searching for a more real(istic) solution in line with experimental data. The solution represents the specific task performed in a specific environment (typically a lab). The generalisation of other everyday activities or environments is not straightforward. Intra-subject variability is also not accounted for. Alternative methods were thus explored.

Neuromotor control as a stochastic process

Towards the end of the twentieth century, scientists started looking at the MR problem from a different perspective. The multitude of possible neural solutions (combinations of muscle forces and activations to produce a specific motion and dynamics) were interpreted as motor abundancy (with a positive connotation) other than redundancy (negative connotation) [135].

Observing how workers used to perform repetitive tasks, Scholz et al [136] and Scholz and Schöner [15] theorised that the CNS is not constantly selecting an optimal solution (in a reductionist sense), rather controls only those muscles and degrees of freedom that needs to be controlled to achieve the

set goal [137]. Motor control was thus considered a stochastic process aimed at identifying a 'good enough' solution that allows for some variability to provide stability to sudden changes or perturbations. This is known as the uncontrolled manifold theory (UMT).

At first, an exploration of natural biological variations in muscle forces (not yet attributable to a stochastic approach) was introduced through the parametric variation of the relative contributions of individual muscles, which were grouped based on their physiological function and role [138], [139]. The activation level of each actuator within a specific agonistic muscle group could vary between 0 (minimum) and 1 (maximum), while the activations of all antagonist muscles were determined *a priori*. Solutions were checked to be physiologically feasible with physiological constraint equations [139]. Such implementation, however, did not account for any goal variation (change in cost function) in response to external environmental factors, which was observed experimentally.

In 2011, Martelli et al [140] suggested expanding the solution space to an m-by-n hyperspace of possible and physiologically plausible muscle force combinations (where m is the number of degrees of freedom and n is the number of modelled muscles), delimited by the combinations resulting in minimal and maximal joint loading. The solution space was then sampled by randomly perturbing the set of muscle forces corresponding to an optimal solution (i.e., null-space algorithm). This method was later refined to ensure that all sampled solutions were within the realm of combinations able to produce the observed kinematics and dynamics (i.e., that respected the dynamic equilibrium) [141]. A Bayesian approach was implemented that interpreted the vector of the unknown (muscle forces) as a multivariate random variable characterised by a probability density function. The solutions were sampled using the Markov Chain Monte Carlo scheme, which provided a more uniform sampling of the full spectrum of possible recruitment strategies. This results in a band of plausible solutions (in contrast to a single solution identified by more traditional optimisation approaches), the width of which is representative of the intra-subject variability in the movement execution, further accounting for experimental data uncertainties.

The stochastic approach was first used to explore the probability of spontaneous hip fractures due to severe osteoporosis and severely sub-optimal muscle control [142]. The same has also been used to explain and quantify the variability in the recruitment strategies adopted by individuals with osteoarthritis following a total knee replacement surgery while walking [104] and to explore possible effects of knee joint overloading (e.g., due to Parkinson disease) on implant wear [64]. A similar approach was employed where the initial solution was identified through EMG-assisted simulations [56], as opposed to static optimisation. Current implementations of the stochastic approach suffer from the same limitations of static optimisation approaches, in that the solution is solved at each time frame, independently of the past and the future.

Alternative applications of the UMT have been proposed over the years. With a focus on highly dynamic tasks, specifically parkour motion (jumping and landing techniques), in 2018, Maldonado et al [143]presented an extension of the UMT based on the task function approach used in robotics. They showed that the CNS hierarchises and controls (sub)tasks to coordinate complex movements.

Explicit modelling of the controller-actuator coupling

Providing a systematic review of the current knowledge on the neurophysiology bases of motor control is beyond the scope of this review. For the sake of simplicity, we can idealise the current understanding in three separate layers that operate in concert: a reflexes layer, a central pattern generator layer, and a voluntary control layer.

Reflexes are muscle contractions that occur unconsciously. Specific sensory organs (e.g., the muscle spindle, which senses the elongation of each skeletal muscle, or the Golgi organs, which sense the tendons force) produce afferent signals that the motoneurons in the spine directly translate into a coordinated pattern of efferent activation signals to selected muscles, according to some predetermined schemes [144].

Voluntary movements always involve the central nervous system. But for stereotypical movements such as level walking, the involvement may be limited to initiating the task. Once in motion, a cluster of motoneurons in the spine is responsible for sustaining it by generating pre-codified activation patterns [145], even in the absence of descending inputs from the higher-level centres (i.e., supra-spinal). It can be considered a low-level (i.e., in spinal cord) controller [146]. This is the essence of the central pattern generator (CPG) theory proposed by Grillner in 1975 [147].

The control of non-stereotypical movements requires continuous control by the central nervous system (CNS). There are many theories on how this works exactly, but a generalisation of some of these theories is that of predictor-corrector control. Because of the non-negligible latency in the transmission of nervous signals, the brain needs to decide not what to do now but what to do in some hundred milliseconds, when the muscles will contract in response to the CNS signalling. To do so, the brain maintains a predictive model of how the body interacts with the physical world, which provides an estimate of the best possible activation pattern to achieve the desired motor target. This estimate is inaccurate for several reasons. Thus, as the movement develops, the CNS use all afferent signals to control and update its prediction and, where necessary, perform some corrections [144].

Modelling such mechanisms is not trivial. In general, this is achieved by adding feedback and feedforward [148], [149], [150] loops triggered by external factors such as muscle elongation (over stretch) [151], [152], [153], [154], [155], [156], joint angles [153], [154], [155], [156], [157], [158] or rate of force development [148], [151], [153], [154], [155], [156], [157]. While more complex to implement than traditional approaches, the inclusion of explicit controller-actuator mechanisms within the models enables predictive simulations, which are useful for investigating cause-effect relationships, gait abnormalities and neuromuscular deficits.

In the following, we will review the existing literature, clustering it around these three control layers.

Central pattern generator for stereotypical movements

One of the first controller-based MSK models implementing a CPG mechanism was introduced in 1991 by Taga and colleagues [159], who developed a torque-actuated model whose movements were based on the phase of the gait cycle through neural oscillators [160]. Later, this model was improved by adding muscles to actuate joints [161]. Stance and swing phases were identified by a foot-contact mechanism that accounted for gait speed and other factors. Accordingly, a series of neural oscillators (one per joint) – coupled to one another – alternatively activated agonist and antagonist muscles. As a result, the MSK model was able to walk normally, in line with experimental data from motion capture systems. The model presented an early and primitive feedback-based behaviour based on joint angle which could modulate (enhance or suppress) the work/action of adjacent neural oscillators. In 2001, Ogihara and Yamazaki suggested a model with both a rhythmic pattern from a CPG mechanism and feedback loops from proprioceptive information [152]. The parameters characterising the whole controller-actuator system were tuned to minimise the energy expenditure (per distance travelled).

The role of reflexes: feedback and feedforward loops

In 2010, Geyer and Herr [155] introduced a different level of the physiological controller, an alternative to a CPG controller, to mimic the role of both the Golgi organs and the muscle spindles; thus, adding muscle reflexes modulation (similarly to the way spinal reflexes send sensory information to alpha motoneurons). The walking pattern was guaranteed by length and force feedback specific for each muscle, depending on the gait phase. A force-sensor acted as an inhibitor, while a controller acted in response to muscle fibre (over)stretch and contraction velocity. Positive and negative feedback were introduced to ensure stability (of leg and trunk segments) and to prevent joint overextension during the execution of the task. In the same years, Similar (or slightly more advanced) models stemmed from this work, e.g. that implemented a feedforward control to stabilise further the gait [148] or neural oscillators driven by synergies extracted via non-negative matrix factorisation methods to control the activation of muscle actuators [162]. Other authors [163], [164] proposed ways to model the stretch reflex instead, which is responsible for muscle hyper-resistance and hyper-excitability in children with cerebral palsy (e.g., in spastic muscles), linking the excitations of specific muscles to the velocity and acceleration at which their fibres were contracting [163] and the muscle force produced.

Indeed, modelling muscle reflexes, combined with new approaches typical of optimal control methods, enables to run predictive simulations combining constraints and model modifications typical of pathological conditions such as age-related modifications [165], weakness of specific muscle groups [154], [158], to evaluate model transition to different gait speeds or to different terrain slope simply using the foot contact information to update the global state and oscillator working frequency [159], [166] or to explore a different combination of performance criteria to predict healthy gait [167]. A combination of CMC and biologically-inspired feedback controls has also been suggested to evaluate the effects of surgery on balance recovery in patients with cerebral palsy [168]. Of note, in 2019, the SCONE software was released, based on work from Geijtenbeek et al [169], [170], with the specific aim to enable the generation of reflex-based models and simulations [169]. Thanks to SCONE, the high complexity of this method has been partially overcome [154], [156], [167], [171].

Optimal control methods

Considering our actions, the result of a continuous refinement operated by the CNS to achieve the desired motor goal, the motor control problem can be seen as an optimal control problem. Hence, it is suitable to be described and solved using optimal control methods, commonly employed in other fields of science to model complex systems [172] and resolve highly non-linear (differential) equations [173].

Optimal control problems require the definition of an initial (tentative but plausible) solution which gets iteratively optimised to meet pre-determined tolerance and convergence criteria. At each iteration, the last or best-performing solution (in a batch of simulations) serves as a starting point for the subsequent round of optimisation, i.e., a predictor-corrector scheme. In an optimal control problem, the cost function describes the task to be performed, its complexity and its purpose through the definition of subgoals. For example, healthy gait could be seen as a combination of criteria to optimise metabolic energy rate, muscle fatigue, joint accelerations, passive torques and upper body muscle's excitations [174]. Optimal control problems can be defined as tracking or predictive problems. In a predictive simulation, task-specific (sub)goals are optimised independently of

experimental data, representing – for a tracking simulation – the overarching objective to follow or to tend to [70].

The first examples of optimal control applied to human gait were proposed by Chow and Jacobson in 1971 [175] and, few years later in 1976, by Hatze [176] who included the work of individual muscles in the optimal control problem. Due to the high computational costs associated with modelling both the motor task(s) and physiologically consistent muscles, until the late 90s, optimal control methods were rarely employed to simulate human locomotion. With the introduction of direct-shooting methods, such as gradient-based algorithms, simulated annealing and sequential quadratic programming [68], [177], [178], the computational time was drastically reduced but remained prohibitive for most applications. In the early 2000s, direct collocation methods disrupted this trend [173], [174], [179], enabling the solution of large-scale problems with several unknowns. Combinations of various performance criteria have been tested since [67], [174], [180], [181], [182], [183], e.g. to model pathological gait [184]. Alternative algorithms, such as the Adams-type predictor-corrector algorithms [185], have been proposed to address the problem of muscle control, with limited following [186].

In the last decades, alternative uses of optimal control methods to solve neuromuscular control problems gained visibility. In 2004, Scott [187] and Todorov [188] suggested employing optimal control methods to iteratively correct the gains of feedback controllers [189], based on an index of performance. Only those variations that are considered relevant to perform the intended task are thus optimised, enabling the identification of "the best possible control scheme for a given task". This approach, known as optimal feedback control, allows the exploration of the redundancy accumulated in task-irrelevant dimensions while correcting deviations that impact the task (according to the "minimal intervention principle") [189]. Optimal feedback control is also strictly connected to another optimal control method: the stochastic optimal control [189], aimed to introduce into simulations physiological noise to predict a more realistic control strategy [190]. More recently, deep reinforcement learning method has been tested out to solve the optimal control problem. The adoption of this method was related to synthesizing physiologically-based human motions based either on a kinematic reference motion [191] or without it [192]. For more details, authors suggest the review article written by Song et al [193] (Figure 3).

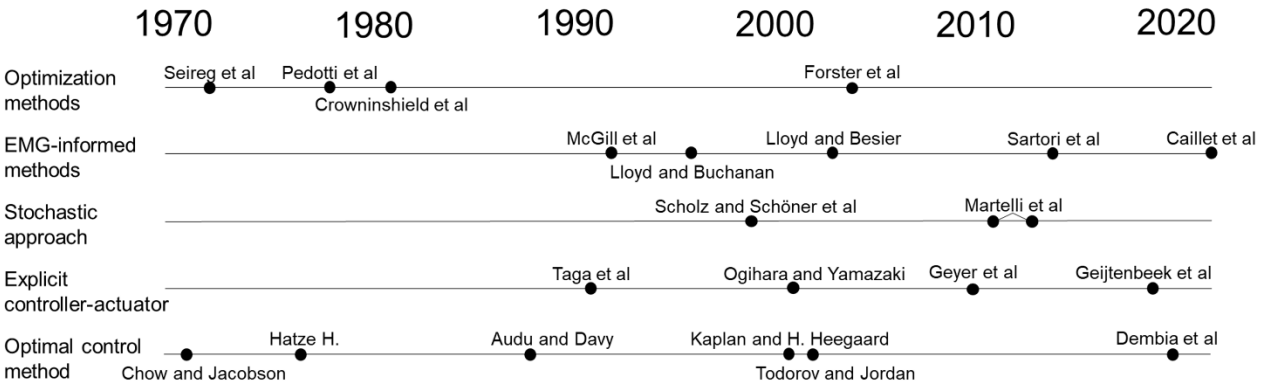

Figure 3. Chronological overview of the approaches to model suboptimal control. The list is not exhaustive but containes the works that in the authors' view contributed to the advancement of the field. EMG indicates electromyography.

Conclusion

This paper reviewed the literature to date on the modelling of neuromuscular control. The work done so far can be clustered into three groups: models based on the classic reductionist approach, which assumes optimal control; the modelling of neuromuscular control as a stochastically optimal process, consistently with the uncontrolled manifold strategy; and a third group of papers that attempt to explicitly model the voluntary control through reflex chains, central pattern generators, or more complex predictor-corrector controllers.

Optimal control plays still an important role in the solution of many biomechanics problems; however, to be clinically relevant in several problems, biomechanics models must be able to handle also suboptimal control.

Assuming a stochastically optimal control can be a very effective approach to model patients with mild degradation of the neuromuscular control; however, it is important that the current approach, where each instant is assumed independent from the following one, may cause unrealistic predictions, and should be extended to include some smoothness constraints over time.

The explicit modelling of motor control still remains extremely challenging. Each author focuses on one of the layers (voluntary control of the reflex chain, central pattern generator for repetitive stereotypical tasks, direct control with predictor-corrector). In contrast, it is probably true that all three mechanisms coexist, combined and overlapped. Modelling this complexity is one of the grand challenges of computational biomechanics in the years to come.

Acknowledgments

This study was partially supported by the EU H2020 project “In Silico World: Lowering barriers to ubiquitous adoption of In Silico Trials” (grant ID 101016503), and the project "ForceLoss: differential diagnosis of force loss in fragile elders" that has received funding from the Italian Ministry of Health (Ricerca finalizzata RF-2019-12369960). The authors would like to thank the Mobilise-D consortium for the support.

Exploring muscle recruitment by Bayesian methods during motions

Mercy Amankwah[1], Alex Bersani[2], Daniela Calvetti[1], Giorgio Davico[2], Erkki Somersalo[1], Marco Viceconti[2,3],

[1] Department of Mathematics, Applied Mathematics and Statistics, Case Western Reserve University, Cleveland, Ohio, USA

[2]Department of Industrial Engineering, Alma Mater Studiorum, University of Bologna, Bologna, Italy

[3] Medical Technology Laboratory, Rizzoli Orthopaedic Institute, Bologna, Italy

Adapted from a publication in:

Chaos, Solitons & Fractals

(2024)

https://doi.org/10.1016/j.chaos.2024.115082

The authors wish to thank Chaos, Solitons & Fractals for providing the permission to re-use the manuscript titled “Exploring muscle recruitment by Bayesian methods during motions” in the present PhD thesis.

Alex Bersani’s contribution to this research is stated in last chapter named “Author contribution”

Abstract

The human musculoskeletal system is characterized by redundancy in the sense that the number of muscles exceeds the number of degrees of freedom of the musculoskeletal system. In practice, this means that a given motor task can be performed by activating the muscles in infinitely many different ways. This redundancy is important for the functionality of the system under changing external or internal conditions, including different diseased states. A central problem in biomechanics is how, and based on which principles, the complex of central nervous system and musculoskeletal system selects the normal activation patterns, and how the patterns change under various abnormal conditions including neurodegenerative diseases and aging. This work lays the mathematical foundation for a formalism to address the question, based on Bayesian probabilistic modeling of the musculoskeletal system. Lagrangian dynamics is used to translate observations of the movement of a subject performing a task into a time series of equilibria which constitute the likelihood model. Different prior models corresponding to biologically motivated assumptions about the muscle dynamics and control are introduced. The posterior distributions of muscle activations are derived and explored by using Markov Chain Monte Carlo (MCMC) sampling techniques. The different priors can be analyzed by comparing the model predictions with actual observations.

Keywords

Inverse Kinematics, Uncontrolled Manifold, Markov Chain Monte Carlo, Feynman-Kac formula

Introduction

Understanding the subtle interplay between the human central nervous system (CNS) and the musculoskeletal system (MS) to generate controlled movements to accomplish specific tasks is one of the central problems in neurophysiology as well as in biomechanics. The musculoskeletal system is characterized by muscle redundancy, whereby the number of muscles actuating a desired movement exceeds the number of degrees of freedom, implying that the desired movement can be accomplished in multiple alternative ways. While this redundancy is crucial for the system to work seamlessly under changing external conditions without being too sensitive to perturbations, it also raises the question of what strategy, if any, the human body follows to attain the desired goal. The reductionist approach assumes the existence of a cost function whose minimizer corresponds to the preferred muscle activation pattern, while the uncontrolled manifold hypothesis assumes that the activation pattern is an approximate optimizer among all possible activations respecting the physiological bounds. The uncontrolled manifold approach is more flexible and can account for patterns effectuating movements in which optimal activation is not possible, as may be the case for non-healthy, non-adult or aged subjects, or tasks performed in challenging environments, for example walking on slippery ground. According to the uncontrolled manifold theory, the CNS controls only those movements – hence the muscles – necessary to perform a given task and achieve a pre-defined goal. The activity of the other muscles – and degrees-of-freedom – is not controlled as tightly, allowing the musculoskeletal system to be flexible, to quickly react to external unpredicted events, e.g., forces or obstacles. This is the reason why a trained person can repeat a task with the same outcome, selecting each time a slightly different strategy, resulting in a different body kinematics. The body segments (e.g., femur, pelvis, tibia) are actuated by the muscles, and move as the muscles contract in response to a signal [15], [135], [136], [137]. Exploring the continuum of possible solutions to the muscle redundancy problem can be done by sampling techniques, including Bayesian

Monte Carlo techniques [140], [141], [194]. For a comprehensive review of the different approaches that have been proposed in the literature, see [195].

As pointed out in the cited review article [195], a shortcoming of most solutions to the muscle redundancy problem is that the algorithms seek the solutions considering one time frame at a time. The reasons for this are twofold: Solving the dynamics of the musculoskeletal system over multiple time frames (e.g. over the entire duration of a task) is more computationally demanding albeit more physiologically plausible than assuming time-independency, as the solution would need to be valid at all frames simultaneously, and requires the definition of rules to mimic the process used by the CNS to select the muscle activation pattern. The model that we propose in this work assumes that under normal activation, i.e., when not performing maximal tasks, the body prefers patterns limiting the total yank [196], defined as the time derivative of the muscle forces. The present approach continues and extends the work in [141], [194] by putting the formalism in a Bayesian statistical context. More specifically, the intrinsic objectives and bound constraints are implemented as a priori information, while the information concerning equilibrium conditions obtained by motion tracking constitutes the likelihood: uncertainties in the tracking process as well as in translating the motion capture data into generalized joint force configurations contribute to the observation noise. In addition, we discuss previously proposed optimization strategies with a reinterpretation in the Bayesian framework providing a uniform framework for the comparison of different objective functions. The remainder of the article is organized as follows. In the next section we present a concise mathematical formulation of the muscle recruitment problem that is a basis for the likelihood model. Section 3 provides an outline of the Bayesian formulation. The full Bayesian model is developed in Section 4, where we introduce prior densities encoding hypotheses about the physiological muscle recruitment principles. Section 5 presents the details of the computational engine, the MCMC sampling algorithm. The performance of the algorithm is demonstrated with computed examples in section 6.

Muscle activation problem

In this section, for completeness, we present a concise derivation of the forwards model relating the muscle forces and the movement that those forces generate, and state the related inverse problem whose solution is the main topic of this paper. The body is modeled as a link-segment system, and the muscle forces generate torques through a lever arm model at the joints with given degrees of freedom which translate into movements of the body. The forward problem consists of computing the trajectories of the joints from known muscle forces, while estimating the muscle forces from partial observations of the movement is the corresponding inverse problem of interest to us.

In biophysics and robotics, the inverse dynamic problem, or inverse structural dynamic problem seeks to find the generalized forces, or torques that applied to joints of a link-segment model of a human or an animal body or a robot effect a desired motion. For the sake of definiteness, we assume that the task of interest is level walking by a human, observed through a motion capture system that records the paths of fiducial markers attached on the surface of the body. Subsequently, the motion is encoded in terms of the degrees of freedom, typically a set of angular variables related to the joints of the link-segment model of the body. This translation is typically based on a weighted least squares process, fitting the dynamic model prediction based on the degrees of freedom to the observations, see, e.g.,[197], and the manual of OpenSim for details of the fitting process. In the following, the dynamics of the link-segment model of the body is encoded in terms of the vector-valued function $\theta(t) \in \mathbb{R}^m, 0 \leq t \leq T,$ where the m components of the vector represent the angular degrees of freedom

associated to the joints characterizing the model of the body. It is assumed that the time course of the generalized coordinates, combined with geometric information including the inertia tensors of the limb segments and the reaction forces completely characterize the dynamics of the system.

To solve the inverse dynamic problem of finding the generalized forces, consider the Lagrangian function of the joint segment system, given by

$$L\left(\theta,\dot{\theta}\right) = E_{kin}\left(\theta(t),\theta\dot{(t)}\right) - U(\theta(t)),$$

where E_{kin} is the kinetic energy of the system, and U is the potential energy [198]. The Lagrange equations

$$\frac{d}{dt}\left(\frac{\partial L}{\partial \dot{\theta_j}}\right) - \frac{\partial L}{\partial \theta_j} = T_{j,} \quad 1 \le j \le m \qquad (1)$$

relate the generalized forces T_j and the equations of motion of the system. Assuming that the generalized coordinates are the joint rotation angles, the generalized forces represent the corresponding torques. By writing the kinetic energy as a quadratic form,

$$E_{kin}\left(\theta,\dot{\theta}\right) = \frac{1}{2}\dot{\theta}^{\mathrm{T}}\mathbf{H}(\theta)\dot{\theta},$$

where $\mathbf{H}(\theta)\epsilon\mathbb{R}^{m\times n}$ is the positive semidefinite (multi-body) inertia matrix of the system, it follows from (1) that the equations of motion can be expressed as

$$T_j = \sum_{k=1}^{m} H_{jk}(\theta)\ddot{\theta} + \sum_{k,l=1}^{n} C_{jkl}(\theta)\dot{\theta}_k\dot{\theta}_l - G_j(\theta), \qquad (2)$$

where C is the Christoffel symbol,

$$C_{jkl} = \frac{\partial H_{jk}}{\partial \theta_l} - \frac{1}{2}\frac{H_{kl}}{\partial \theta_j}, \quad G_j = \frac{\partial U}{\partial \theta_j}$$

Here, the second term on the right accounts for centrifugal and Coriolis forces at the joints. These are the joint torques that the muscles need to effectuate to produce the observed trajectory. Since the time evolution of the generalized coordinates is approximately known, Eq. (2) allows the computation of the torques at times $t_l \le l \le N$, denoted here by $T_j^{exp}(t_l)$. To express the torques in terms of forces, denote by $\vec{F}_{jk}(t)$ vectors of forces of the muscles exerting a torque at the joint related to the *j*th generalized coordinate θ_j, and let $\vec{r}_{jk}(t)$ be the corresponding lever arm vectors. If $\vec{\omega}_j$ is the direction of the *j*th torque vector, we must have

$$\vec{\omega}_j \cdot \left(\sum_k \vec{r}_{jk}(t) \times \vec{F}_{jk}(t)\right) = T_j(t).$$

By collecting the scalar amplitudes of the forces of all n muscles involved in the system into a vector $F(t) \in \mathbb{R}^n$, the torques in a vector $T(t) \in \mathbb{R}^m$, and organizing the coefficients of the above equation into a lever arm matrix $\mathrm{A}(t) \in \mathbb{R}^{m\times n}$, we arrive at the matrix equation,

$$\mathrm{A}(t)F(t) = T(t). \qquad (3)$$

Denote the maximal (tetanic) forces of the muscles by $F_j^*, 0 \le F_j \le F_j^*$, and define the muscle activations q_j by the formula

$$F_j(t) = F_j^* q_j(t), \qquad 0 \le q_j(t) \le 1.$$

We express the equilibrium conditions (3) at the discrete times $t = t_l$ in matrix form as

$$b^l = \mathrm{A}^l q^l + \varepsilon^l, \qquad 0 \le l \le L, \qquad (4)$$

where $b^l \in \mathbb{R}^m$ represents the vector of estimated torques $T^{\exp}(t_l)$, $q^l = q(t) \in \mathbb{R}^n$ is the vector of activations at $t = t_l$,

$$\mathrm{A}^l = \mathrm{A}(t_l)\mathrm{F}^* \epsilon \mathbb{R}^{m \times n}, \ \mathrm{F}^* = diag(F_1^*, \dots, F_n^*),$$

and ε^l represents the uncertainties due to the estimation process of the inverse kinematic problem.

Eq. (4) is the forward model describing how the muscle forces yield the generalized forces acting on joints to effect the observed motion. The corresponding inverse problem, which is the focus of this article, can be stated as follows:

Muscle recruitment problem: Given the lever arm matrices A^l at discrete time instances and the torques b^l estimated with a given accuracy from the motion information, characterize the ensemble of possible muscle activations $q^l \in \mathbb{R}^n, 0 \le l \le L$ that are able to effectuate the observed movement, subject to additional suitable constraints.

In the following section, we discuss possible constraining conditions and develop a systematic Bayesian methodology to solve the muscle recruitment inverse problem.

Bayesian inverse problem: a recap

Before discussing the suitability and implications of different types of constraints, we provide a brief overview of the Bayesian methodology for inverse problems. For further details, we refer to monographs [199], [200].

Consider the problem of estimating an unknown quantity $x \in \mathbb{R}^n$ based on the observation of a related quantity $b \in \mathbb{R}^m$ as well as on a priori information about x. For the sake of clarity, we assume that the unknown and the observation are related to each other through a model

$$b = f(x) + \mathcal{E}, \qquad (5)$$

where $f: \mathbb{R}^n \to \mathbb{R}^m$ is known, and the vector $\varepsilon \in \mathbb{R}^m$ accounts for both observation noise and uncertainties in the model. In the Bayesian framework, all unknown quantities are modeled as random variables regardless of whether the unknown represents a fully deterministic quantity or not: in other words, randomness in the Bayesian framework is an expression of lack of certainty about the value, regardless of the nature of the uncertainty. With that in mind, we interpret Eq. (5) as a model relating the three random variables characterized by the respective probability distributions. We assume here that the variables x and $\mathcal{E}$ are mutually independent. Assuming that the probability distribution of $\mathcal{E}$ is defined through a probability density function π_ε, that is

$$\mathbb{P}\{\varepsilon \in B\} = \int_B \pi_\varepsilon(e)de, \qquad B \subset \mathbb{R}^m$$

the probability density of b conditional on a known value of x is

$$\pi_{b|x}(b|x) = \pi_\varepsilon(b - f(x)).$$

This density, referred to as the *likelihood density*, expresses the distribution of the observed values of b assuming that x is known and fixed. On the other hand, before observing b, we may have some information about the distribution of the unknown x which we encode in the *prior density* π_x,

$$\mathbb{P}\{x \in A\} = \int_A \pi_x(x)dx, \qquad A \subset \mathbb{R}^n$$

by the law of total probability, the *joint probability density* of the pair (x, b) is then given by the expression

$$\pi_{x,b}(x,b) = \pi_{b|x}(b|x)\pi_x(x). \qquad (6)$$

Reversing the role of the variables x and b, the joint probability density of (x, b) can be expressed also as

$$\pi_{x,b}(x,b) = \pi_{x|b}(x|b)\pi_b(b), \qquad (7)$$

where π_b represents the marginal density of the variable b,

$$\pi_b(b) = \int_{\mathbb{R}^n} \pi_{x,b}(x,b)dx = \int_{\mathbb{R}^n} \pi_{b|x}(b|x)\pi_x(x)dx$$

Equating the two equivalent representations (6), (7) of the joint density naturally yields *Bayes' formula*, relating the *posterior density* $\pi_{x|b}(x|b)$ to the likelihood and prior densities,

$$\pi_{x|b}(x|b) = \frac{\pi_{b|x}(b|x)\pi_x(x)}{\pi_b(b)} \propto \pi_{b|x}(b|x)\pi_x(x), \qquad (8)$$

assuming that $\pi_b(b) \neq 0$. In the expression for the posterior, $\pi_b(b)$ represents a scaling factor that is unimportant in most of the analysis and is often omitted, hence the symbol "$\propto$" indicating "proportional up to a scaling factor".

Given the posterior density, it is common to summarize it with either the Maximum A Posteriori (MAP) estimate, or the Posterior Mean (PM) estimates,

$$x_{MAP} = \operatorname{argmax} \pi_{x|b}(x|b), \qquad x_{PM} = \int_{\mathbb{R}^n} x\, \pi_{x|b}(x|b)dx,$$

assuming that the above quantities are well defined. The estimate x_{MAP} is the solution of an optimization problem, while the computation of x_{PM} requires integration in $\mathbb{R}^n$. In high dimensional problems, it is not feasible to integrate using numerical quadratures, and one has to resort to Monte Carlo techniques. A common approach is to use Markov chain Monte Carlo (MCMC) techniques to generate a large sample of realizations,

$$\mathcal{S}_N = \{x^{(1)}, x^{(2)}, \dots, x^{(N)}\}, \qquad (9)$$

Drawn from the distribution $\pi_{x|b}(x|b)$, then using the sample to estimate the posterior mean as

$$x_{PM} \approx \frac{1}{N}\sum_{j=1}^{N} x^{(j)}.$$

Observe that the sample $\mathcal{S}_N$ provides much more information about the posterior distribution than just the posterior mean: For instance, we may approximate the posterior covariance matrix by

$$\mathrm{C} = \frac{1}{N-1}\sum_{j=1}^{N}(x^{(j)} - x_{PM})(x^{(j)} - x_{PM})^{\mathrm{T}}.$$

Moreover, the posterior (marginal) belief intervals of $p\%$ of the components x_k, denoted by $[m_k^p, M_k^p]$, can be determined by sorting the components $x_k^{(j)}$ in increasing order,

$$x_k^{(j_1)} \leq x_k^{(j_2)} \leq \cdots \leq x_k^{(j_N)},$$

and discarding $\frac{1}{2}(100 - p)\%$ of the values from the top and from the bottom. More precisely, letting

$$j_{low} = \left\lceil \frac{1}{2}\left(1 - \frac{p}{100}\right) N \right\rceil, \qquad j_{high} = N - j_{low},$$

we define

$$m_k^p = x_k^{(j_{low})}, \qquad M_k^p = x_k^{(j_{high})}.$$

We end this section by outlining the MCMC sampling algorithm that will be used in the numerical calculations. Consider the current sample point $x^{(j)}$. The Gibbs sampler algorithm provides a method to generate the next sample point $x^{(j+1)}$ in the chain, drawn from the posterior probability distribution in the following way. For notational simplicity, let us denote the posterior density by $\pi(x) = \pi_{x|b}(x|b)$, and let $\pi(x_k|x_1, x_2, \dots, x_{k-1}, x_{k+1}, \dots, x_n)$ denote the one-dimensional posterior density of the component x_k obtained by keeping all components in the density $\pi(x)$ fixed except for the *k*th one. The updating step of the Gibbs sampler consists of *n* random draws from one-dimensional densities: given the current sample point $x^{(j)}$,

$$\begin{aligned}
&\text{draw} x_1^{(j+1)} \text{from} \pi\left(x_1 \middle| x_2^{(j)}, \dots, x_n^{(j)}\right),\\
&\text{draw} x_2^{(j+1)} \text{from} \pi\left(x_2 \middle| x_1^{(j+1)}, x_3^{(j)}, \dots, x_n^{(j)}\right),\\
&\text{draw} x_3^{(j+1)} \text{from} \pi\left(x_3 \middle| x_1^{(j+1)}, x_2^{(j+1)}, x_4^{(j)} \dots, x_n^{(j)}\right),\\
&\vdots\\
&\text{draw} x_n^{(j+1)} \text{from} \pi\left(x_n \middle| x_1^{(j+1)}, x_2^{(j+1)}, \dots, x_{n-1}^{(j+1)}\right).
\end{aligned}$$

The implementation of the Gibbs sampler is, at least in principle, a straightforward task, requiring only random draws from one-dimensional densities. We will discuss the details that need to be addressed for a successful implementation in the context of computed examples.

Bayesian models for the muscle dynamics

In this section, we develop a family of Bayesian prior models designed to encode physiologically meaningful information about the muscle dynamics.

Likelihood model

In the Bayesian framework, we treat the equilibrium conditions (6) as observation models. For reasons of computational simplicity, we assume that the noise vectors ε^l are mutually independent, and moreover, we model them as identically distributed scaled multivariate Gaussian white noise vectors,

$$\varepsilon^l \sim \mathcal{N}(0, \sigma^2 I_n),$$

where $\sigma > 0$ is the noise level, and I_n is the $n \times n$ identity matrix. This yields the Gaussian likelihood model,

$$\pi_{b^l|q^l}(b^l|q^l) \propto \exp\left(-\frac{1}{2\sigma^2}\|b^l - \mathrm{A}^l q^l\|^2\right).$$

We organize the muscle activations into a matrix with columns indexed by the time instances and the rows by the muscles,

$$\mathrm{Q} = \begin{bmatrix} q_1^0 & q_1^1 & \cdots & q_1^N \\ q_2^0 & q_2^1 & \cdots & q_2^N \\ \vdots & \vdots & & \vdots \\ q_n^0 & q_n^1 & \cdots & q_n^N \end{bmatrix} = [q^0\ q^1\ \cdots\ q^N],$$

and we arrange the observations in a similar fashion into a matrix $\mathrm{B} \in \mathbb{R}^{m\times(N+1)}$. To vectorize the calculations, we stack the columns of Q and B into the vectors

$$\mathbf{q} = \mathrm{vec}(\mathrm{Q}) = \begin{bmatrix} q^0 \\ q^1 \\ \vdots \\ q^N \end{bmatrix}, \qquad \mathbf{b} = \mathrm{vec}(\mathrm{B}) = \begin{bmatrix} b^0 \\ b^1 \\ \vdots \\ b^N \end{bmatrix},$$

and we assemble the block diagonal matrix $\mathcal{A}$,

$$\mathcal{A} = \begin{bmatrix} \mathrm{A}^0 & & \\ & \ddots & \\ & & \mathrm{A}^N \end{bmatrix}. \qquad (10)$$

Assuming mutual independence of the identically distributed noise vectors ε^l, the likelihood of the time series of the generalized forces is of the form

$$\pi_{\mathbf{b}|\mathbf{q}}(\mathbf{b}|\mathbf{q}) \propto \exp\left(-\tfrac{1}{2\sigma^2}\textstyle\sum_{l=0}^{N}\left\|b^l - \mathrm{A}^l q^l\right\|^2\right) = \exp\left(-\tfrac{1}{2\sigma^2}\|\mathbf{b} - \mathcal{A}\mathbf{q}\|^2\right). \qquad (11)$$

This likelihood model can be augmented by complementary information, for example electromyographic (EMG) measurements as indicated later in the discussion.

Prior models

In Bayesian analysis of inverse problems, the prior plays a crucial role, as it is a way to augment the observations accounted for in the likelihood with additional information that may be available. In underdetermined ill-posed inverse problems, where the data alone do not suffice to solve the problem in an unambiguous way, the prior can be thought of as adding constraints similar to regularization in the classical deterministic inverse problems framework [201]. In the following subsections we present several prior models, based on physiologically justifiable assumptions, that help explore the uncontrolled manifold in a more insightful manner.

Box prior

Muscle forces must be non-negative and cannot exceed their presumably known tetanic values. These conditions can be expressed in terms of the muscle activations as bound constraints

$$0 \le q^l \le 1, \quad 0 \le l \le N, \qquad (12)$$

with the inequalities to be understood in component-wise sense. We encode these bounds into a *box prior* density of the form

$$\pi_{\mathbf{q}}^{box}(\mathbf{q}) = \textstyle\prod_{l=0}^{T} \mathcal{X}(q^l),$$

where $\mathcal{X}$ is the multivariate indicator function of the unit hypercube in $\mathbb{R}^n$.

Minimum activation prior

The information encoded in the box prior, while reducing considerably the range of possible activations, still allows a lot of redundancy in the determination of the force configurations, some of

which may be physiologically justified under certain conditions, for example co-contraction forces at the joints. While simultaneous activation of agonist and antagonist muscles may occur, e.g., when joint stabilization is necessary, it is unlikely to occur under optimal conditions because it is energetically wasteful. It may be argued that the body, to perform a simple locomotion task such as level walking, may prefer activation configurations that minimize the need of energy metabolism, a hypothesis corroborated by EMG measurements [90], [95]. Following this principle, it is reasonable to hypothesize that the body seeks to minimize muscle activation. This is encoded in the *minimum activation* prior,

$$\pi_{\mathbf{q}}^{MA}(\mathbf{q}) \propto \pi_{\mathbf{q}}^{box}(\mathbf{q}) \exp\left(-\frac{1}{2\omega^2}\|\mathbf{q}\|^2\right),$$

where the prior variance $\omega^2 > 0$ expresses how strongly the minimum activation principle is believed to be followed by the muscles. If there are reasons to believe that the task being performed requires co-contractions (e.g., level walking on ice), a larger variance value may be used to weaken the trust in the minimum energy principle.

Minimum yank prior

The two priors introduced so far assume that the muscle activation patterns at the different times instances t_l are mutually independent. This assumption may not be physiologically justified, because there are limitations for the speed at which an activation configuration can change. Assuming that the velocity at which the activation configuration takes place is a limiting factor, it is reasonable to hypothesize that in a normal continued activity such as level walking, the muscle forces do not change too abruptly in time. While in physics the time derivative of a force has no particular significance, in [196] the authors introduce the term 'yank' to refer to the time derivative of a muscle force. In physiology, yank is an important and useful concept: maximizing the yank improves a predator's chances of reaching a target area, and the prey's chances to escape. In [167] the authors discuss the problem of finding the cost function to be minimized to reduce the redundancies in muscle activations during healthy gait, highlighting the importance of the yank in sensorimotor systems, Furthermore, in support of their position they argue that mitigating the impact of external forces, identified with yank, could be detected by the cutaneous mechanoreceptors in the foot [202], [203], pointing towards the importance of the yank in the feedback mechanism in normal human walking. It has been suggested that controlling the yank is a way for the body to avoid injuries in leg tissues [204], [205], and in [206] it was shown that yank control may be motivated by energetic considerations because fast muscle cells use significantly more ATP than slow muscle cells.

Motivated by these considerations, we introduce a prior model favoring solutions with low yank between time frames over those with large yank. The yank of the *k*th muscle, defined as the time derivative of the force,

$$Y_k(t) = \frac{dF_k}{dt}(t).$$

The average yank over the time interval $[t_{l-1}, t_l]$ is given by

$$\bar{Y}_k^l = \frac{1}{\Delta t}\int_{t_{l-1}}^{t_l} Y_k(t)\,dt = \frac{1}{\Delta t}\left(F_k(t_l) - F_k(t_{l-1})\right) = \frac{1}{\Delta t}\left(F_k^l - F_k^{l-1}\right),$$

where $F^l = F(t_l) \in \mathbb{R}^n$. To formulate the belief about the yank in terms of a probability density function, for each muscle we write

$$F_k^l - F_k^{l-1} = \eta_k^l, \qquad \eta_k^l \sim \mathcal{N}(0, \gamma^2), \qquad l = 1, 2, \ldots, N, \qquad (13)$$

where we assume that $\gamma \to 0$ as $\Delta t \to 0$, guaranteeing continuity of the muscle forces. We can express condition (13) in vectorial form simultaneously for all muscles in terms of the activation vectors q^l with the help of the diagonal matrix F^* of the tetanic forces, so that $F^l = \mathrm{F}^* q^l$. We write the component-wise Eq.(13) for each l as

$$F_k^l - F_k^{l-1} = \mathrm{F}^*(q^l - q^{l-1}) = \gamma\beta^l, \qquad \beta^l \sim \mathcal{N}(0, \mathrm{I}_n).$$

Next we consider all time instances together and write the matrix equation

$$\begin{bmatrix} -F^* & F^* & & & \\ & -\mathrm{F}^* & F^* & & \\ & & \ddots & \ddots & \\ & & & -F^* & F^* \end{bmatrix} \begin{bmatrix} q^0 \\ q^1 \\ \vdots \\ q^N \end{bmatrix} = \gamma \begin{bmatrix} \beta^1 \\ \beta^2 \\ \vdots \\ \beta^N \end{bmatrix}$$

which can be expressed as

$$(\mathrm{L} \otimes \mathrm{F}^*)\mathbf{q} = \gamma\mathbf{e}, \qquad \mathbf{e} \sim \mathcal{N}(0, \mathrm{I}_{\boldsymbol{nN}}),$$

where

$$\mathrm{L} = \begin{bmatrix} -1 & 1 & & & \\ & -1 & 1 & & \\ & & \ddots & \ddots & \\ & & & -\mathrm{F}^* & F^* \end{bmatrix} \in \mathbb{R}^{N \times (N+1)}, \qquad \mathbf{e} = \begin{bmatrix} \beta_1 \\ \beta_2 \\ \vdots \\ \beta_N \end{bmatrix} \in \mathbb{R}^{nN}$$

and $\otimes$ is the Kronecker product.

We are now ready to write the corresponding prior model for the paths $\boldsymbol{Q}$ as

$$\pi_q^{MY}(\mathbf{q}) \propto \pi_q^{box}(\mathbf{q}) exp\left(-\frac{1}{2\gamma^2}\|(\mathrm{L} \otimes \mathrm{F}^*)\mathbf{q}\|^2\right).$$

Observe that unlike the priors defined previously, the yank prior ties the time slice activations together to form paths, thus the realizations at different time slices are no longer mutually independent.

Mixed prior

We end this section with a mixed prior model that interpolates the minimum activation prior and the yank prior. We define the prior density as geometric interpolation of the form

$$\pi_q^{mix}(\mathbf{q}) \propto (\pi_q^{MA}(\mathbf{q}))^{\vartheta} (\pi_q^{MY}(\mathbf{q}))^{1-\vartheta}$$

$$= \pi_q^{box}(\mathbf{q}) \exp\left(-\frac{\vartheta}{2\omega^2}\|\mathbf{q}\|^2 - \frac{1-\vartheta}{2\gamma^2}\|(\mathrm{L} \otimes \mathrm{F}^*)\mathbf{q}\|^2\right), \qquad 0 < \vartheta < 1,$$

where the parameter ϑ determines the relative weight of the two priors. We remark that in the limit $\vartheta \to 0+$ we have the minimum yank prior, while letting $\vartheta \to 1$- we obtain the minimum activation prior. More generally, the priors can be combined as

$$\pi_q^{mix}(\mathbf{q}) \propto (\pi_q^{MA}(\mathbf{q}))^{\vartheta_1} (\pi_q^{MY}(\mathbf{q}))^{\vartheta_2}$$

with mutually independent exponents ϑ_1 and ϑ_2. In our numerical simulations, we restrict the model to the former one to reduce the number of parameters.

Bayesian exploration of the posteriors

In this section we describe different ways to explore the posterior densities corresponding to the priors introduced in Section "Bayesian models for the muscle dynamics". In the computed examples, since the number *n* of muscles exceeds the number *m* of degrees of freedom, the matrices $\mathrm{A}^l \in \mathbb{R}^{m\times n}$ have a non-trivial null space, hence the posterior density for the box prior does not have a unique maximizer. Therefore, in the following discussion, MAP estimates are considered only for the minimum activation, minimum yank, and mixed priors.

MAP estimates by optimization

One popular way to summarize the posterior density is by means of the realization with "highest probability", i.e., the MAP estimate. We start by considering the posterior distribution corresponding to the minimum activation (MA) prior. Since in this case the time slices are mutually independent, it suffices to consider single time slices. In the following, to simplify the notation we omit the superscript referring to the time instance, and write $\mathrm{A} = \mathrm{A}^l, b = b^l$ and $q = q^l$ for $t = t_l$.

With these notations, the posterior density for a single time slice is

$$\pi_{q|b}(q|b) \propto x(q)\exp(-\tfrac{1}{2\sigma^2}\|b - \mathrm{A}q\|^2 - \tfrac{1}{2\omega^2}\|\mathrm{q}\|^2),$$

therefore the MAP estimate q_{MAP} is the solution of

$$\text{minimize} \qquad g(q) = \tfrac{1}{2\sigma^2}\|b - \mathrm{A}q\|^2 - \tfrac{1}{2\omega^2}\|\mathrm{q}\|^2 \quad \text{subject to } 0 \le q \le 1.$$

Since this is a quadratic minimization problem with bound constraints, the solution can be found using a projected Newton algorithm [207]. For completeness, we present an outline of how the algorithm proceeds.

We begin by computing the global unconstrained minimizer q^* of *g*. Since

$$g(q) = \tfrac{1}{2\sigma^2}\left\|\begin{bmatrix}\mathrm{A}\\ \alpha\mathrm{I}_n\end{bmatrix}q - \begin{bmatrix}b\\ 0\end{bmatrix}\right\|^2 = \tfrac{1}{2\sigma^2}(q^{\mathrm{T}}\mathrm{C}q - 2q^{\mathrm{T}}r + \|b\|^2), \qquad \alpha = \tfrac{\sigma}{\omega},$$

where

$$C = \mathrm{A}^{\mathrm{T}}\mathrm{A} + \alpha^2\mathrm{I}_n, \qquad r = \mathrm{A}^{\mathrm{T}}b,$$

it follows from the first order optimality condition that

$$q^* = \mathrm{C}^{-1}r.$$

In general, there is no guarantee that the q^* satisfies the bound constraints, therefore we use it as a starting point for an iterative process leading to a feasible solution. Let

$$q^{(1)} = \mathrm{P}q^*,$$

where P is the orthogonal projector onto the unit hypercube, so that

$$q_j^{(1)} = \max\{\min\{q_j^*, 1\}, 0\},$$

and we identify the set of indices $I_{act} \subset \{1, \dots, n\}$ corresponding to the components on which the constraints are active, that is, $I_{act} = \left\{j \middle| q_j^{(j)} \epsilon \{0,1\}\right\}$, and denote by I_{inact} the set of indices of the

components unaffected by the constraints. If $I_{act} \neq 0$, the global minimizer is inside the feasible set and the algorithm terminates, otherwise we continue as follows. To find the next iterate, we partition the vector q, fixing the components in the active set to the values determined by the projection onto the feasible set. After possibly rearranging the entries of q we have

$$q = \begin{bmatrix} q_1 \\ q_2 \end{bmatrix}, \qquad q_1 = q^{(1)}(I_{inact}), \qquad q_2 = q^{(1)}(I_{act}),$$

where the components of q_2 are known and fixed to the extremal values $\{0,1\}$. Next we partition the matrix C and the vector r according to the active/inactive partitioning of q, obtaining

$$\mathrm{C} = \begin{bmatrix} \mathrm{C}(I_{inact}, I_{inact}) & \mathrm{C}(I_{inact}, I_{act}) \\ \mathrm{C}(I_{act}, I_{inact}) & \mathrm{C}(I_{act}, I_{act}) \end{bmatrix} = \begin{bmatrix} \mathrm{C}_{11} & \mathrm{C}_{12} \\ \mathrm{C}_{21} & \mathrm{C}_{22} \end{bmatrix}, \qquad r = \begin{bmatrix} r(I_{inact}) \\ r(I_{act}) \end{bmatrix} = \begin{bmatrix} r_1 \\ r_2 \end{bmatrix},$$

and we write the objective function as

$$g(q) = g(q_1, q_2) = \frac{1}{2\sigma^2}\left(\left(q_1^{\mathrm{T}}\mathrm{C}_{11}q_1 - 2q_1^{\mathrm{T}}(r_1 - \mathrm{C}_{12}q_2)\right) + \text{terms independent of } q_1\right).$$

We remark that since q_2 is constant, the minimizer q_1^* of $g(q_1, q_2)$ with respect to the free variables q_1 is given by

$$q_1^* = \mathrm{C}_{11}^{-1}(r_1 - \mathrm{C}_{12}q_2).$$

As in the previous step, we project q_1^* onto the feasible set to guarantee that the constraints are satisfied, obtaining thus the next iterate,

$$q^{(2)} = \mathrm{P}\begin{bmatrix} q_1^* \\ q_2 \end{bmatrix}.$$

The process continues until no new active components are found. The process is guaranteed to converge in at most n steps, although usually it terminates much sooner.

The projected Newton algorithm can be used also to find the MAP estimate for the minimum yank (MY) prior and the mixed prior (MX). In the case of the MY prior, we can write the posterior density as

$$\pi_{q|b}(\mathbf{q}|\mathbf{b}) \propto \pi_q^{MY}(\mathbf{q})\pi_{b|q}(\mathbf{b}|\mathbf{q}) \qquad (14)$$

$$\propto \pi_q^{box}(\mathbf{q})\exp\left(-\frac{1}{2\gamma^2}\|(\mathrm{L} \otimes \mathrm{F}^*)\mathbf{q}\|^2 - \frac{1}{2\sigma^2}\|\mathbf{b} - \mathcal{A}\mathbf{q}\|^2\right),$$

Where $\mathcal{A}$ is the block diagonal matrix (7). Recall that in this case the MAP estimate is a vector $\mathbf{q}^* = \mathrm{vec}(\mathrm{Q}^*)$, with each row of $\mathrm{Q}^* \in \mathbb{R}^{n\times(N+1)}$ defining a paths for each muscle, minimizing

$$\text{minimize } G(\mathbf{q}) = \frac{1}{2\sigma^2}\|\mathbf{b} - \mathcal{A}\mathbf{q}\|^2 + \frac{1}{2\gamma^2}\|(\mathrm{L} \otimes \mathrm{F}^*)\mathbf{q}\|^2 \qquad \text{subject to } 0 \leq \mathbf{q} \leq 1.$$

The minimizer can be found with the same algorithm used to find the MAP with the MA prior. The fact that the matrix $\mathrm{L} \otimes \mathrm{F}^*$ has a non-trivial null space may cause technical difficulties. We overcome this shortcoming by assigning boundary conditions at $t = t_0$ and/or at $t = t_N$. Possible choices of boundary conditions will be considered in the next section, where the MCMC sampling from the posterior density is discussed. The same strategy can be adapted for the case of the mixed prior.

MCMC sampling: independent time slices

We begin by discussing the Gibbs sampler algorithm for the posterior density corresponding to the minimum action prior with the box constraint condition. Because of the mutual independence of the time slices, we limit the discussion to a single time slice, omitting the superscript indicating the time instance. The sampling algorithm was inspired by the engine behind the software Metabolica, designed for analyzing steady state reaction and transport fluxes in complex metabolic networks [208], [209], and later employed to investigate the muscle recruitment problem [141], [194].

After computing the singular value decomposition (SVD) of the lever arm matrix A,

$$\mathrm{A} = \mathrm{UDV}^{\mathrm{T}},$$

and substituting it in the term describing the equilibrium condition, we obtain

$$\|b - \mathrm{A}q\|^2 = \|\mathrm{U}(\mathrm{U}^{\mathrm{T}}b - \mathrm{DV}^{\mathrm{T}}q\|^2 = \|b' - \mathrm{D}\xi\|^2,$$

where

$$b' = \mathrm{U}^{\mathrm{T}}b, \qquad \xi = \mathrm{V}^{\mathrm{T}}q.$$

Let $r \leq n$ be the rank of the matrix A, and let d_j, $1 \leq j \leq r$ be its positive singular values. It follows from the orthogonality of the matrix V that

$$\frac{1}{2\sigma^2}\|b - \mathrm{A}q\|^2 + \frac{1}{2\omega^2}\|q\|^2 = \frac{1}{2\sigma^2}\sum_{j=1}^{r}(b_j' - d_j\xi_j)^2 + \frac{1}{2\omega^2}\sum_{j=1}^{n}\xi_j^2.$$

We draw from the posterior using the Gibbs sampler for updating ξ one component at a time. To update the *j*th component we proceed as follows. Denote by ξ_c the current value of ξ, and write

$$\xi(t) = \xi_c + te_j,$$

where e_j is the *j*th canonical Cartesian unit vector. The random variable $\xi(t)$ is distributed according to a one-dimensional Gaussian density with bound constraints. From $q(t) = \mathrm{V}\xi(t)$ it follows that

$$\exp\left(-\frac{1}{2\sigma^2}\|b - \mathrm{A}q\|^2 - \frac{1}{2\omega^2}\|\mathrm{q(t)}\|^2\right) \propto \exp\left(-\frac{1}{2\delta^2}\left(t - t_j\right)^2\right),$$

where

$$\delta_j^2 = \frac{\sigma^2\omega^2}{d_j\omega^2 + \sigma^2}, \qquad t_j = \frac{d_j\omega^2(b_j' - d_j\xi_{c,j})}{d_j\omega^2 + \sigma^2},$$

with the understanding that $d_j = 0$ if $j > r$.

To write the bound constraints confining $q(t)$ inside the unit hypercube in terms of *t*, we observe that *t* must be chosen so that the inequality

$$0 \leq q(t) = \mathrm{V}\xi(t) = \mathrm{V}\xi_c + tv^{(j)} \leq 1, \qquad v^{(j)} = \mathrm{V}e_j = j\text{th column of V},$$

holds component-wise, or equivalently,

$$\alpha \leq tv^{(j)} \leq \beta, \qquad \text{where } \alpha = -\mathrm{V}\xi_c, \qquad \beta = 1 - \mathrm{V}\xi_c.$$

Since $t = 0$ corresponds to the current value of ξ which satisfies the bounds, the set of feasible values of *t* is non-empty. To avoid numerical instabilities, we set the components of $v^{(j)}$ with an absolute value below a threshold $\tau > 0$ to zero, and write the bounds for the components of *t* as

$\frac{\alpha_k}{v_k^{(j)}} \le t \le \frac{\beta_k}{v_k^{(j)}}$ if $v_k^j > \tau$, $\frac{\beta_k}{v_k^{(j)}} \le t \le \frac{\alpha_k}{v_k^{(j)}}$ if $v_k^j < -\tau$.

Denoting the index sets where the above conditions hold by J_+ and J_-, respectively, depending on the sign of $v_k^{(j)}$, we conclude that

$$t_{min} = max\left\{\frac{\alpha(J_+)}{v^{(j)}(J_+)}, \frac{\beta(J_-)}{v^{(j)}(J_-)}\right\}, \qquad t_{max} = max\left\{\frac{\beta(J_+)}{v^{(j)}(J_+)}, \frac{\alpha(J_-)}{v^{(j)}(J_-)}\right\}. \tag{15}$$

Observe that if the Gaussian is centered at $t_j > t_{max}$ or $t_j < t_{min}$, the values of t must be drawn from the tail of the Gaussian. Unfortunately, most of the time the feasible interval is very far in the tail, and the standard error functions cannot be employed. In those cases one needs to resort to numerical quadratures to evaluate the cumulative distribution functions.

Formulas (15) need to be modified when using only the box prior. Formally, the corresponding equations are obtained by the limiting process of letting $\omega^2 \to \infty$. The bound constraints (15) do not change, but the expressions for the mean and variance simplify, giving

$$\delta_j^2 \to \frac{\sigma^2}{d_j}, \qquad t_j \to b_j' - d_j \xi_{c,j} \qquad \text{for } j \le r,$$

while for $r + 1 \le j \le n$, the parameter t is drawn from the uniform distribution over the interval $[t_{min}, t_{max}]$. We remark that the algorithm for sampling from the posterior with the box prior case is the same as the sampling scheme used in the articles [141], [194].

Sampling of paths and Feynman-Kac model

We turn now to sampling from the posterior densities corresponding to minimum yank and mixed priors, respectively. Unlike in the previous cases, the time slices are no longer mutually independent, thus the longitudinal nature of the priors need to be taken into account.

We consider first the posterior associated with the minimum yank prior (14). Monte Carlo sampling generates an ensemble of paths,

$\mathcal{S} = \{q^1, q^2, \dots, q^L\}$, L= sample size.

There is a formal similarity of this procedure with the Feynman–Kac path integral formalism of representing solutions of certain diffusion-type parabolic equations as expectations of integrals over paths [210]. In our case the expectation over paths yields the posterior mean estimate of the muscle activation problem with the yank prior. This connection between Monte Carlo sampling and the Feynman–Kac model has been pointed out, e.g., in [211]. It is because of this formal similarity that we refer to the path sampling as Feynman–Kac model.

Fixed boundary conditions

We are now ready to address the question how to generate samples from the posterior density (14). The modifications needed to make it suitable for the mixed prior are outlined at the end of this subsection. Consider first a case in which the boundary values at $t = t_0$ and $t = t_N$ are fixed, $q^0 = \bar{q}^0$ and $q^N = \bar{q}^N$. In this case, the time slices $q^1, q^2, \dots, q^{N-1}$are drawn from the density

$$\pi_{q^1,\dots,q^{N-1}|b,q^0,q^N}(q_1, \dots, q_{T-1} \mid b, \bar{q}^0, \bar{q}^N) \propto \pi_{q|b}(\bar{q}^0, q^1, q^2, \dots, q^{N-1}, \bar{q}^N \mid b),$$

that is, we consider the posterior density with q^0 and q^N fixed to the given boundary values.

To generate the sample, we consider a *block Gibbs sampler*, where the updating is done time slice by time slice: Given

$q^{k-1} = [\bar{q}^0; (q^1)^{k-1}; \cdots; (q^{N-1})^{k-1}; \bar{q}^N]$, we generate

$q^k = [\bar{q}^0; (q^1)^k; \cdots; (q^N)^k; \bar{q}^N]$ through the following process:

1. Draw $(q^1)^k$ from $\pi_1(q^1) =$;
   $\pi_{q|b}(\bar{q}^0,$
   $q^1,$
   $(q^2)^{k-1},$
   $(q^3)^{k-1},$
   $\cdots,$
   $(q^{N-1})^{k-1},$
   $\bar{q}^N|\mathbf{b})$

2. Draw $(q^2)^k$ from $\pi_2(q^2) =$;
   $\pi_{q|b}(\bar{q}^0,$
   $(q^1)^k, q^2,$
   $(q^3)^{k-1},$
   $\cdots,$
   $(q^{N-1})^{k-1},$
   $\bar{q}^N|\mathbf{b})$

   ⋮

N-1. Draw $(q^{N-1})^k$ from $\pi_{N-1}(q^{N-1}) =$;
   $\pi_{q|b}(\bar{q}^0,$
   $(q^1)^k,$
   $(q^2)^k, \cdots,$
   $(q^{N-2})^k,$
   $(q^{N-1}),$
   $q^N|\mathbf{b})$

Formally, the task is similar to generating sample paths for the diffusion model corresponding to a *Brownian bridge* [212], a Brownian motion in which the initial and final values are pinned down. The path generation is complicated by the need for the forces to satisfy the box constraints and the equilibrium conditions. Before discussing these details, consider the term corresponding to the yank term in the posterior density for a single activation vector q^l, $0 < l < N$, assuming that all other activation vectors are given. We have

$$\|(\mathrm{L} \otimes \mathrm{F}^*)\mathbf{q}\|^2 = \|\mathrm{F}^*(q^l - q^{l-1})\|^2 + \|\mathrm{F}^*(q^{l+1} - q^l)\|^2 + \text{terms independent of } q^l$$

$$= 2\|\mathrm{F}^* q^l\|^2 - 2(\mathrm{F} * q^l)^{\mathrm{T}}\mathrm{F}^*(q^{l-1} + q^{l+1}) + \text{terms independent of } q^l$$

$$= 2\|\mathrm{F}^*(q^l - \tfrac{1}{2}(q^{l-1} + q^{l+1}))\|^2 + \text{terms independent of } q^l.$$

Therefore, ignoring the bound constraints and the equilibrium conditions, the updating of q^l conditional on the rest of the activation vectors corresponds to drawing from a second order smoothness prior weighted by the matrix

F^* [199]https://www.sciencedirect.com/science/article/pii/S0960077924006349, the extra conditions making the process slightly more complicated.

The observations above imply that the *l*th update requires drawing from the density

$$\pi_l(q^l) \propto$$

$$\mathcal{X}(q^l)\exp\left(-\frac{1}{2\sigma^2}\|b^l - \mathrm{A}^l q^l\|^2\right) \times \exp\left(-\frac{1}{\gamma^2}\|\mathrm{F}^*[q^l - \frac{1}{2}((q^{l-1})^k + (q^{l+1})^{k-1})]\|^2 \right. \quad (16)$$

with $\mathcal{X}(q^l)\exp\left(-\frac{1}{2\sigma^2}\|b^l - \mathrm{A}^l q^l\|^2\right) = \pi_l^0(q^l)$

$$= \pi_l^0(q_l)\exp\left(-\frac{1}{\gamma^2}\|\mathrm{F}^*[q^l - \frac{1}{2}((q^{l-1})^k + (q^{l+1})^{k-1})]\|^2, \quad 1 \le l \le N-1,\right.$$

With $(q^0)^k = \bar{q}_0$ and $(q^N)^{k-1} = \bar{q}^N$.

The block Gibbs sampling algorithm outlined above requires thus the updating of each q^l, keeping the other activation vectors fixed. This can be done as for the updating of the independent time slices, giving rise to the following nested *Gibbs-within-Gibbs algorithm*.
Consider the density (16). Denoting

$$\mathrm{F}^l = \mathrm{F}^* q^l,$$

and setting $\lambda = \gamma/2$, it follows that

$$\frac{1}{2\sigma^2}\|b^l - \mathrm{A}^l q^l\|^2 + \frac{1}{2\lambda^2}\|\mathrm{F}^*[q^l - \frac{1}{2}(q^{l-1})^k + (q^{l+1})^{k-1}]\|^2$$

$$= \frac{1}{2\sigma^2}\|b^l - \mathrm{A}^l(\mathrm{F}^*)^{-1}\mathrm{F}^l\|^2 + \frac{1}{2\lambda^2}\|\mathrm{F}^l - \frac{1}{2}[(\mathrm{F}^{l-1})^k + (\mathrm{F}^{l+1})^{k-1}]\|^2.$$

Because the update is computed for one individual time slice at a time, we proceed as in the updating process of independent time slices, using the singular value decomposition of the corresponding equilibrium matrix, scaled by the tetanic forces. Letting

$$\mathrm{A}^l(\mathrm{F}^*)^{-1} = \mathrm{UDV}^{\mathrm{T}}$$

be the SVD of $\mathrm{A}^l(\mathrm{F}^*)^{-1}$, and observing that the matrices U, D and V have a different meaning than before, we write the quadratic expression as

$$\frac{1}{2\sigma^2}\|b^l - \mathrm{A}^l(\mathrm{F}^*)^{-1}\mathrm{F}^l\|^2 + \frac{1}{2\lambda^2}\left\|\mathrm{F}^l - \frac{1}{2}[(\mathrm{F}^{l-1})^k + (\mathrm{F}^{l+1})^{k-1}]\right\|^2$$

$$= \frac{1}{2\sigma^2}\|b' - \mathrm{DV}^{\mathrm{T}}\mathrm{F}^l\|^2 + \frac{1}{2\lambda^2}\|\mathrm{VV}^{\mathrm{T}}\{\mathrm{F}^l - \frac{1}{2}[(\mathrm{F}^{l-1})^k + (\mathrm{F}^{l+1})^{k-1}]\}\|^2,$$

Where $b' = \mathrm{U}^{\mathrm{T}}b^l$. Further, letting $\xi = \mathrm{V}^{\mathrm{T}}\mathrm{F}^l$, we arrive at the expression

$$\frac{1}{2\sigma^2}\|b' - \mathrm{D}\xi\|^2 + \frac{1}{2\lambda^2}\|\xi - c\|^2,$$

where

$$c = \frac{1}{2}\mathrm{V}^{\mathrm{T}}[(\mathrm{F}^{l-1})^k + (\mathrm{F}^{l+1})^{k-1}]. \quad (17)$$

In this manner we have reduced the problem of updating q^l to the problem of drawing the vector ξ from the distribution proportional to

$$\exp\left(-\frac{1}{2\sigma^2}\|b' - \mathrm{D}\xi\|^2 - \frac{1}{2\lambda^2}\|\xi - c\|^2\right) + \text{ bounds},$$

and the process continues component-wise along the lines of the previous subsection.

Sampling the path for the mixed prior is very similar, requiring only the few modifications indicated below. Starting from the formula corresponding to (16),

$$\pi_l(q^l) \propto \mathcal{X}(q_l)\exp\left(-\frac{1}{2\sigma^2}\|b^l - \mathrm{A}^l q^l\|^2 - \frac{\vartheta}{2\omega^2}\|q^l\|^2 - \frac{1-\vartheta}{\gamma^2}\left\|\mathrm{F}^*\left[q^l - \frac{1}{2}((q^{l-1})^k + (q^{l+1})^{k-1})\right]\right\|^2\right),$$

we combine the first two terms in the exponential to obtain

$$\frac{1}{2\sigma^2}\|b^l - \mathrm{A}^l q^l\|^2 + \frac{\vartheta}{2\omega^2}\|q^l\|^2$$

$$= \frac{1}{2\sigma^2}\left\|\begin{bmatrix} b^l \\ 0 \end{bmatrix} - \begin{bmatrix} A^l \\ \mu\mathrm{I} \end{bmatrix} q^l\right\|^2$$

$$= \frac{1}{2\sigma^2}\left\|\begin{bmatrix} b^l \\ 0 \end{bmatrix} - \begin{bmatrix} \mathrm{A}^l \\ \mu\mathrm{I} \end{bmatrix} (\mathrm{F}^*)^{-1}\mathrm{F}^l\right\|^2, \qquad \mu = \frac{\sqrt{\vartheta}\sigma}{\omega}.$$

As previously, we compute the SVD,

$$\begin{bmatrix} \mathrm{A}^l \\ \mu\mathrm{I} \end{bmatrix} (\mathrm{F}^*)^{-1} = \mathrm{UDV}^{\mathrm{T}},$$

where, again, the matrices U, D, and V differ from the earlier definitions, and define

$$b' = U^T \begin{bmatrix} b^l \\ 0 \end{bmatrix}, \quad \xi = \mathrm{V}^{\mathrm{T}} q^l,$$

so that the sampling algorithm becomes formally identical to the one presented before.

Above, it was assumed that the initial and final boundary values were given and fixed. Technically, we could fix only one of the two boundary values and treat the other value as a random variable. In general, assuming one or both boundary values known may have a biasing effect on the paths samples. In the rest of this section, we consider some computationally feasible ways to deal with the restriction. In particular, two physiologically meaningful alternatives are proposed.

Periodic boundary conditions

Periodic boundary conditions are a meaningful alternative when the dynamics represents a repetitive task, such as level walking: In the last time frame after a completed cycle of steps, the musculoskeletal system is approximately in the same equilibrium position as in the beginning of the cycle, and we may identify q^0 and q^N as random variables. Therefore, after initializing the chain by using an initial state $q_0^1 = \bar{q}_0$, we use the block Gibbs sampler, using in (16) for $l = N$ and $l = 0$ formally

$$(q^{N+1})^{k-1} = (q^2)^k, \quad (q^{-1})^k = (q^{N-1})^{k-1}.$$

This sampler is similar to a *Brownian ring* of periodic random walks. To avoid ambiguities, the identification of the distributions of q^0 and q^N require that in the initial and final equilibrium conditions, the replacements

$$\mathrm{A}^0, \mathrm{A}^N \leftarrow \frac{1}{2}(\mathrm{A}^0 + \mathrm{A}^N), \qquad b^0, b^N \leftarrow \frac{1}{2}(b^0 + b^N)$$

are performed before the sampling.

Freeing the fixed boundary values

Another possibility to free the fixed boundary conditions is to postulate prior distributions for the end values, and write

$$\pi_{q|b}(q^0, q^1, \dots, q^{N-1}, q^N \mid \mathbf{b}) = \pi_{q^2,\dots,q^{N-1}|q^1,q^N,\mathbf{b}}(q^1, \dots, q^{N-1} \mid q^0, q^N, \mathbf{b})\pi_{q^0}(q^0)\pi_{q^N}(q^N),$$

where (q^0) and $\pi_{q^N}(q^N)$represent the initial and final distributions.

In practice, we draw the new independent initial and final values from their respective distributions before each block Gibbs updating round. While this extension removes the necessity to specify exactly the boundary values, an initial distribution needs to be entered, which may also bias the outcomes.

Augmenting the likelihood

The main focus of the discussion above was on prior models, while the likelihood was restricted to contain information about the equilibrium condition only. Sometimes, however, we may have additional observations available, such as EMG-recordings of a given set of muscles. While the EMG data do not translate directly to muscle activation (see [54] for a discussion), they carry indirect information that should be taken into consideration in the analysis [213]. Consider, for simplicity, EMG data collected from one single muscle. The most straightforward model is to assume a strictly increasing dependency between the rectified and low-pass filtered EMG recording $\mu(t)$of the *j*th muscle and the activation level of the muscle,

$$q_j(t) = g_j(\mu(t)) + \text{error},$$

where g_j is an appropriately chosen increasing function like a sigmoid, and the "error" refers to a modeling error. A computationally feasible approach is to use the activation model above to define a likelihood interval, requiring that $q_j(t)$satisfies

$$q_{min}(t) = \max\{g(\mu(t)) - \Delta, 0\} \le q_j(t) \le \min\{g(\mu(t)) + \Delta, 1\} = q_{max}(t),$$

where $\Delta > 0$ is the presumed model accuracy. This model translates into the likelihood model by multiplying the likelihood density (11) by the indicator functions of the intervals $[q_{min}(t_l), q_{max}(t_l)]$,

$$\pi_{\mathbf{b}|\mathbf{q}}(\mathbf{b} \mid \mathbf{q}) \propto \exp\left(-\frac{1}{2\sigma^2}\|\mathbf{b} - \mathcal{A}\mathbf{q}\|^2\right) \prod_{l=0}^{N} \chi_{[q_{min}(t_l), q_{max}(t_l)]}(q_j^l).$$

This modification can be effectuated by simply replacing the lower and upper bounds of q_j^l in the box prior (12) by the new bounds, thus the modification of the Gibbs sampler algorithm becomes straightforward.

Computed examples

In this section, we demonstrate the effect of different priors and selections of boundary conditions and parameters.

The generic musculoskeletal model Gait2392 [55] was employed in this study to simulate level ground walking. The model, illustrated in Figure 4, was scaled to closely approximate the

anthropometry of a 86 year old man with an instrumented knee prosthesis, and includes 2 lower limbs and the torso, comprising of total of 12 bodies from the torso down to the toes, 92 actuators representing the muscles, 46 for each leg, and 17 degrees of freedom: 3 at the hip, one at the knee, ankle, subtalar joint, and metatarsophalangeal joint for each leg, and 3 between the pelvis and the torso. The experimental data are part of the fifth dataset of the Knee Grand Challenge [214]. The biomechanical variables were estimated using OpenSim, an open-source platform to perform biomechanical analyses of musculoskeletal dynamics [197]. Joint angles and joint torques were computed by implementing and solving the inverse problem, as described in "Muscle activation problem" chapter. The muscle moment arms defining the moment matrices A^l were obtained through the Analyze Tool of OpenSim once the joint angles were known.

As a starting point, we assume that the inverse dynamic problem is thus completely solved, and the lever arm matrices and the corresponding torque vectors $\{\mathrm{A}^l, b^l\}_{l=0}^{L}$, where $\mathrm{A}^l \in \mathbb{R}^{m\times n}, b^l \in \mathbb{R}^m$, are resolved with accuracy that allows us to use an equilibrium model (4) with noise modeled as

$$\varepsilon^l \sim \mathcal{N}(0, \sigma_l^2 \mathrm{I}_m).$$

In our data set, the number of equilibrium equations is $m = 17$, while the number of muscles included in the model is $n = 92$. The time interval of the full stride is divided in $L = 130$ intervals. Observe that the vectors b^l represent generalized forces, and in order to scale the standard deviation properly, we write

$$\sigma_l = \bar{b}_l \sigma_0, \qquad \bar{b}_l = \frac{1}{m}\|b^l\|,$$

and set $\sigma_0 = 0.001$.

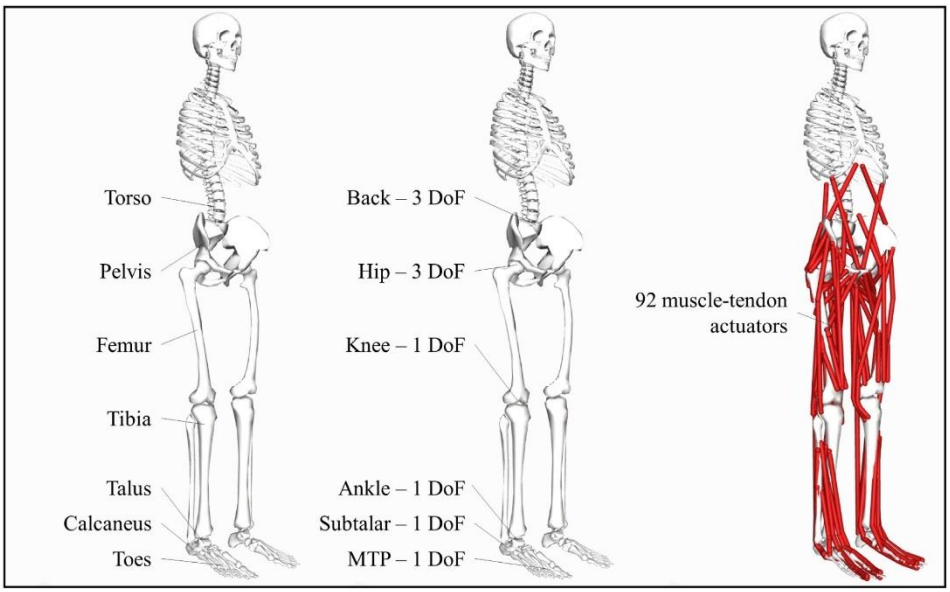

Figure 4. OpenSim model employed in current simulations. The model consists of 12 bodies divided into two lower limbs and a torso as indicated in the figure, 17 degrees of freedom and 92 muscle-tendon actuators, 46 for each leg.

We start the simulations by running the MCMC sampler using the box prior, i.e., including only the physiological bound constraints to muscle activations, and subsequently we compute samplers for three more informative priors, minimum activation (MA), minimum yank (MY) and mixed (MX) priors. In all simulations, the sample size is set at $N = 100k$, while the prior and likelihood variance parameters are set as indicated in Table 2. The results are summarized in figures that show quantile plots as described in detail below. The plots are limited to only eight muscles, four large ones (*Gluteus*

Medius Anterioris L, *Medial Gastrocnemius L*, *Soleus L*, and *Tibial Anterioris L*) and four smaller muscles (*Sartorius L*, *Gracilis L*, *Flexor Digitorum L*, and *Extensor Digitorum L*). The locations of the muscles are shown in Figure 5.

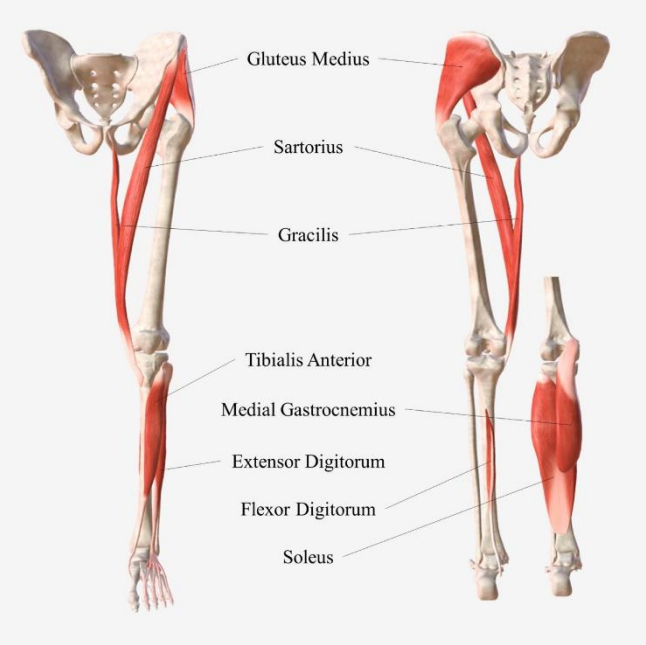

Figure 5. The eight selected muscles of the left leg whose activation patterns are shown in this study. Anterior (left) and posterior (right) view.

Table 2. The values of the parameters used in the simulations. In all simulations, the sample size is N = 100000.

Prior	σ_0	ω	γ_0	θ
Box	0.001			
Min. activation	0.001	0.1		
Min. yank	0.001		0.01	
Mixed	0.001	0.1	0.01	0.5

Figure 6 shows a superposition of the results corresponding to the MA box prior. In the figure, the interval between the minimum and maximum sample value at each time slice of the box prior is indicated by a thin red bar, while the interval of the 75% quantile is plotted with a thick red bar. On top of that, we have plotted the envelopes containing 75% (darker shade) and 100% (lighter shade) of the sample points corresponding to the MA prior sampling. Finally, the median of the MA sample is indicated by a blue curve, and the MAP estimate computed by the optimization algorithm is plotted in red. Using the same color coding, the results corresponding to the smaller muscles are shown in Figure 7.

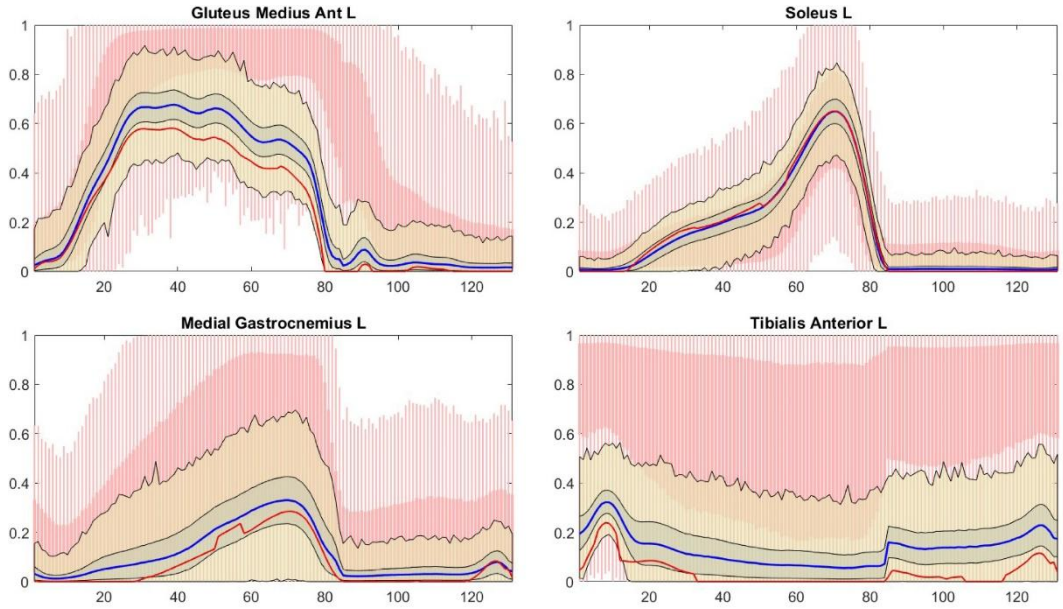

Figure 6. Sampling results corresponding to the MA prior. The thick red bars correspond to the 75% quantile of samples computed with the box prior, while the thin red bars indicate the full range of the samples. Similarly, the dark and light beige envelopes correspond to the 75% quantile and the full range, respectively, of the sample based on the MA prior. The red curve is the computed minimum activation MAP estimate, and the blue curve is the median over the MA sample. The sampling time step in all figures is Δt=0.00833s, the total time interval being therefore about 1.1s. (For interpretation of the references to color in this figure legend, the reader is referred to the web version of this article).

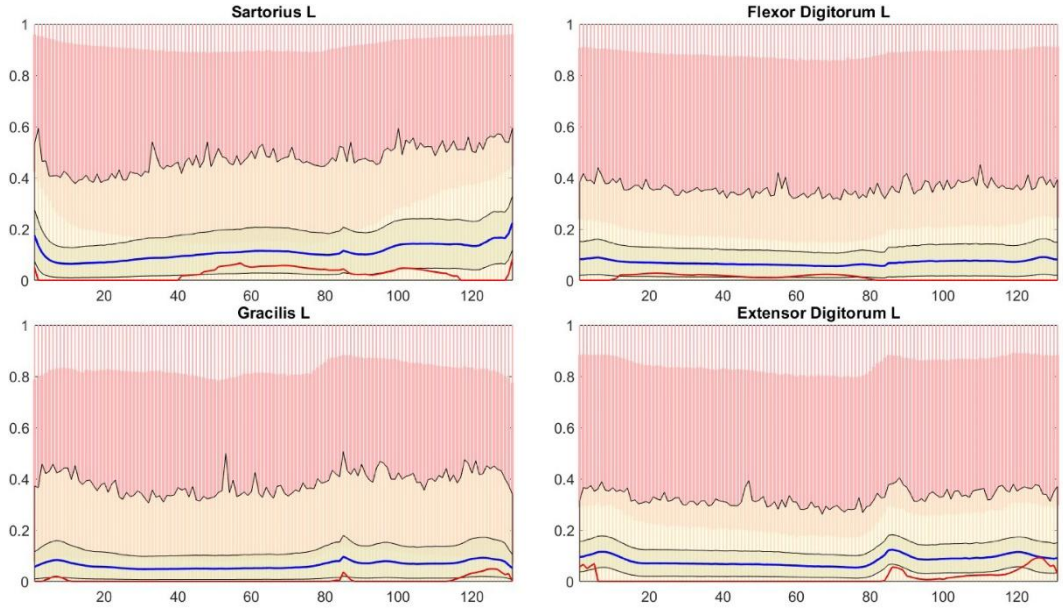

Figure 7. The sampling results corresponding to Figure 6 for the selected smaller muscles. The color coding is as in the previous figure.

The results indicate that as expected, the MA prior drives the sample envelope, and the MAP estimate in particular, to the low end of the box prior feasible intervals. In particular, the samples of the smaller muscles seem to reflect very weakly the performed task of level walking, showing an almost flat response.

We then run the sampler using the minimum yank prior. The standard deviation γ is given in the units of forces (N), the implicit dependency of the length of the time step being suppressed, and in order to have dimensionless parameters, we scale γ by the average of the tetanic forces, writing.

$\gamma = \frac{1}{n}\sum_{j=1}^{n} F_j^* \gamma_0$.

To set the value γ_0, literature about the rate of force development (RFD, [N/s]) or rate of torque development (RTD, [Nm/s]) was consulted [215], [216], [217], [218], [219]. The RFD and RTD parameters represent the ability of a muscle to rapidly develop external force. Based on the experimentally measured values, we defined a plausible range for the yank. Subsequently, to obtain a plausible value for γ, the value range of the yank, originally estimated for one second, was scaled to the time step of the example data, corresponding to $\Delta t = 0.00833\ s$. The value of γ_0 used in the simulations is given in Table 2.

In the first simulation, the initial and final activations patterns, q^0 and q^N, are fixed to be equal to the median values of the corresponding activations of the box prior sample. Figure 8, Figure9 show the envelopes containing 75% of the sampled values as well as the full intervals of the values. For comparison, the envelopes are superimposed on the intervals containing the full intervals of the sampled values using the box prior and the minimum activation priors, respectively, giving an idea of how much the minimum yank prior restricts and translates the values.

To investigate the effect of the fixed boundary conditions on the envelopes, for comparison we run the sampler using the periodic boundary conditions. The results are shown in Figure 10 for the selected larger muscles and in Figure 11 for the smaller ones. The results with the smaller muscles, in particular, indicate that the periodic boundary condition may be overly lax, leaving a large uncertainty in the muscle paths.

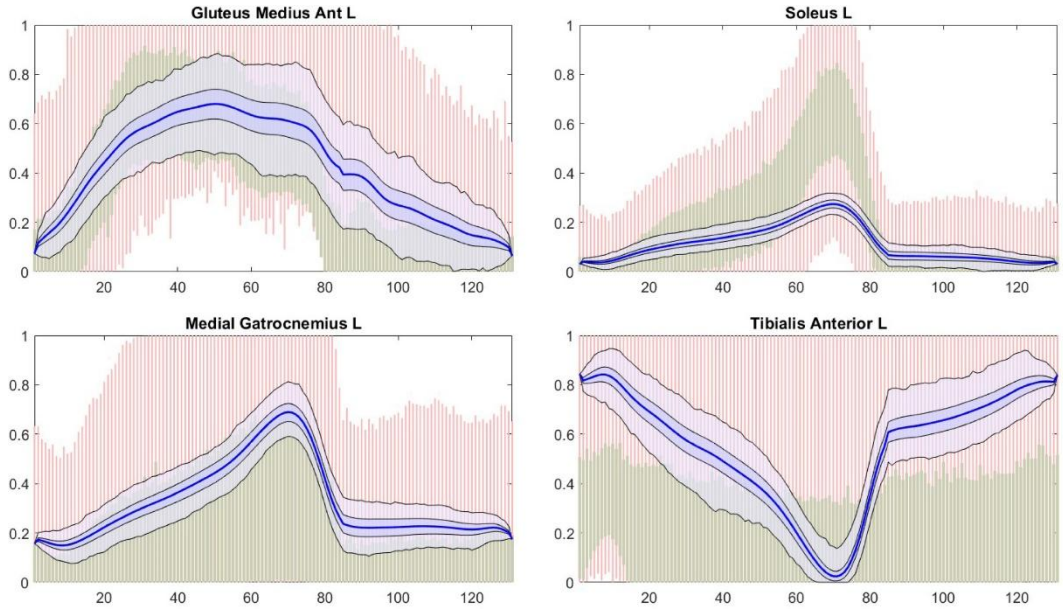

Figure 8. Sampling results corresponding to the minimum yank prior with fixed boundary conditions, the boundary values being fixed at the median value of the sample drawn with the box prior. The red bars indicate the full range of the sample using the box prior, and the green bars correspond to the full range corresponding to the minimum activation prior. The dark and light blue envelopes correspond to the 75% quantile and the full range of the paths drawn with the MY prior, respectively. The blue curve is the median over the MY sample. (For interpretation of the references to color in this figure legend, the reader is referred to the web version of this article.)

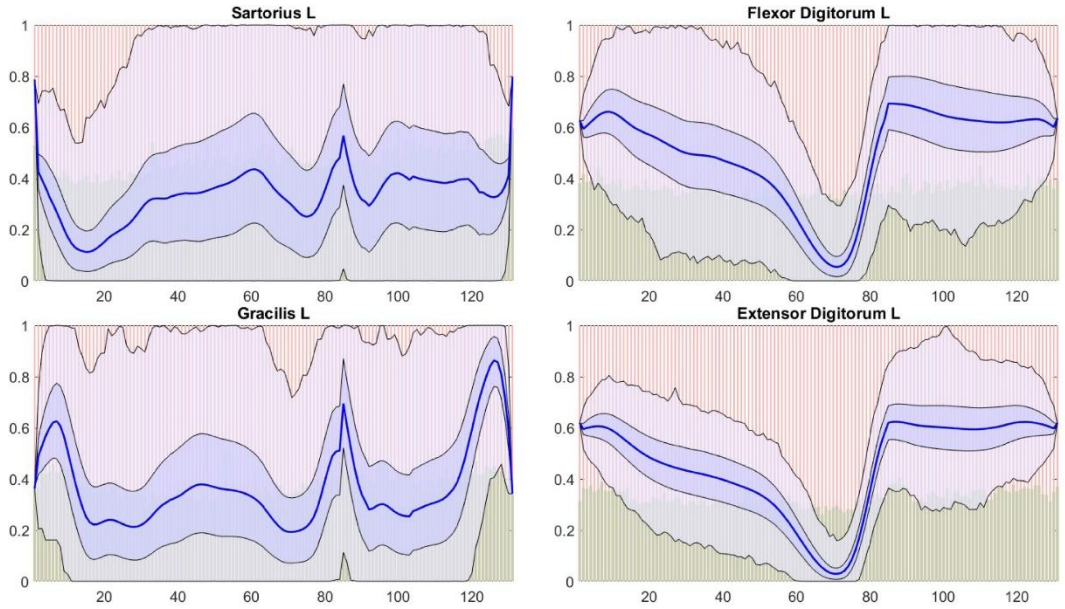

Figure 9. The figure corresponding to Figure 8 for the selected smaller muscles. The color coding is as in the previous figure.

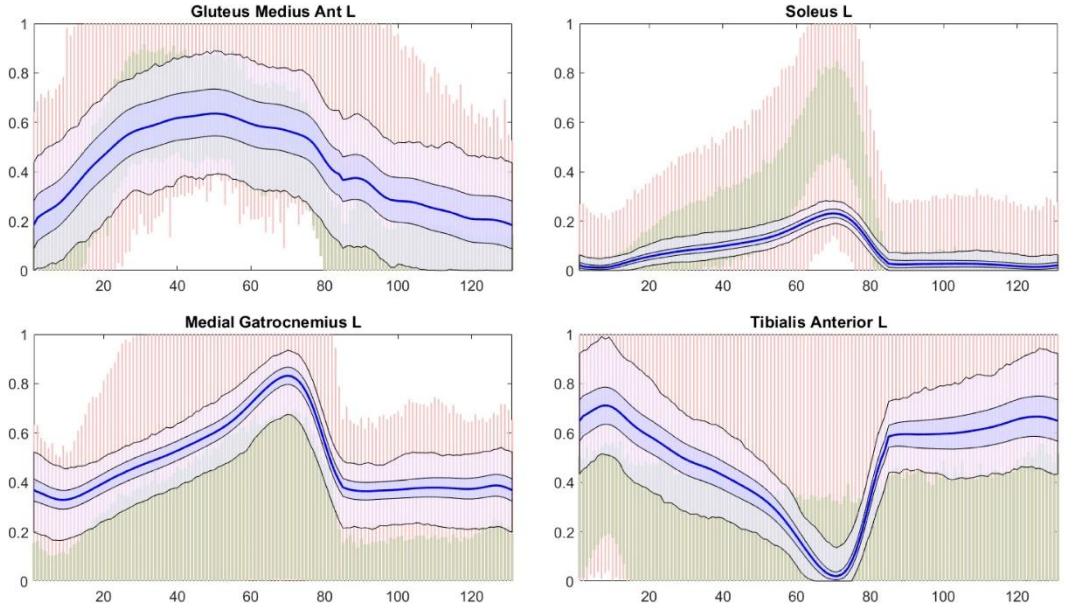

Figure 10.Sampling results corresponding to the minimum yank prior with periodic boundary conditions. The red bars indicate the full range of the sample using the box prior, and the green bars correspond to the full range corresponding to the minimum activation prior. The dark and light blue envelopes correspond to the 75% quantile and the full range of the paths drawn with the MY prior, respectively. The blue curve is the median over the MY sample. (For interpretation of the references to color in this figure legend, the reader is referred to the web version of this article.)

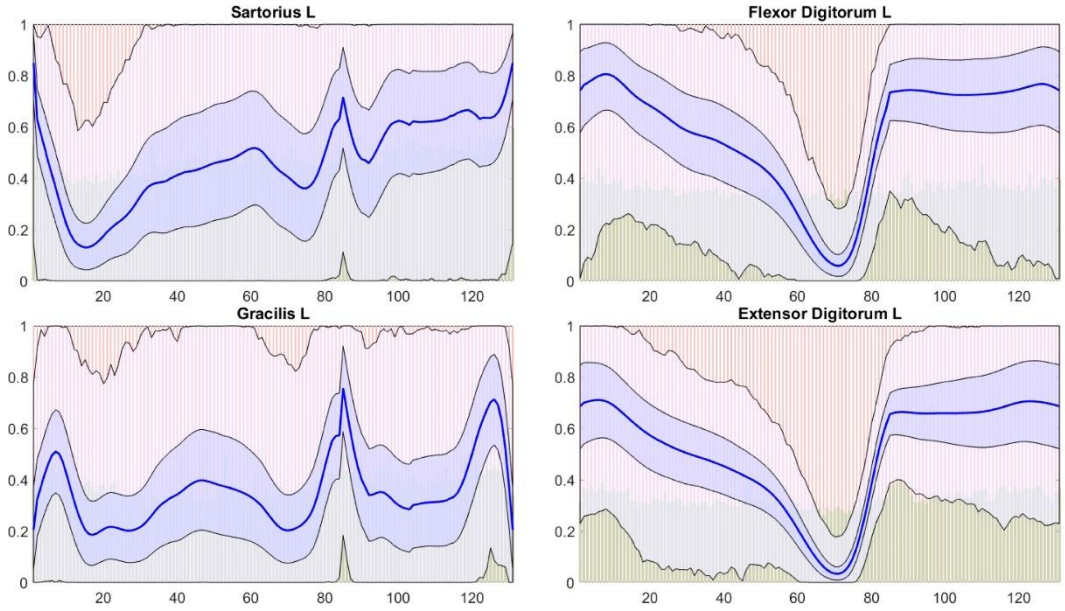

Figure 11. The figure corresponding to Figure 10 for the selected smaller muscles. The color coding is as in the previous figure.

Finally, we generate the samples using the mixed prior, setting the value of the interpolation parameter to $\vartheta = {}^{1}/_{2}$. Figure 12, Figure 13 show the envelopes corresponding to the fixed boundary conditions. Here, the initial and final values were set to be equal to the median values of q^0 and q^N over the sample corresponding to the minimum activation prior. Again, the envelopes of 75% quantile and full range are plotted against the full range of the box prior (red bars) and the minimum activation prior (green bars). For comparison, the corresponding plots using the periodic boundary condition are shown in Figure 14, Figure 15, respectively.

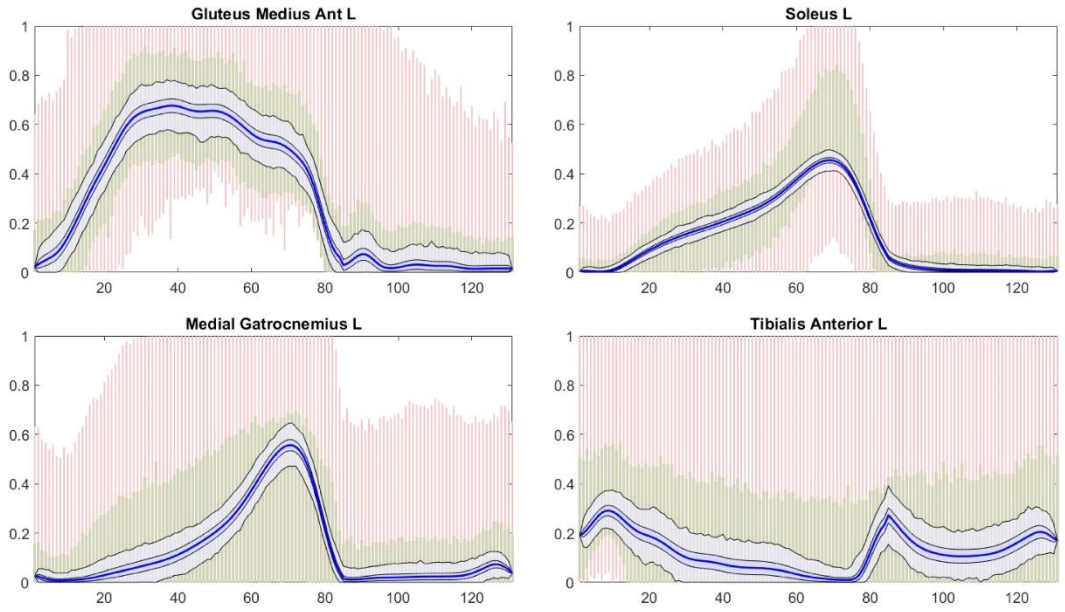

Figure 12. Sampling results corresponding to the mixed prior with fixed boundary conditions, the boundary value as before fixed at the median value over the minimum activation prior sample. The red bars indicate the full range of the sample using the box prior, and the green bars correspond to the full range corresponding to the minimum activation prior. The dark and light blue envelopes correspond to the 75% quantile and the full range of the paths drawn with the MX prior, respectively. The blue curve is the median over the MX sample. (For interpretation of the references to color in this figure legend, the reader is referred to the web version of this article.)

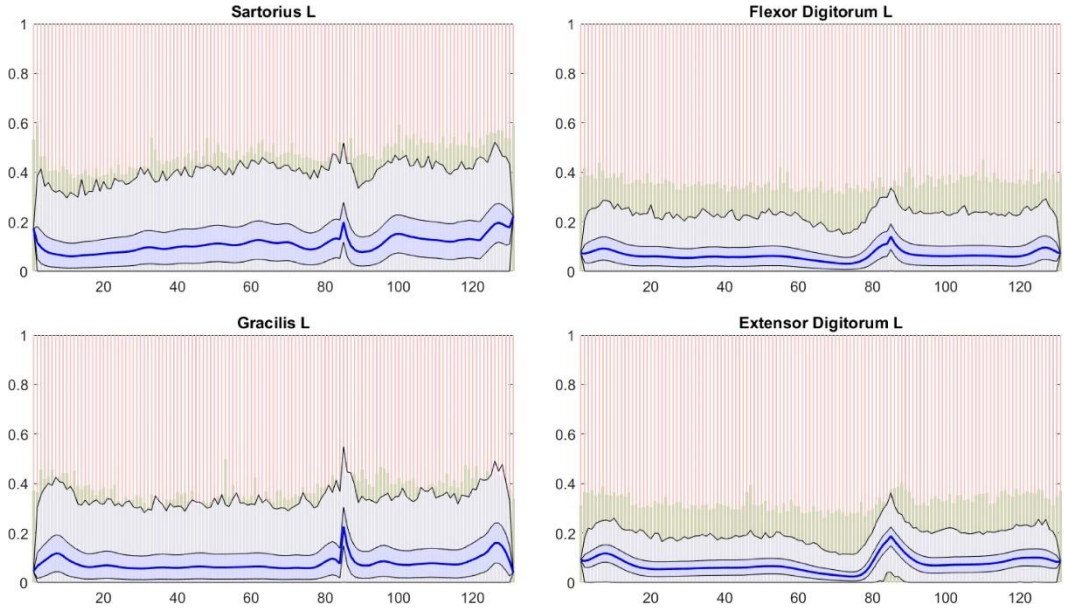

Figure 13. The figure corresponding to Figure 12 for the selected smaller muscles. The color coding is as in the previous figure.

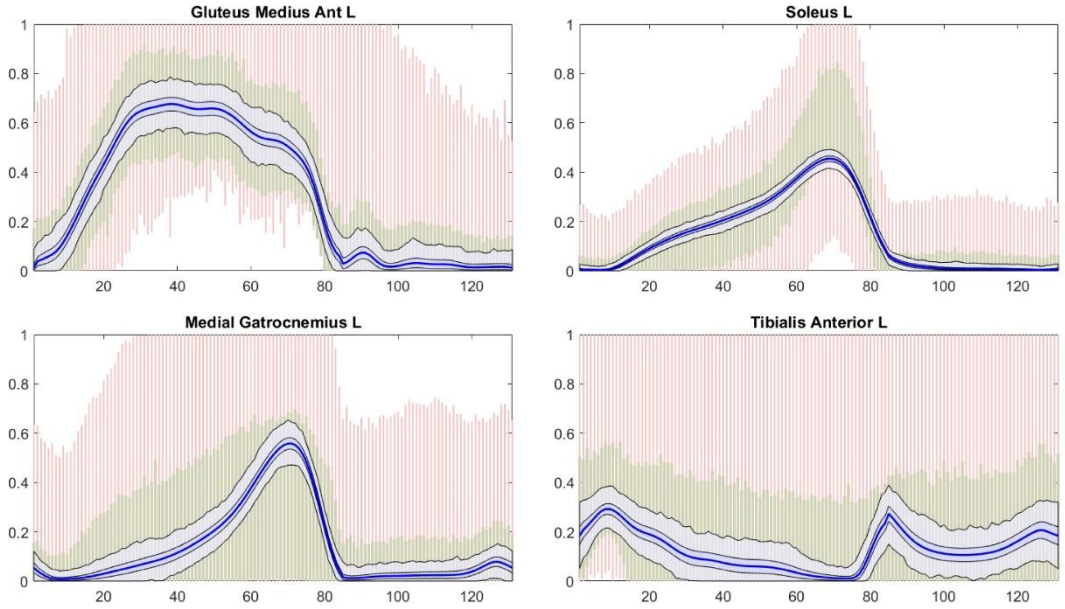

Figure 14. Sampling results corresponding to the mixed prior with periodic boundary conditions. The red bars indicate the full range of the sample using the box prior, and the green bars correspond to the full range corresponding to the minimum activation prior. The dark and light blue envelopes correspond to the 75% quantile and the full range of the paths drawn with the MX prior, respectively. The blue curve is the median over the MX sample. (For interpretation of the references to color in this figure legend, the reader is referred to the web version of this article.)

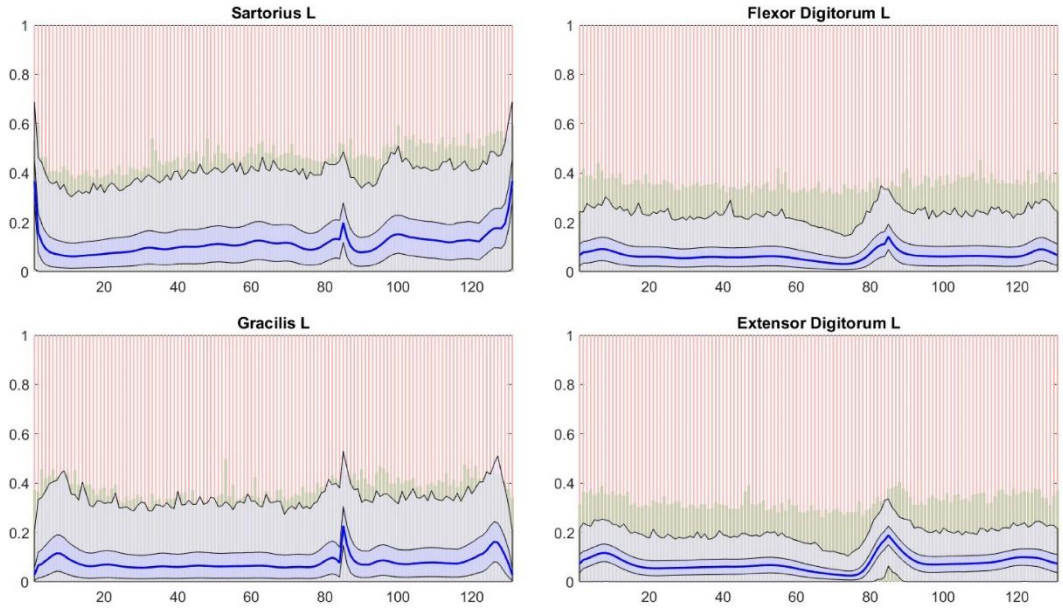

Figure 15. The figure corresponding to Figure 14 for the selected smaller muscles. The color coding is as in the previous figure.

Discussion

The Bayesian framework provides a rich environment of investigating the muscle recruitment problem by sampling the probability distributions representing possible activation configurations that respect the equilibrium conditions up to a prescribed accuracy. The previous works [141], [194] were limited to consider equilibrium solutions with the minimum prior assumption that the natural bound constraints were satisfied with no other preferential properties given. Here, the formalism is extended to include further prior information. Unlike the minimum activation prior that still assumes the different time slices to be independent, the minimum yank and mixed priors introduce longitudinal prior structure, tying together the time slice realizations through a smoothness prior of first order. While the minimum activation prior can be justified, e.g., through energetic considerations, the longitudinal prior structure is meaningful as the musculoskeletal system under normal conditions and outside the regime of extreme movements is likely to favor smooth paths without jerky activations that may even be harmful for the muscles. Considering the results, significant differences in the activation patterns can be seen both in the large and small muscles. For instance, comparing the activation pattern of the soleus muscle in Figure 6 on one hand and in Figure 8, Figure 10, we see that the minimum activation prior allows a significantly higher activation level than the minimum yank prior, regardless of the boundary condition, indicating that while the minimum activation prior aims overall to favor lower activation levels, in single muscles, the desired effect is achieved by restricting the yank. Conversely, comparing a smaller muscle such as extensor digitorum muscle in Figure 7 with those in Figure 9, Figure 11, the minimum yank prior leads to a higher activation level. In fact, the minimum activation prior seems to favor solutions that are close to zero, which, while possible from the point of view of the equilibrium, may not correspond to a typical activation during normal level walk, see, e.g., the supplementary EMG data in [125], and foot EMG data in [220]. These considerations promote models with longitudinal priors, however, further evidence to definitely justify the use of one prior over another is required. Future tests for model validation include a comparison of the joint contact forces predicted by the models based on the muscle forces to the in vivo recordings from the instrumented implants.

A standard deterministic approach to solve the muscle recruitment problem is to use optimization tools to find a single trajectory that minimizes or maximizes a given objective function. The Bayesian formulation described here can be used to produce such optimal solutions by maximizing the posterior density, or, equivalently, minimizing the corresponding Gibbs energy, defined as the negative logarithm of the posterior probability density. Formally, the Gibbs energy corresponds to a penalized least squares solution with bound constraints. In particular with the minimum yank prior, a caveat concerning the MAP estimate is in order. The MAP estimate is easy to find by using the projected Newton algorithm described in this paper. However, while the minimum yank prior favors smooth solutions with no sudden jerks, the hard boundary conditions may make the MAP estimate to be non-smooth: When the smooth solution meets the boundary, typically an abrupt flattening of the curve ensues, creating a sudden kink that does not respect the smoothness requirement. For this reason, the MAP estimate does not necessarily represent the typical paths. We point out that there is also a physiological reason to assume that the muscles anticipate the change in the activation state: Human walking is sometimes characterized as "controlled falling" [221], and the muscles secure the joints through co-contractions before the reactive forces activate. The sampled solutions with the MY and MX priors do qualitatively demonstrate this behavior. The fact that the MAP estimate may not be a good representative of the density is nothing new in the Bayesian context, which is the reason why the computations of MAP estimates are sometimes not recommended in the literature.

Declaration of competing interest

The authors declare that they have no known competing financial interests or personal relationships that could have appeared to influence the work reported in this paper.

Acknowledgments

The work of MA and ES was partly supported by the National Science Foundation grant DMS 2204618, and DC by the National Science Foundation grant DMS 1951446

Author contribution

AB contribution to this research has been Conceptualisation, Methodology, Software, Writing – Review & Editing. In particular, the biomechanical data and the musculoskeletal model adopted as inputs in this research have been prepared by AB (also Figures 4 and 5 are part of the work done by AB). Subsequently, AB evaluated the plausibility of the predicted outputs.

Myobolica: a stochastic approach to estimate physiological muscle control variability

Alex Bersani[1], Mercy Amankwah[2], Daniela Calvetti[2], Erkki Somersalo[2], Marco Viceconti[1,3], Giorgio Davico[1]

[1] Department of Industrial Engineering, Alma Mater Studiorum, University of Bologna, Bologna, Italy

[2] Department of Mathematics, Applied Mathematics and Statistics, Case Western Reserve University, Cleveland, Ohio, USA

[3] Medical Technology Laboratory, Rizzoli Orthopaedic Institute, Bologna, Italy

Adapted from a publication in:

IEEE Transactions on Neural Systems and Rehabilitation Engineering

(2024)

https://doi.org/10.1109/TNSRE.2024.3447791

The authors wish to thank IEEE Transactions on Neural Systems and Rehabilitation Engineering for providing the permission to re-use the manuscript titled “Myobolica: a stochastic approach to estimate physiological muscle control variability” in the present PhD thesis

Abstract

The inherent redundancy of the musculoskeletal systems is traditionally solved by optimizing a cost function. This approach may not be correct to model non-adult or pathological populations likely to adopt a "non-optimal" motor control strategy. Over the years, various methods have been developed to address this limitation, such as the stochastic approach. A well-known implementation of this approach, Metabolica, samples a wide number of plausible solutions instead of searching for a single one, leveraging Bayesian statistics and Markov Chain Monte Carlo algorithm, yet allowing muscles to abruptly change their activation levels. To overcome this and other limitations, we developed a new implementation of the stochastic approach (Myobolica), adding constraints and parameters to ensure the identification of physiological solutions. The aim of this study was to evaluate Myobolica, and quantify the differences in terms of width of the solution band (muscle control variability) compared to Metabolica. To this end, both muscle forces and knee joint force solutions bands estimated by the two approaches were compared to one another, and against (i) the solution identified by static optimization and (ii) experimentally measured knee joint forces. The use of Myobolica led to a marked narrowing of the solution band compared to Metabolica. Furthermore, the Myobolica solutions well correlated with the experimental data (R^2 = 0.92, RMSE = 0.3 BW), but not as much with the optimal solution (R^2 = 0.82, RMSE = 0.63 BW). Additional analyses are required to confirm the findings and further improve this implementation.

Index Terms

Suboptimal control, Muscle recruitment, Stochastic approach, Markov Chain Monte Carlo, OpenSim.

Introduction

Reductionism in biomechanics favors the separation between biomechanics and neurology of human movement. The number of muscles that the central nervous system may choose to produce the same movement is considerably higher than the number of degrees of freedom of a human body (defined by the body's allowed movement); this discrepancy results in a redundancy situation for the muscular system [16], where the muscle activation patterns that may be selected to reach the same goal are essentially endless. Traditionally, the biomechanics community tended to reduce the complexity of neuromuscular control with the assumption that among all possible control strategies that satisfy the physical and physiological constraints, the central nervous system will choose one minimizing some cost functions representative of a physiological criterion (reductionist approach) [71]. With this assumption, musculoskeletal dynamics models can predict the muscle activation patterns given measured kinematics plus ground reactions using inverse dynamics and static optimization [95]. Several studies have confirmed that this is an acceptable approximation for healthy adults who perform sub-maximal stereotypical tasks such as level walking [65], [66]. Unfortunately, much biomechanics research focuses on pathological subjects whose neuromuscular control deviates more or less significantly from this assumption (sub-optimal control).

Several approaches have been proposed to overcome this limitation [195] such as electromyography(EMG)-based [113], [121], [222], [223] and feedback-based approaches [224]. A different approach was proposed in [141], where the problem of constrained control was formulated in terms of Bayesian statistics, and a Markov Chain Monte Carlo (MCMC) algorithm was used to sample the solution space of all muscle activation patterns that satisfy the dynamic equilibrium and the tetanic limits. Instead of searching for an optimal solution, we sampled all possible solutions using

a software implementation called *Metabolica*, originally developed for analyzing metabolic networks [208]. The advantage of this approach is that it does not rely on the EMG information and makes no assumption of synergies, thus considering also the least optimal muscle activation patterns. The Metabolica approach was successfully used in studies where the question was how sub-optimal control could increase joint loading [56], [64], [104], [194].

However, Metabolica assumes that each instant of the locomotion cycle is independent of the others; the solution space is built assuming instantaneous equilibrium without concern about whether a muscle was already activated or not in the previous instant. However, this is not physiologically correct: a muscle cannot abruptly change its activation level (and therefore its force).

The aim of this study was to evaluate whether the neuromuscular control variability predicted assuming as constraints only the equilibrium of forces and moments and the tetanic limit for each muscle (i.e., Metabolica approach [208]) changed (and to which extent) when the muscle force generation velocity was accounted for. We named this new approach Myobolica and hypothesized that it would narrow the solution band (compared to Metabolica), including only the more physiologically plausible estimates.

The reader is referred to [225] for a mathematical dissertation on the Myobolica approach.

Material and Methods

Experimental data

The experimental data used in this study, which include motion capture, ground reaction forces, and in vivo knee contact forces measured with an instrumented implant on an 83-year-old male subject, are part of the sixth Grand Challenge Competition dataset [214] In particular, the first available overground gait trial (DM_ngait_og3) was selected for our case study and processed to ensure that a full gait cycle was included, i.e. that the first and last frames corresponded to two consecutive right heel strikes on the force plate.

Musculoskeletal model

A personalized single-leg musculoskeletal model was employed to perform the simulations. The model, built off the available post-operative medical imaging data of the subject under study, was inherited from previous work [103] and included 5 bodies (pelvis, femur, patella, tibia, and foot), 11 degrees of freedom (3 for the hip, 1 for the knee and the ankle, 6 connecting the model to the ground) and 43 muscle-tendon actuators.

OpenSim workflow – optimal solution

The open-source software OpenSim (v4.1) [197] was used to estimate joint kinematics and kinetics, as well as the musculoskeletal parameters such as the muscle lever arms. The OpenSim's static optimization tool was then employed to predict the 'optimal' and reference solution, i.e. set of muscle forces and activation patterns, that minimized the sum of squared muscle activations [90], henceforth referred to as optimal solution, and the resulting total knee joint contact forces (JCF).

Stochastic approach

Stochastic simulations were performed with Metabolica and Myobolica through MATLAB (v2021b), setting the number of solutions to be identified to 8×10^5. This number was deemed sufficient considering that in previous studies where Metabolica was employed such value was set to 1×10^5 and 2×10^5, respectively [64], [141].

Once the solutions had been generated, the knee JCFs were predicted by leveraging on the OpenSim API for MATLAB (similarly to what was done to compute the JCFs corresponding to the optimal solution).

Of note, in Metabolica no manifold was applied, i.e., the solution space was not restricted, and the sampler could explore the entire space of solutions.

The mathematical concepts behind Myobolica and the rationale and procedure to select the key parameters defining how it works (Table 3) are summarized in the following sections. For a complete description of the mathematics behind Myobolica, we refer the reader to [225].

Table 3. Myobolica parameters defined for this case study.

Parameter	Value	Description
Samples	800000	Number of solutions to be identified
Step analyzed	2^{nd}	Reduce the dependence on the optimal solution
Sigma	0.12	Modeling of uncertainties in equilibrium equation
Gamma	0.0022	Modeling muscle force development velocity control

Myobolica – Equilibrium condition

The Myobolica tool considers muscle forces as random variables based on observations on joint torques and muscle moment arms (1) and a priori information to constrain muscle forces (2):

$$M = B \times F_{mus} + \varepsilon \quad (1)$$

$$F_{min} \leq F_{mus} \leq F_{tetanic} \quad (2)$$

Where B is the matrix of muscle lever arms, M is the joint torques vector, F_{mus} is the unknown muscle forces vector bounded between its minimum value (F_{min}) and maximum value ($F_{tetanic}$). The parameter ε models noise and uncertainties as Gaussian white noise:

$$\varepsilon \sim N(0,\ \sigma^2 I_n) \quad (3)$$

By adopting a Bayesian statistics methodology, Myobolica describes the unknown muscle forces vector as a posterior Probability Distribution Function (PDF):

$$\pi(F_{mus}|M) \propto \pi_{pr}(F_{mus})\pi(M|F_{mus}) \quad (4)$$

Where $\pi(F_{mus}|M)$ is the posterior PDF of the muscle forces, $\pi_{pr}(F_{mus})$ is the prior PDF and $\pi(M|F_{mus})$ is the likelihood.

Sigma (σ) is the parameter modeling noise and uncertainties in the equilibrium condition equation, and it represents the standard deviation of the Gaussian PDF in (3). To define a plausible range for the σ parameter we estimated the error ε (1) by propagating the experimental error of the instrumented knee prosthesis adopted in our example dataset [214].

Myobolica – Muscle force development velocity control

The classical formulation for the Bayesian statistic (adopted in Metabolica) would assume that PDFs at different timeframes are mutually independent. This lacks physiological accuracy – due to the natural limits of the muscle activation velocity (and, as a result, of the muscle force development velocity); in other words, different timeframes cannot be mutually independent. To overcome this, in Myobolica, we modeled the concept of "yank", which is the time derivative of a muscle force [196]. In particular, we defined the yank as a PDF:

$$F_{mus,t} - F_{mus,t-1} = \eta t \quad (5)$$

$$\eta t = N(0, \gamma^2) \quad (6)$$

Modeling the yank binding through this prior PDF – discussed in detail in [225] – allows us to compute a solution that keeps track of each simulation timeframe information. Notably, the sampling of longitudinal paths rather than single solutions (required to obtain solutions which respect the new yank constraint) is achieved through the Feynman-Kac model [211]. Briefly, the Feynman-Kac path formalism (developed for diffusion-type parabolic equations) introduces a probability distribution in the space of path over time and represents solutions as expectation of integrals over paths similarly to how in our modelling problem the muscle force posterior PDF is defined by the yank prior PDF [225].

Gamma (γ) represents the standard deviation of the gaussian PDF describing the yank variance (6). In particular, γ (which controls the yank) relates to an experimental parameter frequently measured or estimated in experimental muscle characterization studies: the rate of force development (RFD), at times reported as the rate of moment/torques development (RMD). The RFD describes the capacity of a muscle to rapidly generate force [215] and is measured in Newton per second [N/s] (or Nm/s, when derived from torques). The RFD is calculated during maximal voluntary isometric contraction tests (MVIC tests) of sports gestures for athlete's performance evaluation or constrained to an instrumented chair in the clinical environment. Commonly, the parameter is estimated during the first 300-400 ms of the executed task [215] and clustered into shorter intervals.

Myobolica – Consecutive steps analysis

To run, Myobolica requires a first tentative solution (i) to compute an early value of the muscle force development velocity control and (ii) to define the initial conditions at the first timeframe of the simulation (the initial set of muscle forces).

To limit the dependency of the Myobolica solutions on the tentative solution, which corresponds to the optimal solution from static optimization, we simulated two consecutive steps. More specifically, assuming that the kinematics variability between steps is little to negligible [226], the median muscle force patterns among the Myobolica solutions estimated after the first run were provided as tentative

solutions for the simulation of the second step. In addition, the pool of plausible initial conditions to guide the initial sampling for the second step was set to the values of the Myobolica solutions at the last timeframe of the first step.

Henceforth, with the term Myobolica solutions we refer to the solutions of the second step.

Data Analysis

A schematic summary of the work done in this paper is reported in Figure 16. For both Myobolica and Metabolica, the resulting solution space (i.e. set of muscle forces) was initially sorted in ascending order to facilitate the identification of the minimum and maximum solutions, along with the 10^{th}, 25^{th}, 75^{th}, and 90^{th} percentiles as well as the median solution. Similarly, the estimated knee JCF profiles were first normalized to the subject's body weight and then sorted in ascending order.

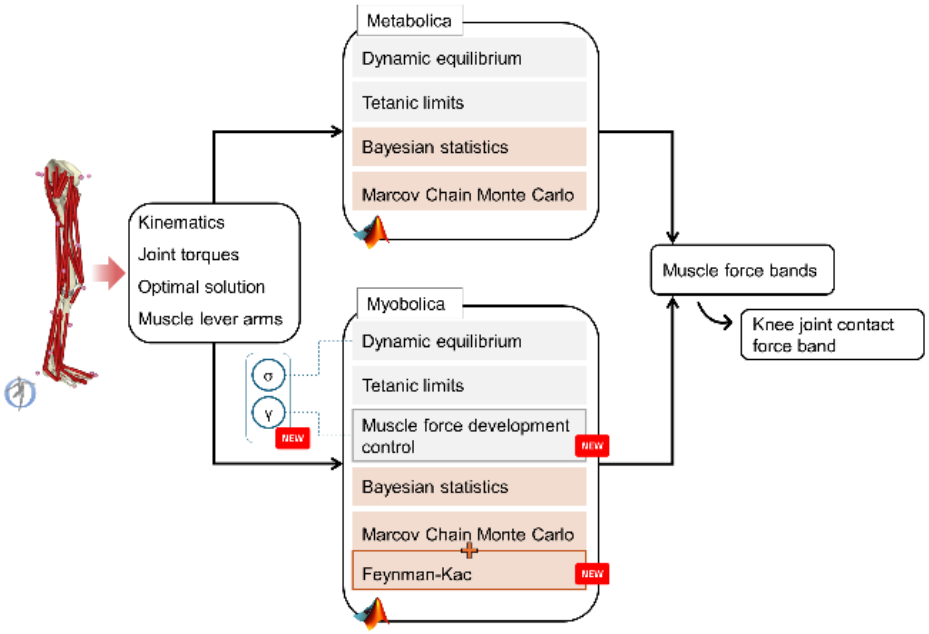

Figure 16. Summary of the workflow done. Firstly, biomechanical parameters are extracted from the musculoskeletal model. Then, an implementation of the stochastic approach is executed (Myobolica or Metabolica). In the end, both implementations provide as output a band of plausible muscle forces, in turn used to compute a band of plausible knee JCF profiles. In Myobolica, σ and γ are parameters related to uncertainties modelling and the new "yank" constraint and the mutual independency among frames is reached through the Feynman-Kac model path sampling.

The comparison between the results from Metabolica and Myobolica is performed employing descriptive statistics and similarity metrics (i.e., R^2 and root mean square error - RMSE) as well as through the quantification of the range of variation (min to max solution), further complemented by a qualitative analysis.

In addition, the Myobolica solution space was compared to the optimal solution and to the experimental knee JCFs (i) measuring the overlap (as percentage, throughout time), (ii) computing the R^2 and RMSE, and (iii) comparing the ranges of variation.

Results

For clarity and to keep the Results section concise, we hereby only report the results for a subset of muscles, i.e., *triceps surae*, *vastii*, and *hamstrings* (see Figure 17). Additional comparisons and results may be found in the Appendix.

Overall, the inclusion of an additional constraint (yank parameter) to control the force-generating capability of a muscle when exploring the solution space through a stochastic approach (i.e., Myobolica implementation) led to a significantly narrower solution band compared to the output from Metabolica (previous implementation of the stochastic approach where no manifold was applied and the solutions at consecutive frames were independent of one another, thus allowing for abrupt changes in muscle force).

On average, the bandwidth (spectrum of solutions) across all modeled muscles was 659.4 N for Metabolica and 205.5 N for Myobolica (see Figure 18). More specifically, for the *soleus* muscle, the force range estimated by Metabolica was 2385.7 N, compared to 415.3 N from Myobolica; for the *vastus medialis* 1207.7 N compared to 180.2 N; for the *medial gastrocnemius,* 1454.1 N compared to 371.7 N.

Similarly, the spectrum of the knee JCFs – computed from the identified set of muscle forces – ranged from 0.45 BW to 2.9 BW in Myobolica (see Figure 19) and from 0.14 BW to 13.2 BW in Metabolica, with an average solution variability of 0.6 BW for Myobolica and 9.7 BW for Metabolica.

From a qualitative assessment, for both approaches, the peak force was observed at around 55% of the gait cycle (in correspondence of the typical second characteristic peak of knee JCF force in a walking trial). The profiles of the solution spaces between Myobolica and Metabolica were similar in shape (R^2 = 0.87, RMSE = 4.5 BW, between the medians of the two solution bands). In S.Fig.1 a comparison between muscle activation solution bands estimated by Myobolica and the experimental EMG signals is provided.

Compared to the true value, i.e., data from the instrumented knee implant, the Myobolica solution band showed a high correlation level (R^2 = 0.92 and RMSE = 0.3 BW, between Myobolica median solution and experimental JCF profile). Furthermore, the implant data were almost completely enclosed in the solution space identified by Myobolica (for approximately 72.8% of the gait cycle; see Figure 20).

By contrast, the knee JCF resulting from the optimal solution identified via the classical static optimization approach (Figure 20, green line), thus hypothesizing optimal muscle control, was characterized by a first characteristic peak larger than the second characteristic peak (i.e., overall maximum identified around initial heel contact, at ~8% of the gait cycle, compared to ~55% in both the experimental data and the Myobolica solutions). Shape-wise, the optimal solution was not as similar to the Myobolica band of solutions as the implant data (i.e., R^2 = 0.82, RMSE = 0.63 BW,

between the medians of Myobolica solutions band and the optimal solution), and fell mostly outside of it (i.e., 15.9% overlap across the gait cycle).

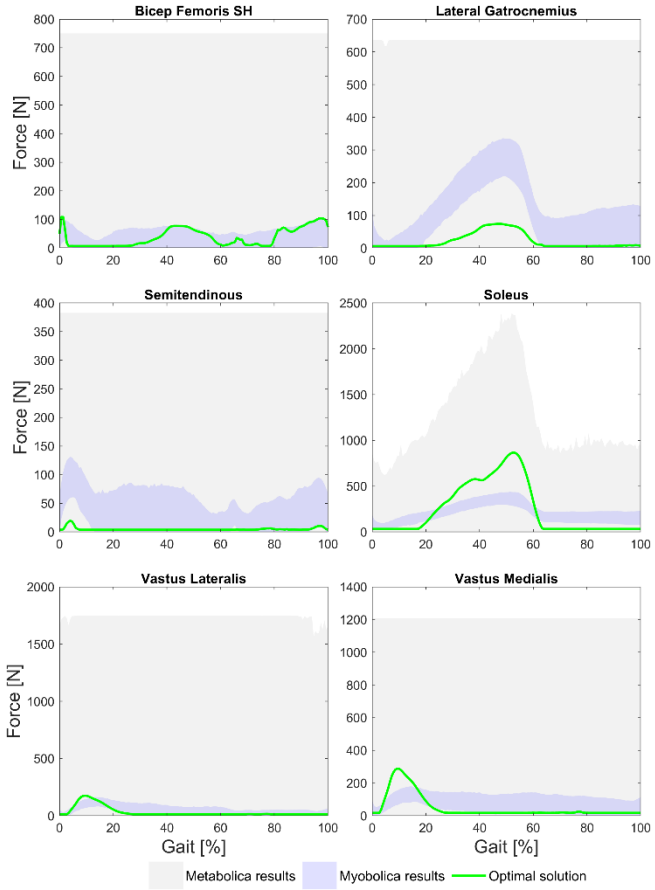

Figure 17. Muscle force solutions bands comparison between Myobolica (blue) and Metabolica (grey). The optimal solution is plotted in green.

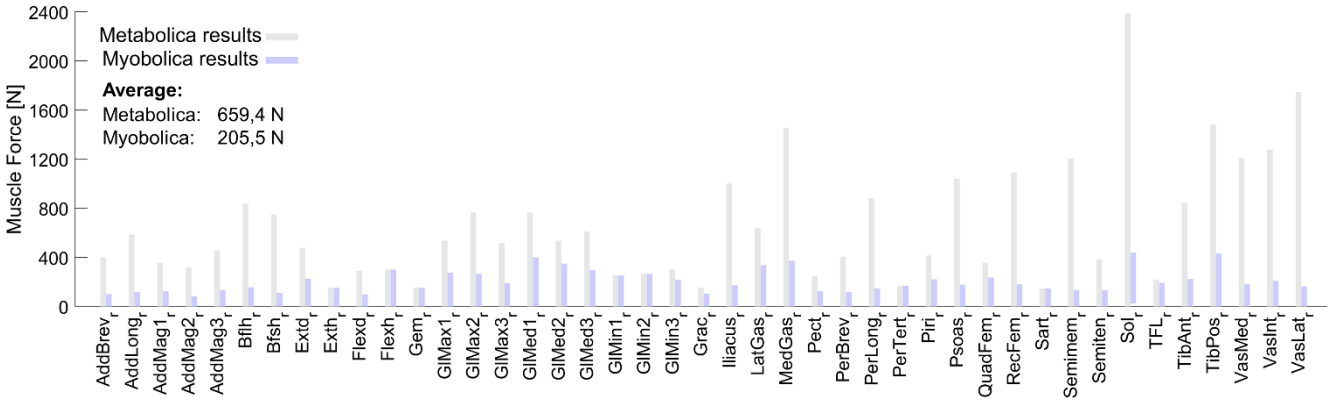

Figure 18. Comparison of muscle range of forces estimated by Myobolica (blue) and Metabolica (grey).

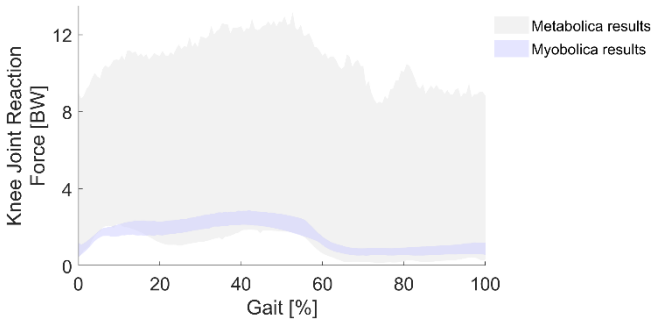

Figure 19. Comparison of the knee JCF solution bands estimated by Myobolica (blue) and Metabolica (grey).

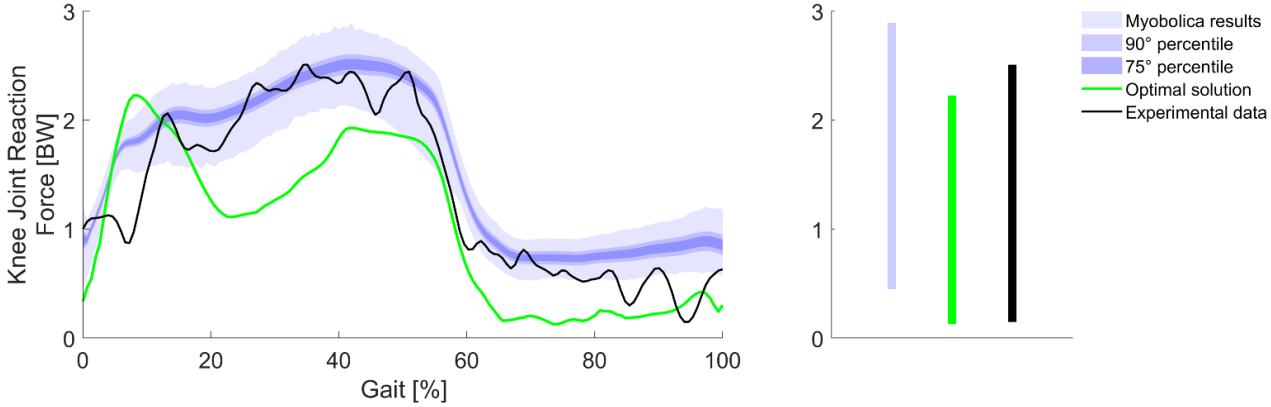

Figure 20. Comparison of knee JCF estimated by Myobolica (blue shade bands), optimal solution (green) and experimentally measured data (black). Right: min-to-max range of the solutions estimated by the two methods and the experimentally measured value.

Discussion

The aim of this paper was twofold: to present the results of Myobolica, a tool to implement a stochastic approach to predict physiologically plausible muscle forces and activation patterns accounting for neuromuscular control variability while constraining the ability of muscles to rapidly generate force, and to compare the obtained variability to the variability predicted assuming as constraints only the equilibrium of forces and moments and the tetanic limit for each muscle (i.e., Metabolica).

As hypothesized, introducing a term to discourage abrupt changes in muscle force led to a marked narrowing in the solution band (in terms of knee joint contact forces, from 13 BW to 2.4 BW, Figure 18 and Figure 19), compared to results from Metabolica [141], [208]. While part of the solution space obtained with Metabolica may be considered physically plausible as the identified solutions satisfy both the dynamics of the system (equilibrium) and the tetanic limits of the muscles (i.e., maximal isometric force values), those same solutions may not be physiologically plausible. In fact, when the γ parameter (to control the yank) was introduced, a large portion of the Metabolica solution space was no longer explored (Figure 19). This may suggest that even in a subject adopting a suboptimal control (such as the subject under study), some variability in neuromuscular control is physiological, but it may be less than previously hypothesized.

In addition, the knee joint contact force profiles calculated from the solution space identified by Myobolica more closely approximated the experimental data from the instrumented implant. This may be reconducted to the higher muscle-co-contraction resulted by Myobolica. The introduction of the γ and σ parameters to control the yank and the uncertainties in the equilibrium condition, respectively, had thus a twofold (positive) effect: to reduce the band of solutions and to enable more

accurate predictions. Interestingly, the optimal solution (generated hypothesizing optimal muscle control – i.e., minimization of sum squared muscle activations) is close to but not comprised within the range of Myobolica solutions. This circumstance calls for further investigation.

The authors are aware of the limitations of this work. For instance, the computational cost is non-negligible. While a single Myobolica solution (i.e., set of muscle forces and activations plus the resulting knee joint contact force) can be generated in as little as 0.3 seconds, the overall time required to compute the whole band of solutions (e.g., 8×10^5 solutions) is in the order of hours due to a lack of parallelization in the current implementation. Moreover, the γ parameter – related to the yank control – may vary between populations, with significant differences between trained and untrained subjects. Additional tests should be performed to study the effect of such parameters on different subjects. The authors point out that this paper was conducted on one subject with an explorative purpose, and the set γ parameter was comparable to values found in the literature.

A future development, to improve the physiological accuracy of Myobolica, will be the introduction of the force-length and force-velocity relationships into the likelihood component of the Bayesian framework. In its current implementation, Myobolica assumes the muscle force to be linearly proportional to the muscle's tetanic force and activation. This choice was made for computational and pragmatic reasons: introducing a more realistic muscle model at this stage would have required additional parameters and complexity to the problem. This simplification aligns with the adoption of static optimization as a tentative solution, which – in OpenSim – does not account for the physiological tendon compliance by design and for the force-length and force-velocity relationships in our simulations. The enhancement introduced by Myobolica relative to the previous stochastic approach tool (namely, the constraint on muscle force generation velocity) imposes a physiological constraint that could be interpreted as a first step toward the incorporation of the force-length and force-velocity relationships. Moreover, it will be further deepened by realistically adapting the ranges where Myobolica can control muscle forces.

The analysis of more subjects is planned in the near future to confirm the conclusions the authors drew in this document, along with a sensitivity analysis to quantify the effect of the values assigned to γ and σ (hereby carefully selected, but likely different depending on the characteristics of the population) and a convergence analysis to identify the minimum number of solutions to be sampled and consecutive steps to be performed to minimize the computational cost.

If future analysis will confirm results emerged in this study, new application scenarios may be hypothesized where the stochastic approach could be used to enhance "what if" kind of study and provide an extended band of what the subject is able to do (in terms of muscle forces) given the kinematics and the subject specific muscle condition.

Appendix

Appendix I – Toolbox parameters

The study for the definition of physiological ranges for Myobolica governing parameters was accomplished for two we defined "gamma" (γ) and "sigma" (σ).

To define a physiological range for the γ parameter we estimated the rate of moment development (RMD) from data collected in our laboratory on 31 people (both young and old individuals. ClinicalTrials ID: NCT05795348, NCT05854316 [227]) who performed maximal voluntary

isometric contraction (MVIC) tests of the lower limbs on a Biodex System 4 Pro isokinetic dynanometer (Biodex Medical System, New York, NY, USA).

The experimental results (i.e., computed RMDs) were clustered into 3 intervals based on the selected analysis window: 0-50 ms, 0-100 ms, 0-200 ms. No specific cluster was chosen, and the results were pooled together, as the peak performance reached in a MVIC test (experimental task) is unlikely to be reached during an overground walk (simulated task). The values thus extracted were in line with the literature [215], [216], [217], [218], [228], [229].

The computed RMDs were later scaled to the timescale of the employed simulation data (in our case, 0.008334 seconds):

$$RMD_{scaled} = RMD \times \Delta t_{specific} \quad \text{(A1)}$$

As in Myobolica the yank is described as a gaussian PDF with average value and standard deviation respectively equal to 0 and γ, to ensure all yank values are described by the gaussian distribution (the authors remind the reader that 99.7% of the values lie within 3 times the standard deviation) we modelled the γ parameter starting from the average RMD value typical of elderly subjects, as in (A2):

$$3 \times \gamma > RMD_{experimental} \quad \text{(A2)}$$

Where $RMD_{experimental}$ was the RMD normalized to the measured peak torques and scaled to the simulation timescale. The overall largest value (across clusters) was selected. The purpose of normalization is to enable comparison of results across studies where different motor tasks are studied.

To define a plausible range for the σ parameter we estimated the error ε (1) by propagating the experimental error of the instrumented implant worn by the subject under study [214]:

$$\varepsilon_{Force,\,knee} = \sum_{i=1}^{Nmuscles} k_i(t) \cdot \varepsilon_{Force,i}(t) \quad \text{(A3)}$$

$$k_i(t) = \frac{F_{mus,i}(t)}{F_{knee,\,resultant}(t)} \quad \text{(A4)}$$

Where $\varepsilon_{Force,knee}$ is the maximum absolute error measured during the calibration of the instrumented prosthesis [230] – i.e., about 1% of the maximum value measured during trial acquisition.
Assuming that the contribution of each muscle to the knee joint force (and so to the error of that measure) is proportional to the force generated by the same muscle, we defined $\varepsilon_{Force,knee}$ as a linear combination of muscle force errors ($\varepsilon_{Force,i}$) weighted by their contribution to the knee resultant force (A3). The contribution k_i was set to 0 for muscles not insisting on the knee joint.

The joint torque error ε was estimated propagating the muscle force error $\varepsilon_{Force,i}$ in (1):

$$M + \varepsilon = B \times [F_{mus} + \varepsilon_{Force,mus}] \quad \text{(A5)}$$

This way, an ε value for each simulation time frame was estimated, and the biggest one, around the second peak of the gait cycle ε reached the value of 0.36 Nm, was chosen as reference value.

To ensure noise and uncertainties in (1) to be described by a gaussian distribution with average value 0 and standard deviation σ, we modelled the σ parameter starting from the previously described ε:

$$3 \times \sigma > \varepsilon \qquad \text{(A6)}$$

Appendix II – Step selection

The analysis of a second consecutive step is mainly motivated by the need to obtain a solution independent from the initial optimal solution, but it led to the estimation of a significantly different solution space. To explore how the periodization of the gait cycle could affect the outcome, a third consecutive step was simulated searching for differences in the resulting solution spaces between the second and the third steps. The median muscle activation pattern estimated in the second cycle is assigned as required tentative solution in the third one and the last timeframe's solution of the second gait cycle is carried out as the pool of plausible initial conditions for the third gait cycle.

The comparison between the Myobolica solution for the first and second steps is shown in A.Fig. 1. The average muscle force range across muscles is 226.7 N in the first step and 205.5 N in the second step. The largest difference was found for the soleus muscle (from 855.5 N in the first to 415.3 N in the second step. A.Fig. 2(a)).

While the knee joint force solution spaces resemble (R^2 = 0.97 and RMSE = 0.28 BW between medians of the two solution bands) with force estimated in the first step generally lower than the one estimated in the second one (A.Fig. 3); in the first step, the estimated spectrum ranged from 0.14 BW to 2.4 BW while in the second step from 0.45 BW to 2.9 BW.

Further tests have been performed to determine whether simulating a third step would lead to much different estimates (A.Fig. 4). No significant differences emerged when comparing individual muscle bands (the largest difference emerged for the tibialis posterior bandwidth: from 429.9 N in the second to 434.8 N in the third step. A.Fig. 2(b)). Similarly, the knee joint force solution spaces were very much alike (R^2 = 0.99 and RMSE = 0.04 BW between medians of the two solution bands. A.Fig. 5).

Considering the computational time to complete a simulation, the authors deemed the difference between the results from the second and the third step not to be significant enough to require a third step to be performed.

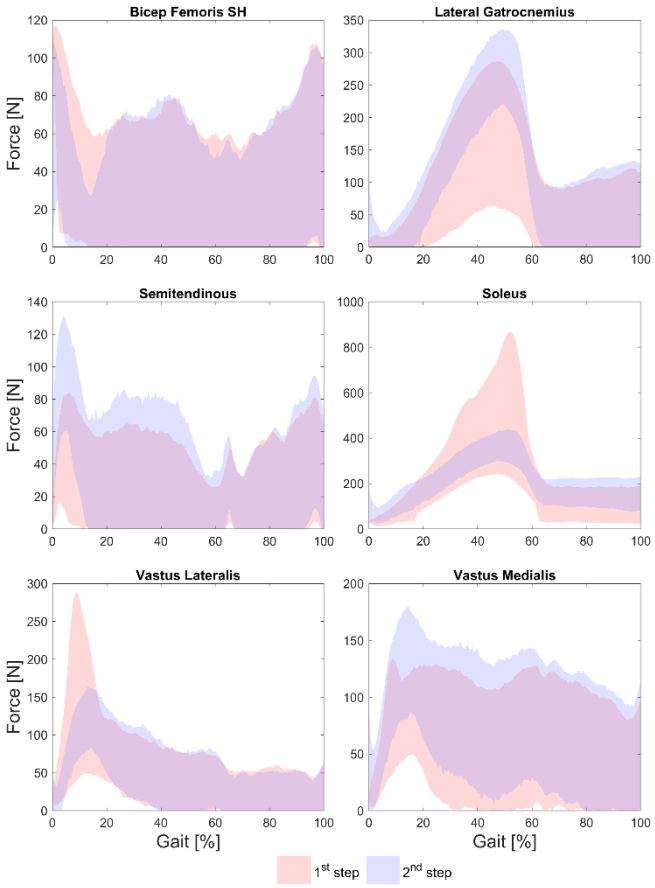

A.Fig. 1. Muscle force solutions bands estimated by Myobolica. Comparison of the first (red) and the second (blue) simulated step.

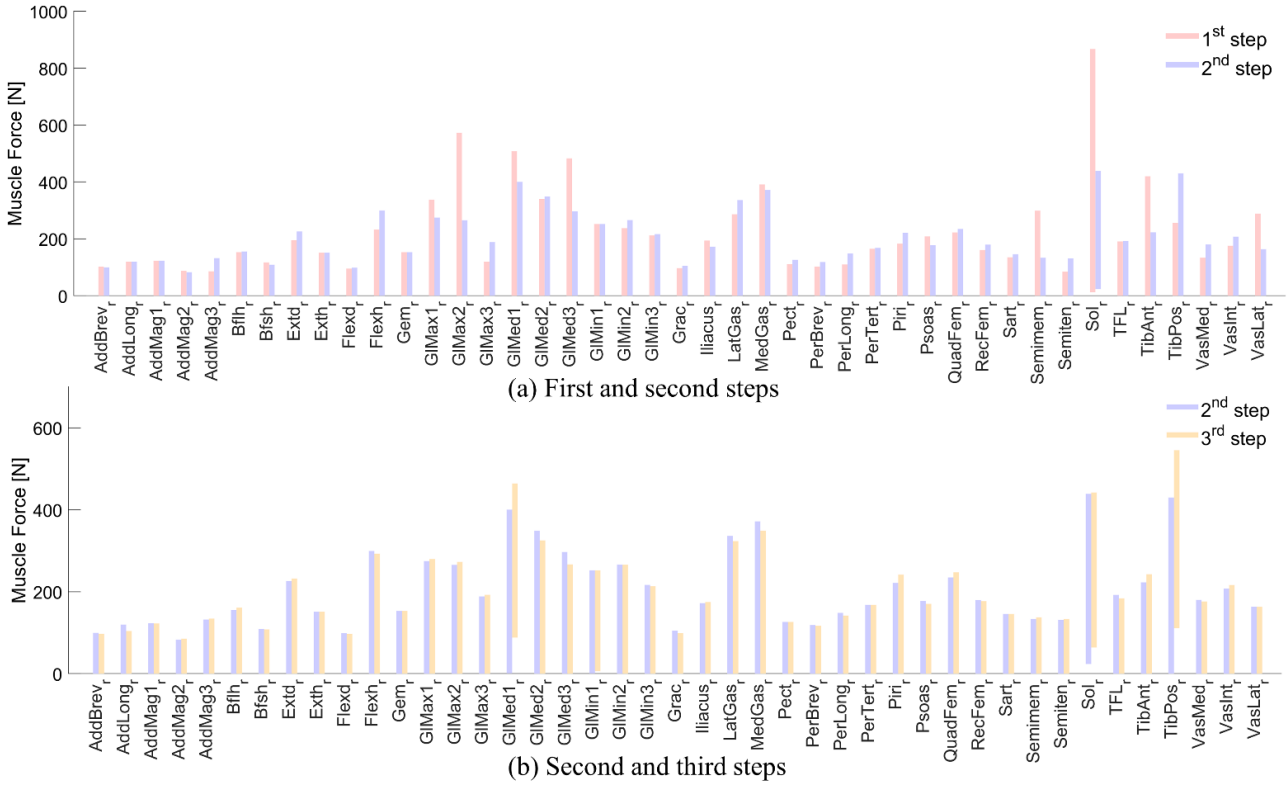

A.Fig. 2. Comparison of muscle range of forces estimated by Myobolica. In (a), comparison between the first (red) and second (blue) simulated step; in (b), comparison between the second (blue) and third (orange) simulated step.

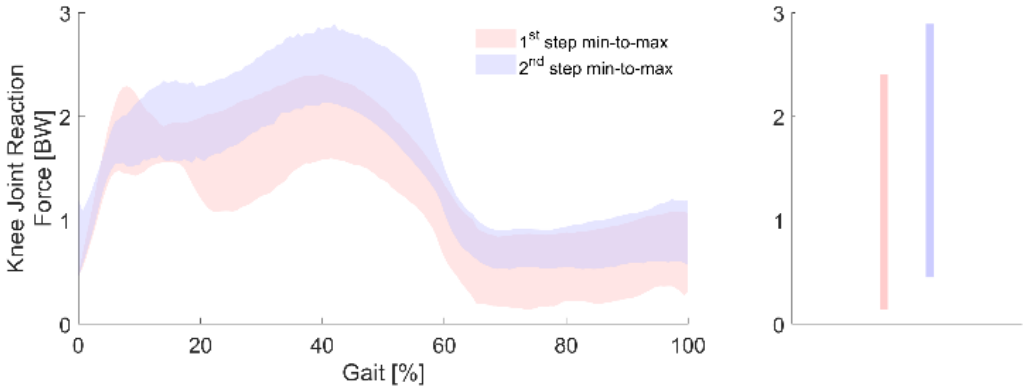

A.Fig. 3. Comparison of the knee JCFs estimated by Myobolica in the first (red) and the second (blue) simulated step.

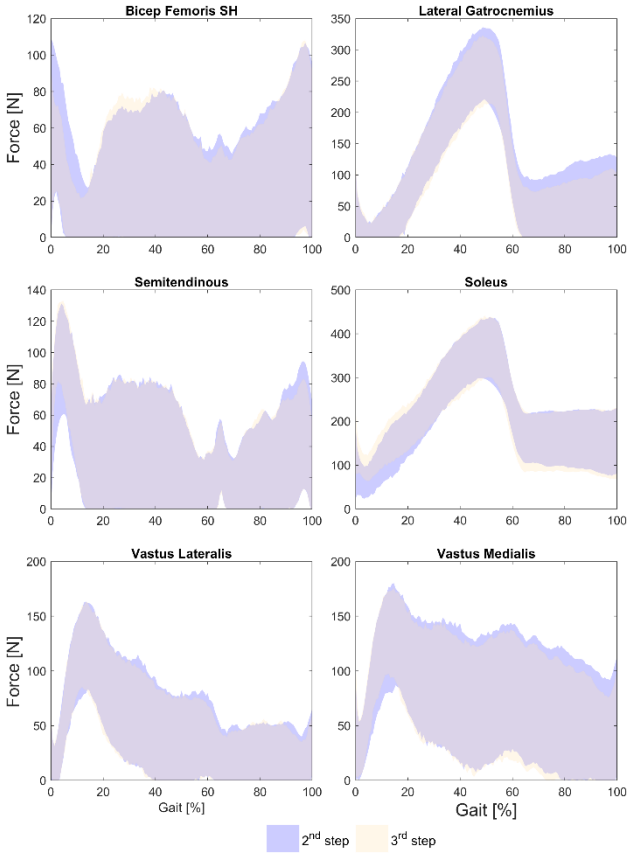

A.Fig. 4. Muscle force solutions bands estimated by Myobolica. Comparison of the second (blue) and the third (orange) simulated step.

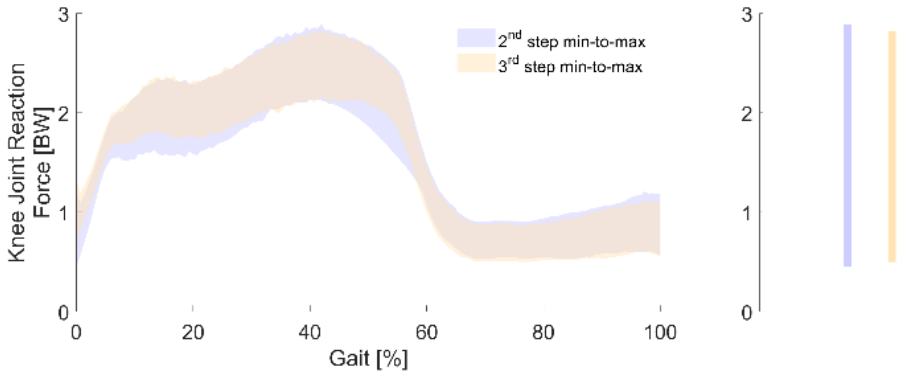

A.Fig. 5. Comparison of the knee JCFs estimated by Myobolica in the second (blue) and the third (orange) simulated step.

Acknowledgment

G. D. would like to thank the European Commission for the support through the European Union - NextGenerationEU through the Italian Ministry of University and Research under PNRR - M4C2-I1.3 Project PE_00000019 "HEAL ITALIA" to Marco Viceconti – CUP J33C22002920006. The views and opinions expressed are those of the authors only and do not necessarily reflect those of the European Union or the European Commission. Neither the European Union nor the European Commission can be held responsible for them.

Supplementary Material

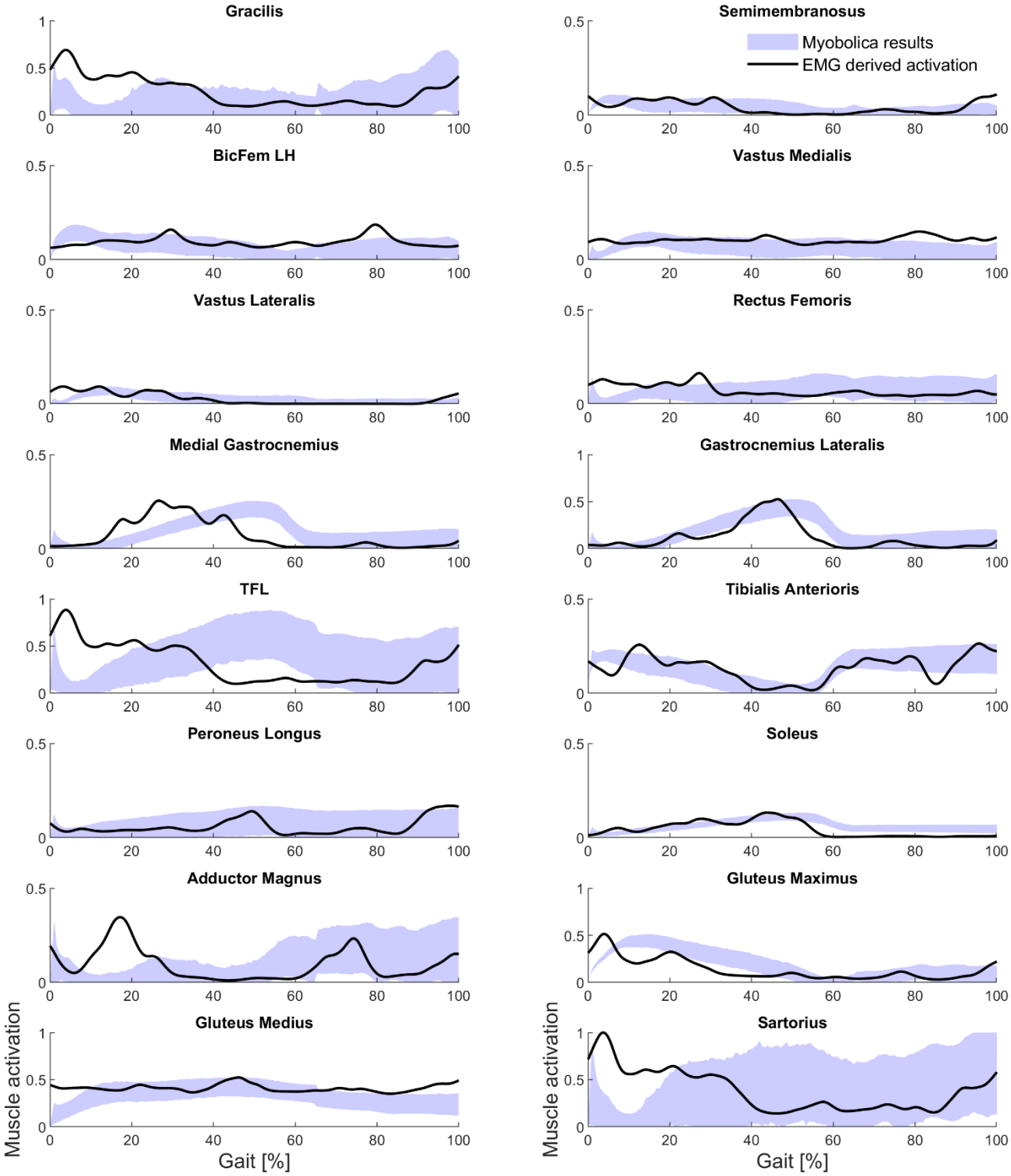

Supp.Fig. 1. Comparison of muscle activation solution bands estimated by Myobolica and EMG signals. EMG signals were band-pass filtered between 30-300 Hz, full wave rectified, and low-pass filtered at 8 Hz using a 4th order zero-lag Butterworth filter. Subsequently, EMG data were normalized to be in the same amplitude range of each corresponding Myobolica solution band. To be considered, Y axis is not the same one in each graph.

Stochastic modelling of muscle control during shoulder abduction

Alex Bersani[1], Saulo Martelli[2,3], Maxence Lavaill[2,3], Giorgio Davico[1]

[1] Department of Industrial Engineering, Alma Mater Studiorum - University of Bologna, Bologna, Italy

[2] School of Mechanical, Medical and Process Engineering, Queensland University of Technology, Brisbane, Australia

[3] Centre for Biomedical Technologies, Queensland University of Technology, Brisbane, Australia

Adapted from a publication in:

Journal of Biomechanics (2025)

https://doi.org/10.1016/j.jbiomech.2025.112993

The authors wish to thank Journal of Biomechanics for providing the permission to re-use the manuscript titled “Stochastic modelling of muscle control during shoulder abduction” in the present PhD thesis

Abstract

The intrinsic variability of the shoulder joint motion is a critical factor in the characterisation of the shoulder joint. However, traditional computational approaches struggle to account for it. On the other hand, the stochastic approach allows to identify a set of plausible solutions. In this study, the Myobolica toolbox, which yielded promising results in the lower limb, was employed to simulate a shoulder abduction, with twofold aims: to assess its generalisability to other joints, and to evaluate an electromyography (EMG)-informed version of Myobolica.

Publicly available kinematics, EMG, and glenohumeral joint force (GJF) data measured by an instrumented implant on a 64-year-old man executing three weighted shoulder abductions were used. A previously developed shoulder musculoskeletal model was employed to compute stochastic simulations informed and not with EMG data, sampling 1×10^5 solutions every 30 timeframes. The predicted GJF were compared to the experimental data, and the variance in the solutions across simulations was computed.

Overall, the correlation between the GJF predicted by Myobolica and the experimental values increased when the EMG-based constraint was applied (from approximately R^2=0.06, RMSE=1.82 BW to R^2=0.6, RMSE=0.73 BW when all available EMG data were employed). Using EMG led to a reduction (from 2.3 to 0.65 BW) in the solution bandwidths.

Providing EMG data to inform the simulations helped improve their accuracy. However, the results obtained otherwise remain promising. Additional work is required to minimize the computational cost of the Myobolica approach. A consistency gap between experimental data and the model is reported.

Keywords

Shoulder modelling, Suboptimal control, Stochastic muscle recruitment, Stochastic approach, Electromyography

Introduction

The glenohumeral joint is central in the execution of activities of daily living [231], [232]. This is particularly evident in individuals with non-healthy shoulders, whose motion may be severely compromised [233], [234]. In this scenario, the importance of having a reasonable estimation of musculoskeletal biomarkers, such as muscle or joint contact forces, for treatment and rehabilitation purposes [235], [236] or to optimise prosthetic design [237], becomes apparent.

Traditional methods to predict musculoskeletal forces include static optimisation and electromyography (EMG)-informed approaches. The first one assumes that muscles are controlled according to a physiological criterion modelled through a cost function to be optimised [90], [238] but tend to underestimate joint forces [238], [239] by discouraging muscle co-contraction [240], [241], and the second one is often adopted to ensure the solution tracks experimental muscle excitations [60], [115] but may suffer from the intrinsic problems of the EMG acquisition [242]. In addition, optimal control methods where different optimisation algorithms are used to solve complex tasks and to perform both inverse and forward [243] dynamics simulations, but can show convergence and high CPU time issues [243], [244].

Alternatively, in the last decade, a stochastic modelling approach has been proposed to solve the muscle recruitment problem while accounting for muscle co-contractions, modelling errors and the muscle control intrinsic variability [141], [245]. Based on the uncontrolled manifold theory [15], the stochastic approach relies on Bayesian statistics and a Monte Carlo (or Markov Chain Monte Carlo) algorithm to sample a band of feasible solutions [208], [225], [245], albeit requiring a non-negligible computation time. Adopted various times to estimate the impact of a sub-optimal control [64], [104], [194], the stochastic approach has been recently improved by constraining time changes of muscle forces either explicitly [225], [246] or by modulating the peak muscle force boundaries [56]. Constraining the force generation rate led to promising results in the lower limb [246], but those are yet to be generalised for application to other joints. In addition, the possibility to combine EMG-informed and stochastic modelling approaches towards more physiologically plausible estimates remains a largely unexplored scientific space. The aim of the present study was twofold: i) to evaluate the Myobolica toolbox to model muscle control of the shoulder joint; ii) to understand the impact of adding EMG signals as a new physiological constraint to the proposed stochastic approach.

Materials and methods

Experimental data

The experimental data employed in this study were collected on a 64-year-old man (labelled S2R) implanted with an instrumented right shoulder prosthesis, part of a publicly available dataset [238], [247]. The dataset included motion capture data, the EMG signals from seven superficial muscles, and the in vivo glenohumeral joint contact force measured by the instrumented implant [248]. A single trial, composed of three consecutive shoulder slow abductions while the subject held a 2.4 kg weight, was selected for the simulations.

The EMG data were filtered to compute the linear envelopes of the signals by implementing a zero-lag 8^{th} order Butterworth filter (40-400 Hz), followed by a full-wave rectification and a zero-lag 8^{th} order low-pass Butterworth filter at 5Hz, and normalised to the maximum value from the available functional, force and maximal voluntary contraction tests [249].

The musculoskeletal model was inherited from previous work [63]. It consists of seven bodies (thorax, clavicle, scapula, humerus, ulna, radius, and hand), eleven degrees of freedom (three for the sternoclavicular, the acromioclavicular and the glenohumeral joints, one for the elbow, and the radioulnar) and 91 muscle-tendon actuators ("Millard2012EquilibriumMuscle" muscle model [250]).

Simulations workflow

An outline of the workflow is summarised in Figure 21. The open-source software OpenSim 4.1 [197] was employed to estimate model kinematics, kinetics, and the muscle lever arms. The OpenSim static optimisation and joint reaction tools were used to predict an optimal solution for the muscle and joint contact forces, which was later used as an initial tentative solution to Myobolica for the stochastic simulations. Due to the limited actuation of the thoracoscapular joint made by the adopted model (the Delf Shoulder and Elbow Model, DSEM)[63], reserve actuators stronger than those recommended in OpenSim guidelines [251] were required for the sternoclavicular, the acromioclavicular, the elbow, and the radioulnar degrees of freedom.

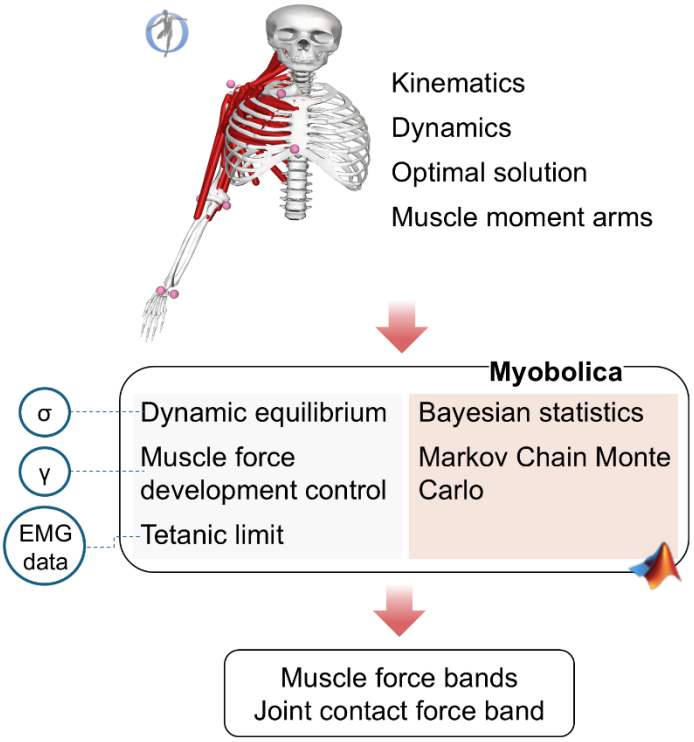

Figure 21. Summary of the workflow. Biomechanical parameters are extracted from the musculoskeletal model; then, the stochastic approach (Myobolica) is adopted to predict bands of plausible muscle and joint contact forces.

Stochastic simulations were performed within Myobolica [225], [246] through MATLAB (v2021b). Myobolica works by sampling the posterior probability distribution function of the unknown variable (i.e., muscle forces) estimated with Bayesian statistics (Equation 1) [225].

$$\pi(F_{mus}|M) \; \alpha \; \pi pr(F_{mus}) \; \pi(M|F_{mus}) \qquad (1)$$

where

$$M = B \times F_{mus} + \varepsilon \qquad (2)$$

$$\varepsilon = N(0, \sigma^2) \qquad (3)$$

$$F_{mus,t} - F_{mus,t-1} = \eta t \qquad (4)$$

$$\eta t = N(0, \gamma^2) \qquad (5)$$

With F_{mus} as the muscle forces vector, M the joint torques vector, B the matrix of muscle lever arms, and "N" representing a Gaussian distribution with 0 mean and σ or γ as the standard deviations. In the present work, the parameter sigma (σ), modelling noise and uncertainties in the equilibrium condition equation (Equation 2 and Equation 3), was set to 0.12 as per [246], while the gamma (γ), which models how fast each muscle is able to generate force (Equation 4 and Equation 5), was set to 0.45, based on the rate of force development (RFD) derived from the literature experimental data [252] and normalised to the current simulation timeframe, as per [246].

Overall, after internal tests to reduce the computational cost while minimising the loss of accuracy, 1×10^5 solutions were sampled, and the system equations were evaluated every 30 timeframes. Each solution consisted of a set of 91 muscle forces.

We then updated the gamma values for the muscles that were modelled with multiple actuators (e.g., the deltoids muscle is modelled with 15 actuators), by normalising the experimentally determined gamma value to the number of actuators (Supplementary Table 1) to address the possible overestimated force generation issue when assigning a gamma value, representative of a whole muscle behaviour, to each subcomponent of the modelled muscle, and run Myobolica a second time. Following, we performed a new batch of stochastic simulations, informed by EMG data. In this case, the initial tentative solution was replaced by the EMG-derived force for the deltoids, triceps, biceps, and trapezius muscles. The latter was obtained by multiplying the processed and normalised EMG signal by the maximal isometric force of the specific muscle. The operating boundaries for the sampler were modulated assuming a 50 % error for the EMG-derived force. The error value has been selected to provide the sampler with smaller boundaries than the default Myobolica simulation without over-constraining the system.

For all simulations (Table 4), the resulting glenohumeral joint contact force solution space was estimated using the OpenSim API for MATLAB.

Table 4. Overview of all simulations performed and corresponding simulation labels. Columns show whether the muscle-specific (MS) gamma parameter and each available muscle EMG data are exploited.

Simulation	Muscle-specific gamma parameter	Deltoid EMG	Biceps EMG	Triceps EMG	Trapezius EMG
Default					
MS gamma parameter	✓				
Delt. EMG	✓	✓			
Bic. EMG	✓		✓		
Tric. EMG	✓			✓	
Trap. EMG	✓				✓
All EMGS	✓	✓	✓	✓	✓

Data analysis

The resulting glenohumeral (GH) joint contact force solutions were sorted in ascending order, normalised to the subject's body weight, with the median solutions and range between the minimum and maximum solutions plotted against the shoulder elevation angle for consistency with the literature [249]. The median solution was plotted as well. Solution profiles are reported only for the first trial for conciseness; the remaining are reported in the Supplementary file.

To assess how the stochastic approach performed, we compared the output of the various simulations to the experimental GH joint force by computing the R^2 index and the root mean square error (RMSE), as well as the overall solution space area (calculated as the top solution minus the bottom solution for each timeframe). In the Results section, average values across the three trials are reported, with each

trial's values reported in Table 5. To assess the impact of the EMG constraint on the solutions, we compared the average bandwidth of the EMG-informed and Default stochastic simulations (reported in the Supplementary Files only).

Results

The use of EMG data to inform the stochastic simulations was associated with a general improvement in the output from Myobolica (Figure 22). The resulting solutions better approximated the implant data ($R^2 > 0.16$, RMSE < 1.38 BW), compared to the simulations where no EMG data were employed. The best results were achieved when data from all four muscle groups were utilised (All EMGs simulation, $R^2 = 0.6$ and RMSE = 0.73 BW, on average across the three trials) (Table 5).

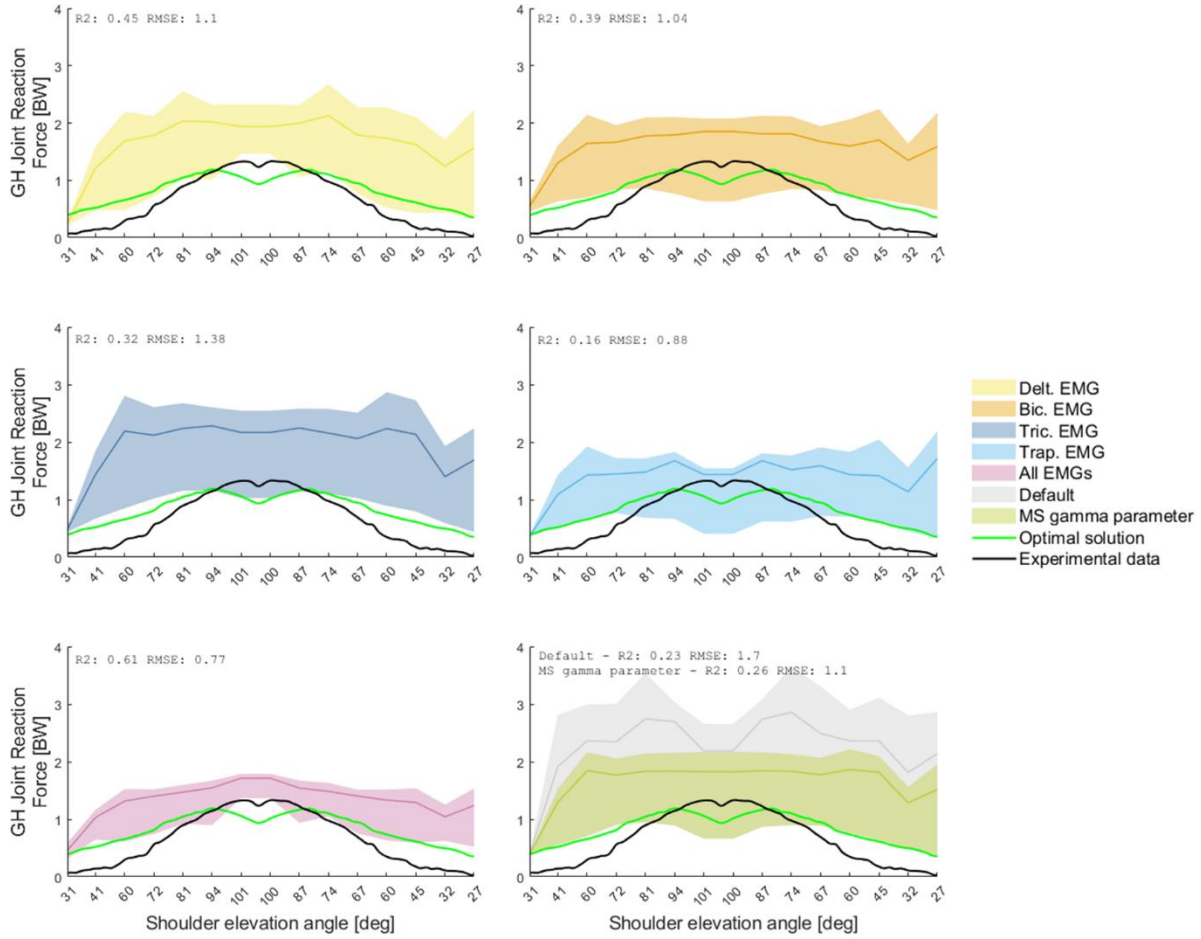

Figure 22. Comparison of the first trial GH joint contact forces predicted by Myobolica (shaded areas), optimal solution (green), and experimentally measured data (black). R^2 and RMSE between the first trial Myobolica median solutions and the experimental data are reported. Myobolica solutions were computed, in order, enforcing only deltoid muscles EMG (yellow), only biceps EMG (orange), only triceps EMG (dark blue), only trapezius EMG (light blue), all the previously mentioned EMGs (light purple), and without enforcing any muscle EMG (earls green); all the previously mentioned simulation were obtained normalising the gamma parameter. The default Myobolica result, without enforcing any muscle EMG or normalising gamma, is reported in grey.

Not enforcing EMG constraints led to the lowest correlation with the experimentally measured joint force in the Default simulation, as reported in Figure 22. Updating the gamma parameter (MS gamma parameter simulation) led to a substantial reduction in the RMSE (~ 30% from the Default simulation), but left almost unaltered and close to 0 the R^2 value (0.06 vs 0.09, Table 5). Informing

the activity of a single muscle with EMG data led to improvements less conspicuous than in the simulation where all EMG data are utilised ($R^2 \leq 0.45$ and RMSE $\leq$ 1.03 BW, where the best metrics were observed in Delt. EMG simulation) (Figure 22).

The width of the predicted GH joint force solution space always decreased when adding the new EMG-based constraint (Figure 23), reaching a reduction of ~70 % (from the Default simulation) in the All EMGs simulation (Table 5). Less marked reductions (up to 40%) were observed when single muscles were informed by EMG data (Figure 23).

Table 5. R^2 and RMSE between Myobolica median solutions and the experimental data for the three trials, and the GH joint contact force average solution space among the three trials.

Simulation	R^2			RMSE [BW]			Solution space average bandwidth [BW]		
	Trial 1	Trial 2	Trial 3	Trial 1	Trial 2	Trial 3	Trial 1	Trial 2	Trial 3
Default	0.23	-0.03	-0.03	1.70	1.81	1.94	2.24 ± 0.67	2.31 ± 0.76	2.35 ± 0.80
MS gamma parameter	0.26	-0.08	0.09	1.10	1.46	1.10	1.25 ± 0.40	1.49 ± 0.6	1.33 ± 0.47
Delt. EMG	0.45	0.29	0.61	1.10	1.10	0.907	1.40 ± 0.49	1.32 ± 0.47	1 ±0.46
Bic. EMG	0.39	0.006	0.19	1.04	1.35	1.11	1.26 ± 0.39	1.50 ± 0.48	1.31 ±0.42
Tric. EMG	0.32	0.09	0.18	1.38	1.46	1.49	1.47 ± 0.48	1.48± 0.53	1.48 ± 0.57
Trap. EMG	0.16	-0.06	-0.09	0.88	1.07	0.97	1.20 ± 0.45	1.34 ± 0.52	1.17 ± 0.52
All EMGs	0.61	0.42	0.76	0.77	0.78	0.63	0.72± 0.24	0.67 ± 0.26	0.55 ± 0.25

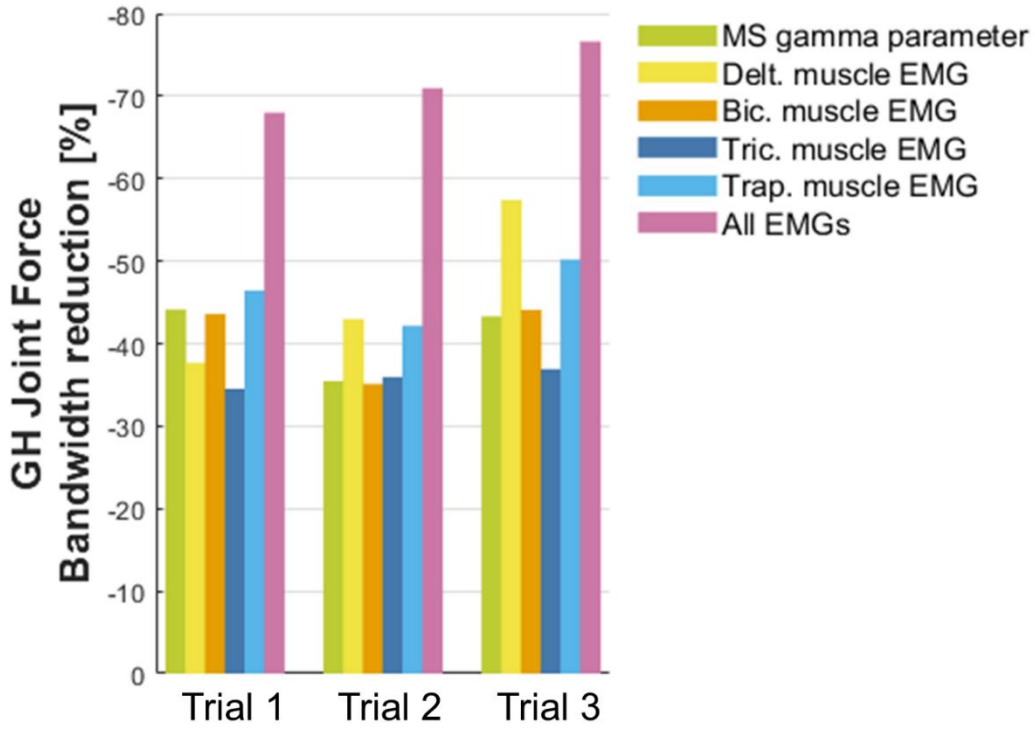

Figure 23. The reduction of the GH joint force solution space from the Default simulation to each subsequent simulation for the three trials. Myobolica solutions were computed, in order, without enforcing any muscle EMG (earls green), enforcing only deltoid muscles EMG (yellow), only biceps EMG (orange), only triceps EMG (dark blue), only trapezius EMG (light blue), and all the previously mentioned EMGs (light purple); all the previously mentioned simulation were obtained normalising the gamma parameter.

Discussion

In this work, a novel stochastic approach was employed to simulate a shoulder abduction task, aiming to test the feasibility of applying Myobolica to predict a spectrum of plausible solutions for the shoulder joint and seeking to evaluate the impact of a new physiological constraint based on EMG data. To this end, publicly available data and a previously developed musculoskeletal model were used. In a model such as the shoulder, characterised by high muscle redundancy required to permit a variety of movements, including more information in the model by adding EMG data as a constraint may reduce the variance of the spectrum (Figures 22 and 23). The improvement changes with the input, likely depending on model sensitivity and measurement errors. The deltoid muscle played a major role in the task, significantly influencing the shape of the predicted solution space. Also, constraining muscles less active in the optimal solution (e.g., biceps and triceps) resulted in a marked impact. In addition, results showed how modelling each actuator's velocity of force generation can become relevant to significantly reduce the solution space (Figure 22 and Table 5). Compared to a previous implementation of the stochastic approach (Metabolica) employed on a shoulder model [249], we have been able to reach narrower – and potentially more accurate – solution spaces. Myobolica predicted a GH joint force solution space from ~64 % in the Default up to ~90 % in the All EMGs simulation smaller than the solution space predicted by Metabolica in [249].

A limitation of this work is the computation time of such an approach. More work is needed in the future to improve the computational efficiency of the method and, even though every solution complies with the equilibrium conditions (Equation 2) and the physiological constraints (Equation 4 and the muscle activation boundaries), to run Myobolica on multiple trials and subjects without

recurring to a subsampling. As already pointed out in a previous work [249], a lack of consistency between the experimental data and the model predictions stands out.

In fact, noticeably, no simulation setups allowed Myobolica to predict same joint force values as the experimental data, especially for low abduction angles. This discrepancy is likely caused by limitations in the underlying musculoskeletal model rather than in the functioning of Myobolica. This is a limitation of the current work which cannot be solved unless a different musculoskeletal model is chosen; however, the adopted musculoskeletal model has been rigorously built and validated by Lavaill and colleagues [63], [249], representing a valid state-of-the-art shoulder musculoskeletal model. It brings out a weak point of Myobolica, that is to be addressed in the future in order to mitigate the impact of the underlying musculoskeletal model's defects on the predicted solution space. A planned development will be the replacement of the deterministic inverse dynamics model, currently in use to estimate the joint torques, with a stochastic one, following what has already been done with the stochastic model predicting the muscle forces. This improvement will allow to take into account the uncertainties coming from the inverse dynamics model and to propagate them into the subsequent model that estimate the muscle forces.

The results showed how small perturbations in muscle control could lead to significantly different joint contact forces, suggesting again the importance of remembering that non-healthy subjects may control muscles in a completely different way than we may hypothesise. Providing a spectrum of solutions – instead of an individual solution – can be more suitable for a clearer glance at the specific subject muscle control.

Declaration of competing interest

The authors declare that they have no known competing financial interests or personal relationships that could have appeared to influence the work reported in this paper.

Acknowledgments

GD received funding from the European Union - NextGenerationEU through the Italian Ministry of University and Research under PNRR - M4C2-I1.3 Project PR_00000019 "HEAL ITALIA" to Marco Viceconti (CUP J33C22002920006). The Australian Research Council (IC190100020, FT180100338) is also gratefully acknowledged. The authors declare that they do not have any financial or personal relationships with other people or organisations that could have inappropriately influenced this study.

Supplementary file

Muscle forces solution spaces analysis – Material and Methods

As explained in the main document, the experimental data were collected on a 64-year-old man implanted with an instrumented right shoulder prosthesis, which was part of a publicly available dataset. The data is composed of three consecutive shoulder slow abductions while holding a 2.4 kg weight. Stochastic simulations were performed with Myobolica sampling 10^5 solutions every 30 timeframes of the simulation. In particular, in the EMG-informed stochastic simulations the initial tentative solution – for the muscles informed with EMG – was the EMG-derived force with a 50 % error. Supplementary Table 1 reports the updated the gamma values for the muscles that were

modelled with multiple actuators (e.g., the deltoids muscle is modelled with 15 actuators), by normalising the experimentally determined gamma value to the number of actuators.

To assess the impact of the EMG-based constraint on the muscle force solution spaces, the reduction of the solution space was estimated as the difference between the average bandwidth in the initial simulation (labelled Default, not EMG-informed with experimentally derived – non-muscle-specific – gamma values) and each subsequent one.

Muscle forces solution spaces analysis – Results and Discussion

The width of the muscle force solution spaces tended to decrease when the EMG-based constraint was introduced (Supplementary Figure 1). The largest variation (compared to the Default simulation) was observed when the EMG data from the deltoids, biceps, triceps and trapezius muscles were provided altogether (All EMGs simulation; Supplementary Figure 1). However, while in the All EMGs simulations the width of the muscle force solution spaces was substantially reduced (by approximately 60-70 %) for the muscle more involved in the analysed task (i.e., deltoid, biceps, triceps), it increased (by up to ~140-220%) for other muscles, such as pectoralis and latissimus dorsi, which are marginally involved in a shoulder abduction task (i.e., they generate little force in absolute terms) and for which no experimental data were provided; this should not mislead the reader, since the few muscles significantly increasing the width showed a very close to zero activation level both in the Default simulation (which led to a high percentage variation) and in the optimal solution. A notable exception is represented by the trapezius muscle: the width of its solution space increased by ~180 % when informed by experimental EMG data (All EMGs simulation; Supplementary Figure 2). As shown in the figures below, the new constraint influenced also the solution space predicted for muscles not informed with EMG data (e.g., the supraspinatus and the subscapularis muscles).

Supp.Table 1. Summary of the number of muscle-tendon actuators modelling each muscle and the muscle-specific gamma parameter adopted for all actuators of each muscle. Trapezius and deltoid muscles are listed with the names they are more often described for clarity.

Muscle name	Number of actuators	Specific gamma value
Trapezius clavicularis (descending)	2	0.2250
Trapezius scapularis (transverse)	8	0.0562
Trapezius scapularis (ascending)	3	0.1500
Deltoid scapularis (posterior)	3	0.1500
Deltoid scapularis (medial)	8	0.0562
Deltoid clavicularis (anterior)	4	0.1125
Coracobrachialis	3	0.1500
Infraspinatus	6	0.0750

Teres minor	3	0.1500
Teres major	4	0.1125
Supraspinatus	4	0.1125
Subscapularis	11	0.0409
Biceps long head	1	0.4500
Biceps short head	2	0.2250
Triceps long head	4	0.1125
Latissimus dorsi	6	0.0750
Pectoralis major toracic	6	0.0750
Pectoralis major clavicularis	2	0.2250

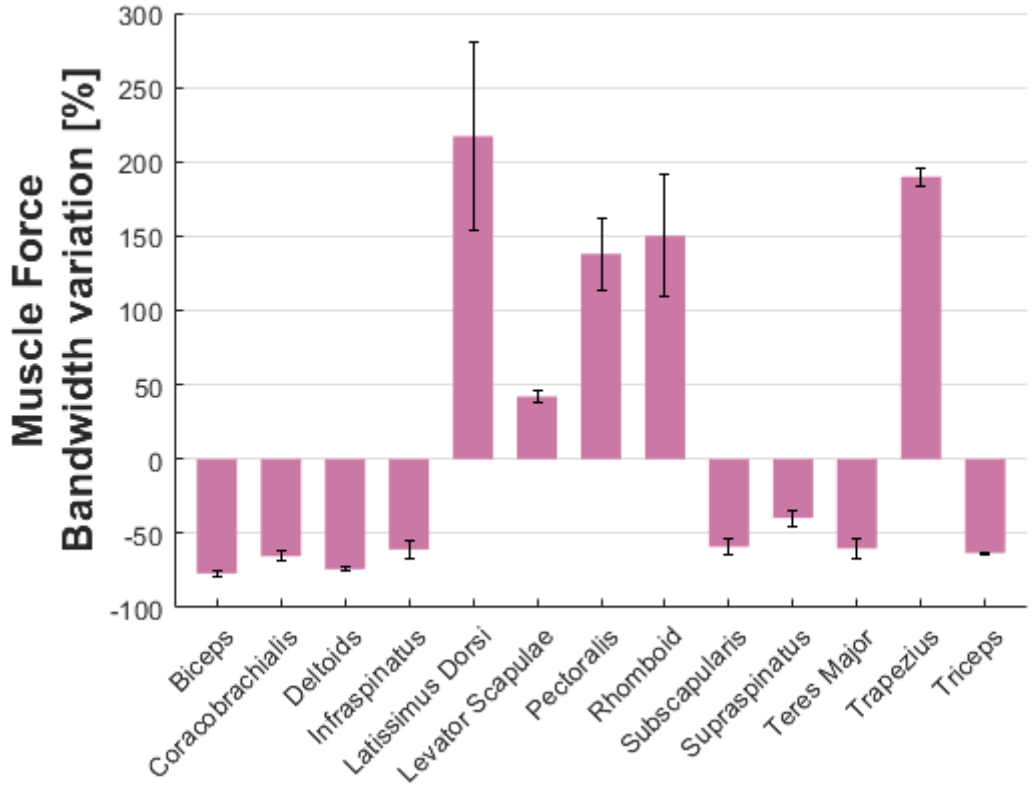

Supp.Fig. 2. Mean and standard deviation across the three trials of each muscle group solution space variation between the Default simulation and the All EMGs simulation.

Results from all analysed trials

Glossary

Default: Myobolica simulation obtained without applying the muscle-specific gamma parameter and the EMG-based constraint.

MS gamma parameter: Myobolica simulation obtained by applying the muscle-specific gamma parameter but not the EMG-based constraint.

Delt. EMG: Myobolica simulation obtained by applying the muscle-specific gamma parameter and the EMG-based constraint with the deltoid muscle EMG data.

Bic. EMG: Myobolica simulation obtained by applying the muscle-specific gamma parameter and the EMG-based constraint with the biceps muscle EMG data.

Tric. EMG: Myobolica simulation obtained by applying the muscle-specific gamma parameter and the EMG-based constraint with the triceps muscle EMG data.

Trap. EMG: Myobolica simulation obtained by applying the muscle-specific gamma parameter and the EMG-based constraint with the trapezius muscle EMG data.

All EMGs: Myobolica simulation obtained by applying the muscle-specific gamma parameter and the EMG-based constraint with the deltoid, biceps, triceps and trapezius muscle EMG data.

Optimal solution: Solution obtained by using OpenSim tools (Static Optimization tool and Analyze tool).

Experimental data: Glenohumeral (GH) joint contact force measured with the instrumented shoulder prosthesis.

Glenohumeral joint contact force

Comparison of the glenohumeral (GH) joint contact force – normalised to the subject's body weight – predicted with the distinct Myobolica simulations, the optimal solution, and the experimental data for the three trials (named trial 1, trial 2, and trial 3). The R^2 and RMSE between the experimental data and the median solution of each Myobolica bandwidth are reported.

Trial 1

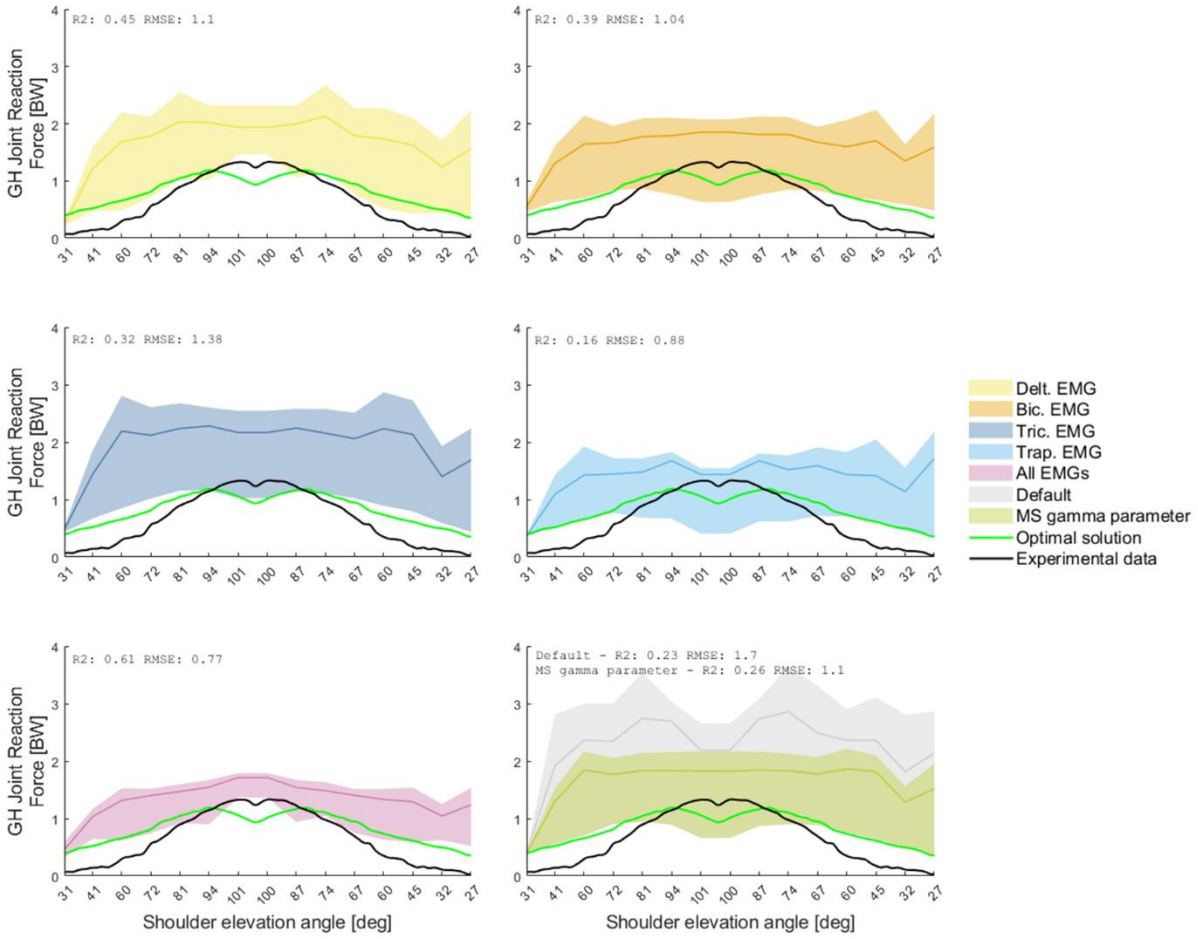

Trial 2

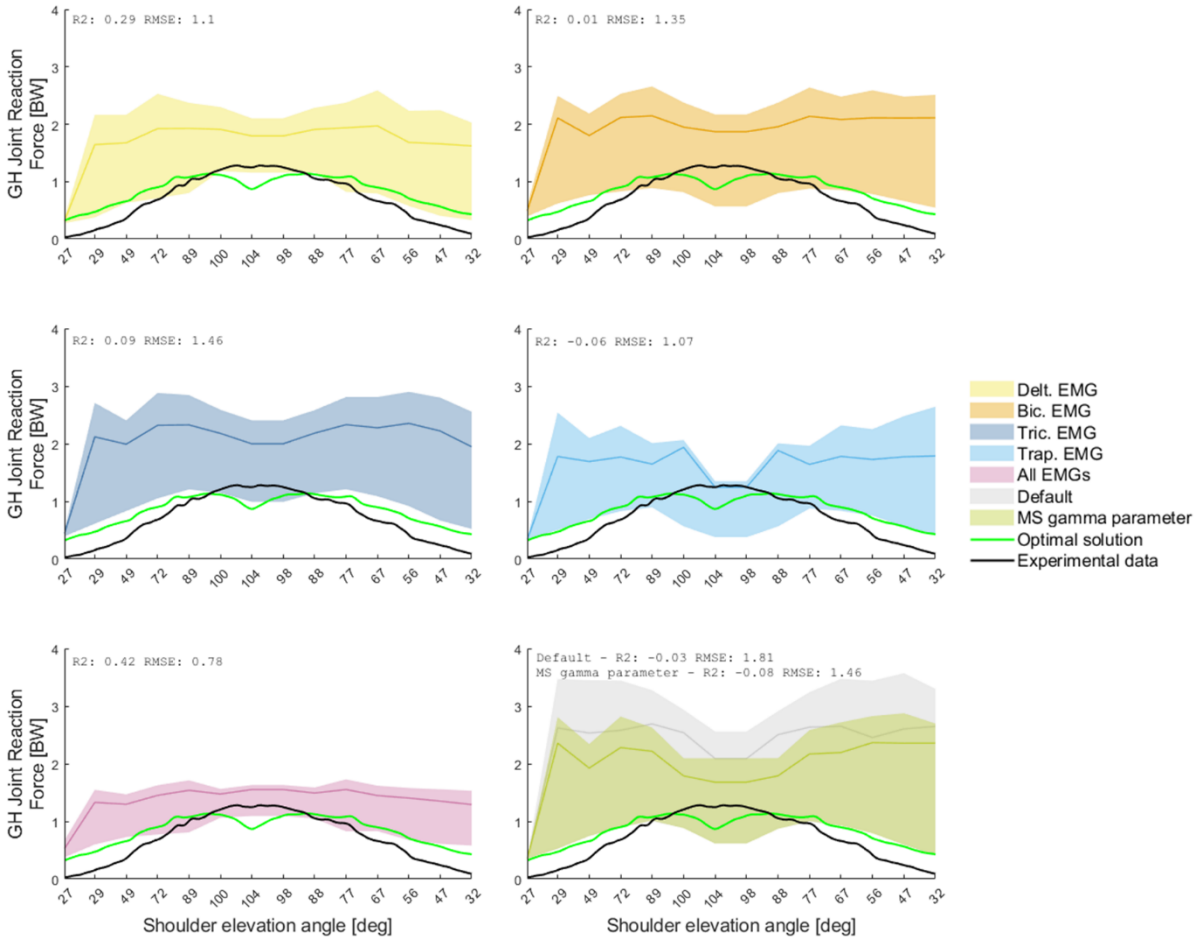
R2: 0.29 RMSE: 1.1
R2: 0.01 RMSE: 1.35
R2: 0.09 RMSE: 1.46
R2: -0.06 RMSE: 1.07
R2: 0.42 RMSE: 0.78
Default - R2: -0.03 RMSE: 1.81
MS gamma parameter - R2: -0.08 RMSE: 1.46
GH Joint Reaction Force [BW]
Shoulder elevation angle [deg]
27 29 49 72 89 100 104 98 88 77 67 56 47 32
Delt. EMG
Bic. EMG
Tric. EMG
Trap. EMG
All EMGs
Default
MS gamma parameter
Optimal solution
Experimental data

Trial 3

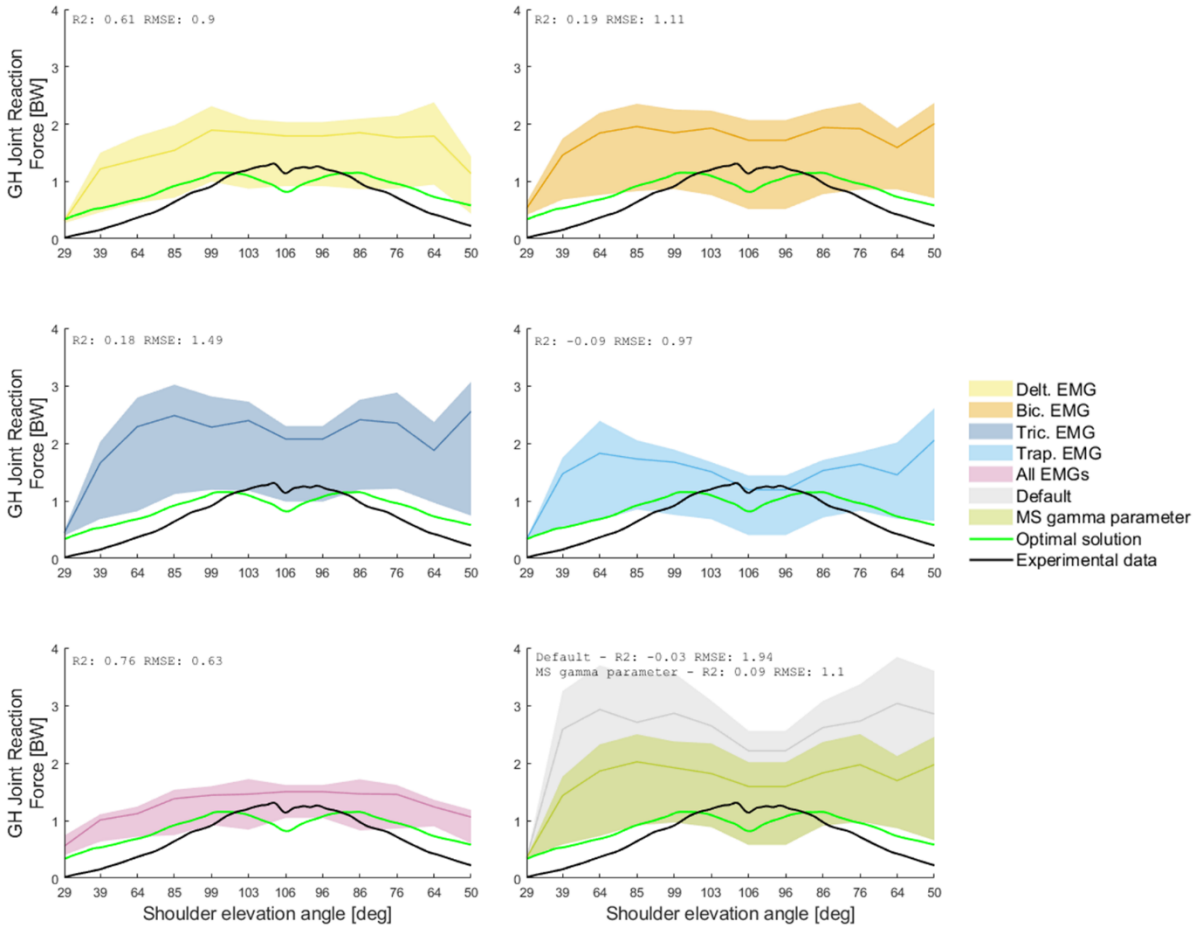

Supp.Table 2. R^2 and RMSE between Myobolica median solutions and the optimal solution estimated with OpenSim for the GH joint contact force of the three trials. In the last row, the R^2 and RMSE values between the experimental data and the optimal solution are shown.

Simulation	R^2			RMSE [BW]		
	Trial 1	Trial 2	Trial 3	Trial 1	Trial 2	Trial 3
Default	0.44	0.91	0.15	2.31	2.43	2.57
MS gamma parameter	0.39	-0.05	0.34	1.68	2.03	1.72
Delt. EMG	0.59	0.45	0.74	1.72	1.74	1.59
Bic. EMG	0.47	0.11	0.41	1.63	1.96	1.75
Tric. EMG	0.48	0.25	0.39	1.99	2.1	2.14
Trap. EMG	0.26	0.05	0.03	1.43	1.64	1.52
All EMGs	0.61	0.50	0.81	1.37	1.40	1.29
Experimental data	0.88	0.86	0.76	0.78	0.80	0.78

Muscle force solution spaces

Comparison of muscle force solution spaces for ten muscles of interest predicted with the distinct Myobolica simulations, the optimal solution, and the normalised EMG for the three trials (named trial 1, trial 2, and trial 3). The chosen muscles are biceps short head, deltoid clavicularis, deltoid scapularis, subscapularis, supraspinatus, trapezius clavicularis, trapezius scapularis, triceps long head. The term “head (*number*)” stands for the selected muscle actuator chosen among the actuators modelling the single muscle.

Trial 1

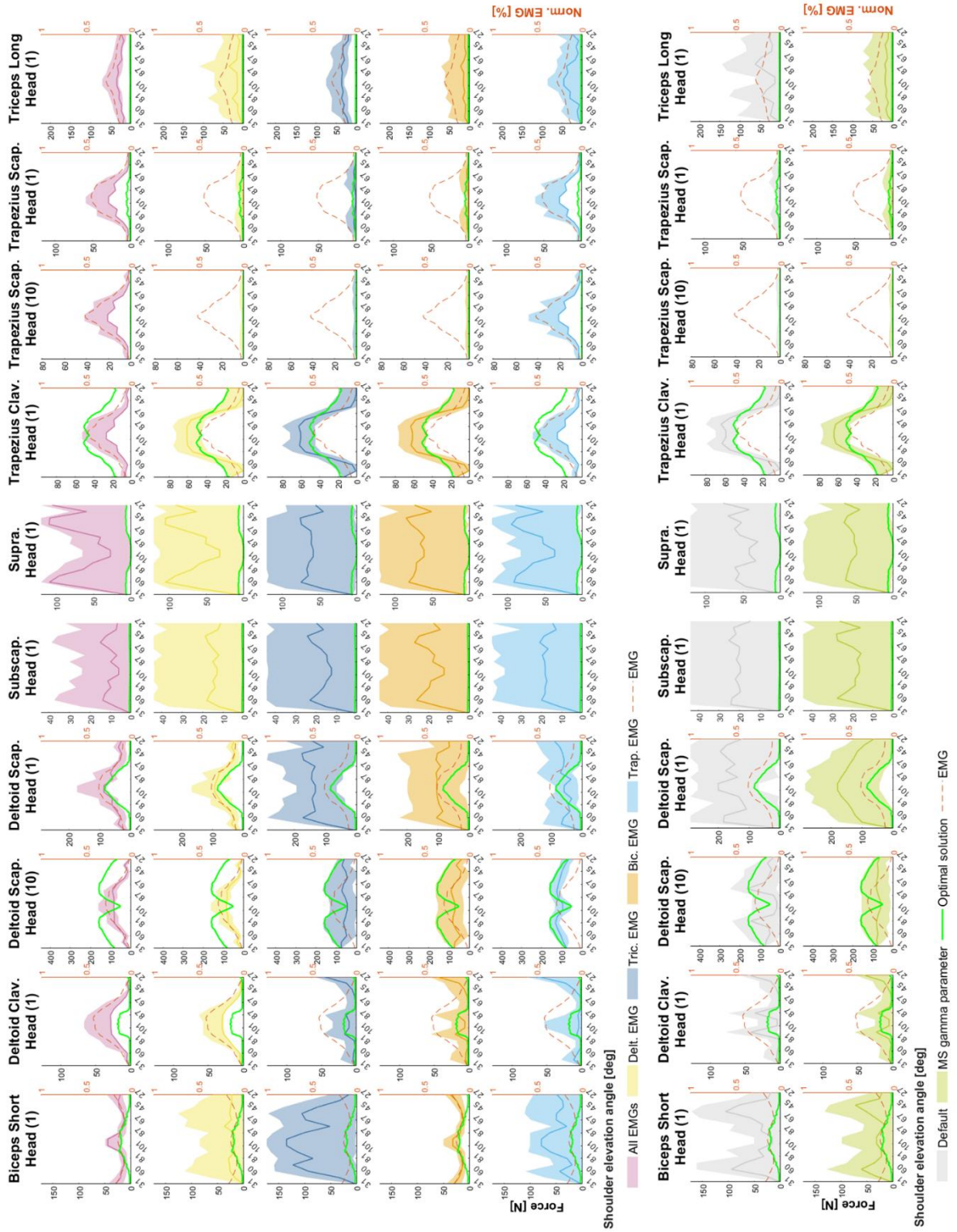
Biceps Short Head (1)
Deltoid Clav. Head (1)
Deltoid Scap. Head (10)
Deltoid Scap. Head (1)
Subscap. Head (1)
Supra. Head (1)
Trapezius Clav. Head (1)
Trapezius Scap. Head (10)
Trapezius Scap. Head (1)
Triceps Long Head (1)
Norm. EMG [%]
Force [N]
Shoulder elevation angle [deg]
All EMGs
Delt. EMG
Tric. EMG
Bic. EMG
Trap. EMG
EMG
Default
MS gamma parameter
Optimal solution
EMG

Trial 2

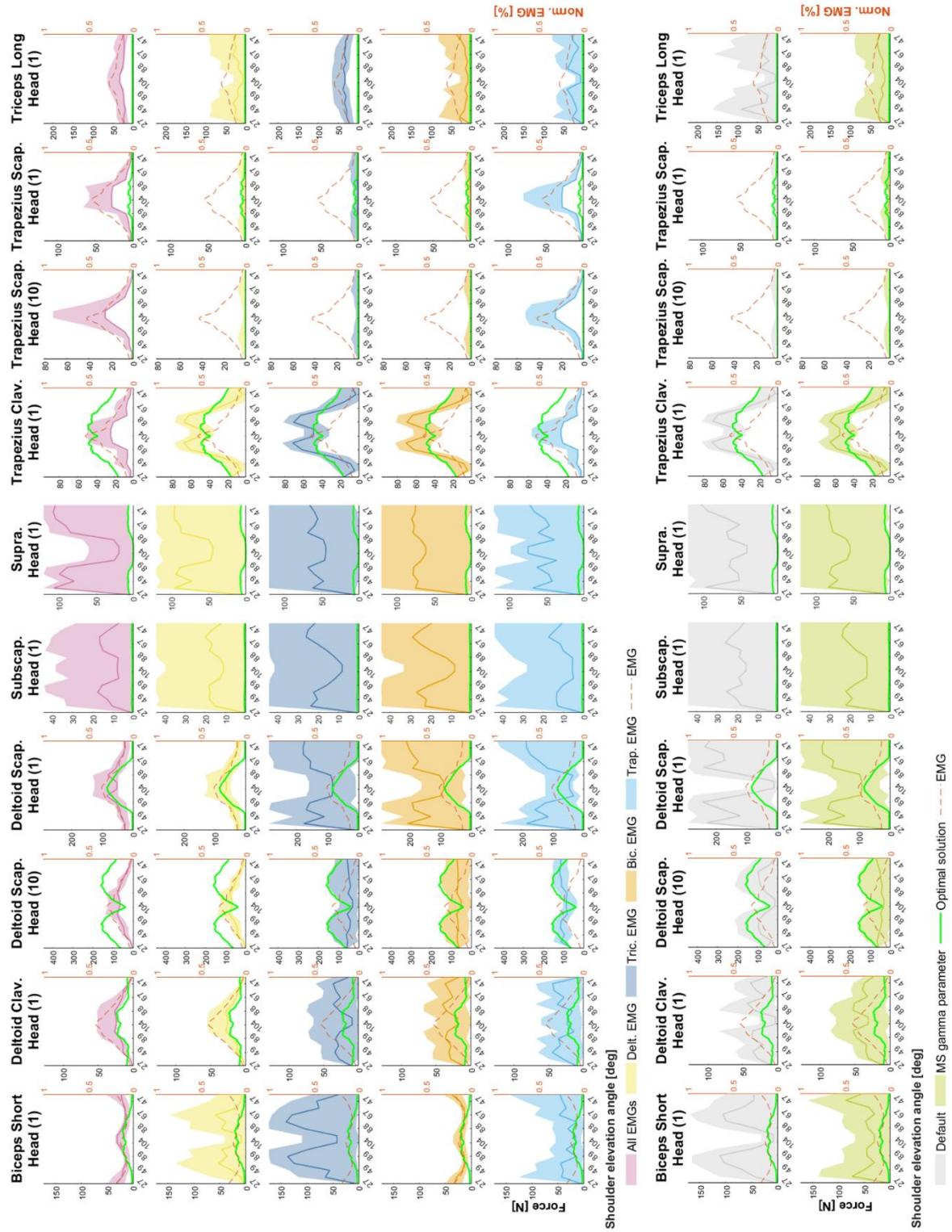
Biceps Short Head (1)
Deltoid Clav. Head (1)
Deltoid Scap. Head (10)
Deltoid Scap. Head (1)
Subscap. Head (1)
Supra. Head (1)
Trapezius Clav. Head (1)
Trapezius Scap. Head (10)
Trapezius Scap. Head (1)
Triceps Long Head (1)
Norm. EMG [%]
Force [N]
Shoulder elevation angle [deg]
All EMGs
Delt. EMG
Tric. EMG
Bic. EMG
Trap. EMG
EMG
Default
MS gamma parameter
Optimal solution

Trial 3

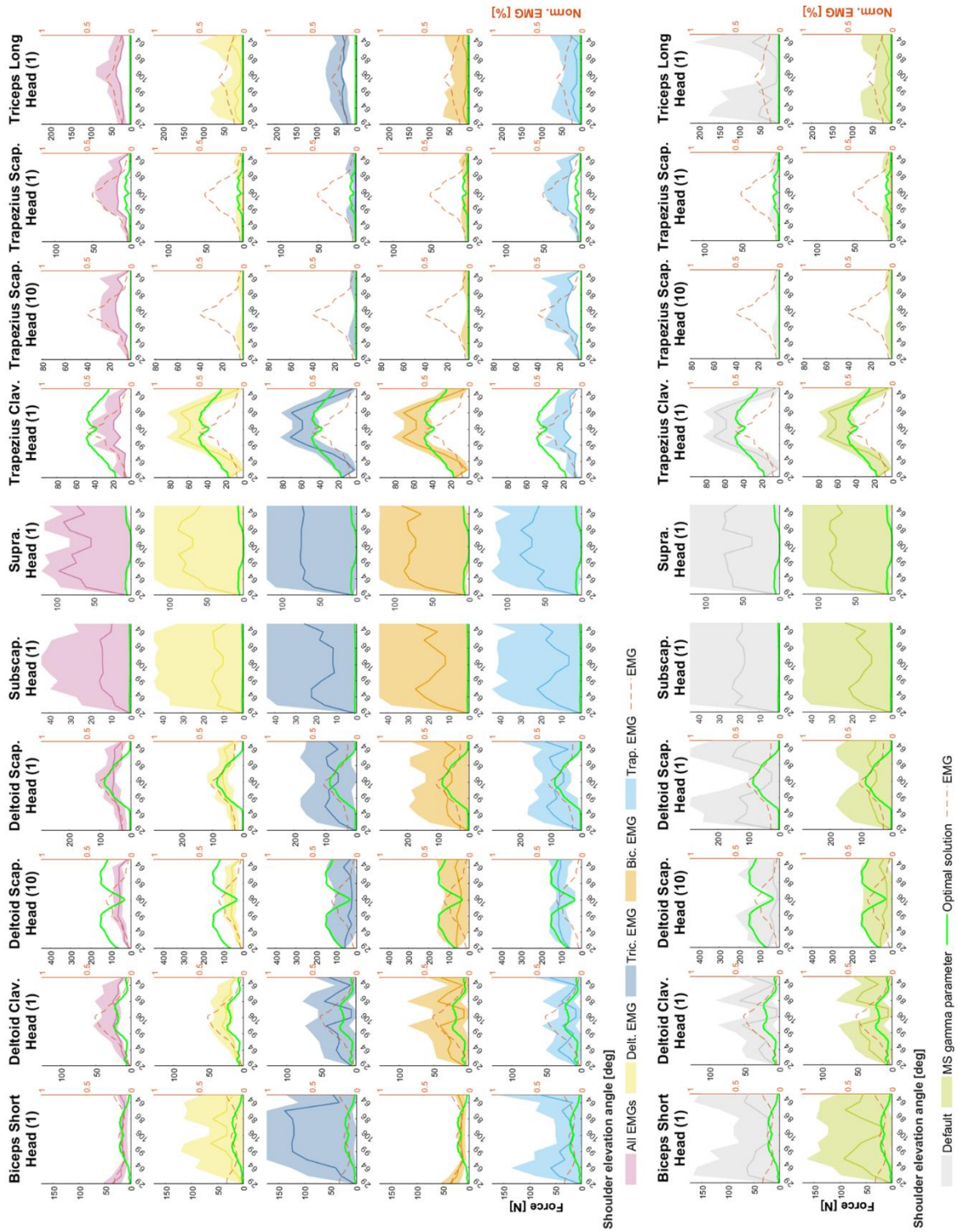
Biceps Short Head (1)
Deltoid Clav. Head (1)
Deltoid Scap. Head (10)
Deltoid Scap. Head (1)
Subscap. Head (1)
Supra. Head (1)
Trapezius Clav. Head (1)
Trapezius Scap. Head (10)
Trapezius Scap. Head (1)
Triceps Long Head (1)
Norm. EMG [%]
Force [N]
Shoulder elevation angle [deg]
All EMGs
Delt. EMG
Tric. EMG
Bic. EMG
Trap. EMG
EMG
Default
MS gamma parameter
Optimal solution
EMG

Explorative assessment of the knee joint load variability in four patients with Parkinson's disease

Introduction

Parkinson's disease (PD) is a neurodegenerative disorder affecting about 1-2 % of the population over the age of 65 [253], [254]. PD is mainly caused by the formation of Lewy bodies, aggregates of α-synuclein proteins in the *substantia nigra,* and a degradation of the dopaminergic neurons [253], [255]. As a result, people with PD present substantial motor impairments, including tremor, slowness of movements, rigidity, reduced gait speed, and step length, which worsen as the disease progresses [34]. Disease severity and progression are commonly evaluated employing the Hoehn & Yahr scale (H&Y) [256] or the Unified Parkinson's Disease Rating Scale (in the version revised by the Movement Disorder Society, MDS-UPDRS) [32]. Both are globally recognised and adopted by the reference clinical community, and rate motor and non-motor disease aspects to provide information about the clinical picture [257]. Early-stage symptoms are often unilateral [34], [258] and generally comprise reduced joint range of motion and muscle power at the hip, knee, and ankle [259], [260]. As the disease progresses, symptoms can get bilateral, with shuffling steps, increased double limb support, reduced arm swing, and blocks in motor function, reduced balance and dyskinesia [259].

There is currently no cure for PD. Treatments mainly aim to reduce the impairments with dopaminergic medications [34]. In particular, the gold standard medication is the Levodopa (L-DOPA) which is a direct precursor of dopamine [254]. The use of the precursor is necessary to penetrate the blood-brain barrier and thereafter convert to dopamine in situ (on the opposite, directly administering dopamine would poorly penetrate that barrier) [254]. The administration of the dopaminergic medication generally establishes a fluctuation in the symptoms control. When the medication is working effectively, symptoms tend to be more controlled; clinicians commonly name it as "on" phase (or state). Conversely, when the medication effect decrease, symptoms resurface; the common name used by clinicians is "off" phase (or state) [253]. Although pharmacological treatment is often preferred, deep-brain stimulation (DBS) may be performed [261]. Some non-pharmacological interventions are also documented and based on rehabilitation exercises to improve motor control, strength, and balance [259], [262]. Studying the movements of subjects with PD can help improve the clinical case interpretation, for example, predicting disease severity and progression, and outlining an individualised treatment intervention [35], [42]. Unfortunately, the variability of motor symptoms given by the individual PD phenotype, the disease stage, the responsiveness to the treatment, compounded with ageing, does not always allow for a unidirectional relation of a muscle control pattern to altered locomotion parameters [260]. Muscle force reduction [263] and variability in the produced force [264] may manifest together with a decrease in the rate of force development [26], [264]. Weakness might be imputed to impaired muscle contraction [22] or central activation deficits [28], as it is seen for other neurological disorders [25]. In response to the above motor impairments, people with PD are likely to adopt compensatory strategies while performing their activities of daily

living (ADLs) [265]. However, this mechanism tends to produce less optimal locomotion [260] and generate a high intra- and inter-subject variability.

This variability should be accounted for if computer models and simulations are to be used to support the clinical management of people with PD. Traditional methods to estimate the muscle activation patterns and muscle forces that produce a specific motion fail to capture such variability, as they rely on motion capture data (that cannot provide information on the neuromotor behaviour) and implement cost functions yielding solutions that can be considered valid for healthy individuals performing simple locomotor tasks [90] but not to model pathological neural control [266]. To this end, researchers may leverage experimental electromyography (EMG) data to estimate more physiological muscle activations via EMG-informed or EMG-assisted approaches, which can result in more accurate simulations when modelling subjects affected by neurological disorders [266], [267]. However, EMG data may not always be available (or of high enough quality) and are typically only collected on a small subset of muscles.

New methods have been studied to address this limitation. One option is to employ factorisation methods, such as the non-negative matrix factorisation, to assess patterns in the coordinate activation of muscles (i.e., muscle synergies) and reduce the number of experimental EMG signals collected [58], [268]. Alternatively, one could perform predictive simulations to simulate different control strategies by optimising one or more performance criteria without requiring experimental data [269]. Unfortunately, this modelling approach is very computationally demanding, requiring several hours to estimate one motor task, and often lacks the accuracy of predictions of individual patients. Another recent modelling approach, the stochastic approach, can estimate a plausible band of several muscle activation patterns modelling the variability in the muscle control by adopting Bayesian statistics [141], [246], but with the drawback of dependency on the same kinematics. It also requires several hours, but in return provides a band of solutions instead of an individual one [246], enabling characterisation of the subject.

The aim of this work is to assess the impact of impaired kinematics on variations in the knee joint loading force patterns in subjects with PD. To this end, we will employ a stochastic approach (i.e., Myobolica) to investigate subjects with PD from a publicly available kinematics dataset. The hypothesis we would like to test in this work is the possibility of highlighting differences in the on and off medication phases.

Materials and methods

The data employed in this study are part of a publicly available dataset, including motion capture, demographical, and clinical data from a cohort of patients with PD performing overground walking trials in a gait laboratory [270]. Specifically, experimental data from four participants (2M/2F, weight = 76.39 ± 16.88 kg, height = 172 ± 4.83 cm, age = 59.75 ± 12.61 years. Table 6) were selected. The dataset contained clinical data regarding the disease assessment, such as ongoing rehabilitation, comorbidities, and H&Y or UPDRS scales scores. Notably, the dataset comprised both “on” and “off” medication conditions for all participants, where “on” meant that the patients took dopaminergic medication one hour before the session, and “off” meant that no medications were taken in the 12 hours prior to the test.

About 15 to 37 walking trials (complete strides) per patient had the patient correctly stepping on the force platforms and were elaborated and employed in the simulations. Both left and right steps (on the force platform) were considered for the biomechanical simulations to gather a significant amount

of experimental data for the on and off phases; in addition, to account for all the possible variability without unbalancing the dataset toward one leg or one medication phase, all appropriate data were employed leading to the analysis of different number of trials for different subjects (SUB02: 15 trials; SUB15: 16 trials; SUB17: 37 trials; SUB19: 25 trials). The raw data (in C3D file format) were processed in MOtoNMS [271] to obtain files compatible with the open-source modelling and simulation software OpenSim [197].

Table 6. Subject information (gender, age, height and weight) was reported together with information related to the pathology severity, which is described by specifying if the subject showed episodes of "freezing of gait" and by the score on the Hoehn & Yahr scale for Parkinson's disease (1 is the lowest stage, five is the most severe one).

ID	SUB02	SUB15	SUB17	SUB19
Gender	F	F	M	M
Age	53	66	46	74
Height [cm]	170	168	171	179
Weight [kg]	62.55	86.95	61.5	94.55
Dominant hand	Right	Right	Left	Right
Freezing of Gait	Non-freezer	Freezer	Freezer	Non-freezer
Levodopa equivalent dose (mg/day)	275	600	1200	250
Hoehn & Yahr (on / off medication)	1 / 1	4 / 4	1 / 2	3 / 3
UPDRS III (on / off medication)	7 / 10	38 / 35	2 / 6	15 / 29
UPDRS III – rigidity (on / off medication)	3 / 2	5 / 9	0 / 1	1 / 5
UPDRS III – walking (on / off medication)	0 / 0	2 / 2	0 / 1	1 / 1

The generic musculoskeletal model "Full Body Model" [272] was scaled to match each subject's anthropometry, using the dedicated tool in OpenSim [197]. Subsequently, the upper body was removed to minimise the computational cost and to focus on the lower limb. The employed model comprised 12 bodies (femur, tibia, patella, talus, calcaneus, and toes, on both sides), 14 degrees of freedom (three at the hip, one at the knee, ankle, subtalar, and metatarsophalangeal joint for each leg), and 80 muscle-tendon actuators (Figure 24).

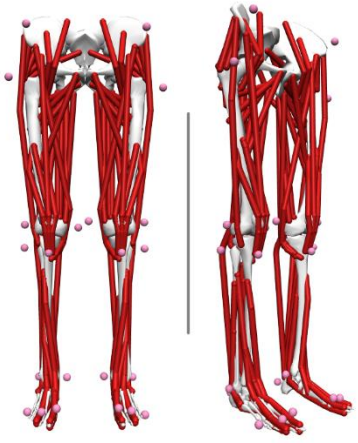

Figure 24. The musculoskeletal generic model was adopted in this study. The torso has been removed after the scaling procedure. It is composed of 12 bodies, 14 degrees of freedom, and 80 muscle-tendon actuators.

A set of muscle forces was estimated with static optimisation, the relative knee joint contact force (JCF) solution and the muscle lever arms following the classic inverse approach in OpenSim. Consequently, stochastic simulations were performed within Myobolica [225], [246] to estimate 200k feasible solutions (i.e., muscle force profiles); with the generated solutions, the knee JCFs were calculated employing the OpenSim API for MATLAB (The MathWorks, Inc., 2022. MATLAB version: 9.11 - R2021b). The knee JCF was calculated – for each trial – only for the knee of the leg stepping on the force platform. A summary of the work pipeline is reported in Figure 25.

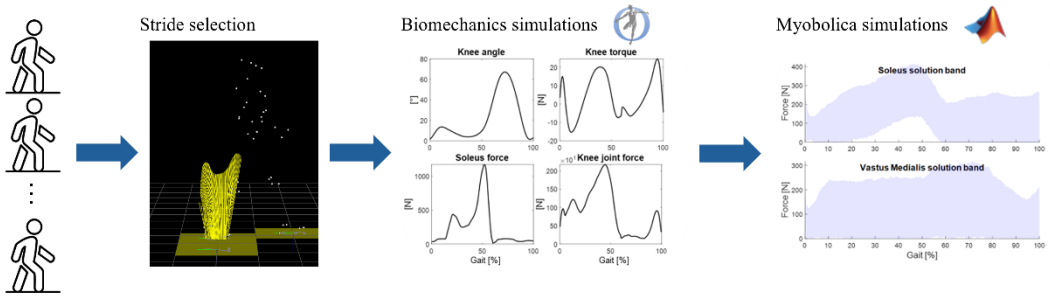

Figure 25. Workflow of this study. Experimental data were chosen to match setup criteria. Then, biomechanics simulations were performed using OpenSim, and lastly, the stochastic solution bands were estimated using Myobolica.

Myobolica stochastic tool uses Bayesian statistics to estimate the posterior probability density function of the variable (accurately described in Chapters 3 and 4). The functioning of Myobolica is strictly linked to two parameters, σ and γ: the first models noise in the equilibrium equation, and the second models the muscle's force development velocity. In this work, σ is defined and set as per Chapter "Myobolica: a stochastic approach to estimate physiological muscle control variability" (Appendix I; σ = 0.12); to define γ, the process described in Chapter "Myobolica: a stochastic approach to estimate physiological muscle control variability" (Appendix I) was followed, while adding in the analysis more values synthetised to estimate a Gaussian distribution with average value zero and standard deviation equal to the γ value (γ=0.005).

Data analysis

For each subject, the predicted knee JCFs were normalised to their bodyweight and sorted in ascending order to select the maximum, minimum, and median Myobolica solutions.

To enable preliminary qualitative comparisons, the selected maximum, minimum, and median solutions from all analysed trials per subject were interpolated to vectors of 101 points, to be expressed in per cent of the gait cycle, and overlayed on the same graph. Similarly, each subject's knee flexion angle was interpolated, and the mean and standard deviation were reported in graphs clustered in the on and off medication phases.

Then, a quantitative assessment was performed by computing the coefficient of determination (R^2) and the root mean squared error (RMSE) between each selected Myobolica solution and the optimal solution from static optimisation, hereby used as reference.

In addition, for each participant, the bandwidth of the Myobolica solution space was calculated for each trial as the difference between the maximum and minimum values at every time step, averaged across the entire gait cycle. For simplicity and conciseness, the average bandwidth values were later reported as mean and standard deviation across the analysed trials, for all subjects independently.

Results

Noticeable differences between the optimal and Myobolica solutions emerged (Table 7). Average values for R^2, RMSE, and the solution bandwidth, across all simulated trials, are reported in Table 7. The lowest correlation with the optimal solution resulted in SUB15 (H&Y 4) and the largest RMSE and average solution bandwidth (Table 7). Moreover, SUB15 showed the largest variability in those parameters. Conversely, SUB02 (H&Y 1) showed the lowest RMSE and average solution bandwidth, but not the highest R^2 observed for SUB17 (H&Y 1-2, on-off).

Clustering the solution by the medication highlighted differences between the two phases (Figure 26 shows the knee JCF profiles for all the analysed subjects, clustered in "on" versus "off" medication). A substantial difference emerged for SUB15, for which the predicted solution spaces differed by 0.77 BW (compared to differences in the clustered optimal solutions of about 0.04 BW; Table 8). For SUB15, the R^2 was lower when the subject was 'off medication' (Table 9; R^2: 0.66 and 0.47, on vs off medication). However, the difference between groups is not larger than each group's variance, while the RMSE is significantly larger (on vs off RMSE: 2.56 vs 3.30). On the contrary, for SUB02 and SUB19, R^2 was lower in the on than in the off medication phase (SUB02 on vs off R^2: 0.67 and 0.71. However, the difference between groups was not larger than each group's variance; SUB19 on vs off R^2: 0.70 and 0.77. The largest bandwidth difference between the on and off medication phase emerged in SUB15 (0.464 BW); the subjects for which those differences are bigger than the measured variances are SUB15 and SUB19. Listed results are coherent with the differences in the subjects' knee kinematics (Figure 27).

Table 7. Average r^2 and root mean square error (RMSE) between knee JCF solutions estimated with Myobolica, the optimal solution estimated via static optimisation, and the average width of the solution band. All trial analysis.

	R^2	RMSE [BW]	Bandwidth [BW]
SUB02	0.695±0.069	0.955±0.065	1.301±0.171
SUB15	0.599±0.210	2.793±0.257	3.467±0.310
SUB17	0.790±0.058	0.984±0.084	1.373±0.193
SUB19	0.733±0.055	0.787±0.056	1.031±0.119

Table 8. Differences across Myobolica median solution profiles of the on and off medication clusters. The average differences between the optimal solutions for the compared cluster are reported for comparison.

	Differences on vs off [BW]	
	Myobolica	Optimal solution
SUB02	0.075±0.055	0.003±0.215
SUB15	0.772±0.209	0.039±0.201
SUB17	0.106±0.075	0.144±0.294
SUB19	0.040±0.092	0.206±0.368

Table 9. Comparison of r^2 and root mean square error (RMSE) between knee JCF solutions estimated with Myobolica and the optimal solution estimated via static optimisation in the on and off medication phases. The average width of the solution bands is reported for both clusters.

	On medication			Off medication		
	r^2	RMSE [BW]	Bandwidth [BW]	r^2	RMSE [BW]	Bandwidth [BW]
SUB02	0.668±0.073	0.955±0.061	1.297±0.185	0.713±0.066	0.955±0.068	1.313±0.186
SUB15	0.659±0.197	2.564±0.251	3.322±0.327	0.465±0.237	3.296±0.270	3.786±0.302
SUB17	0.797±0.057	0.987±0.083	1.379±0.173	0.784±0.059	0.982±0.085	1.368±0.266
SUB19	0.696±0.060	0.798±0.042	0.954±0.133	0.768±0.051	0.777±0.070	1.103±0.127

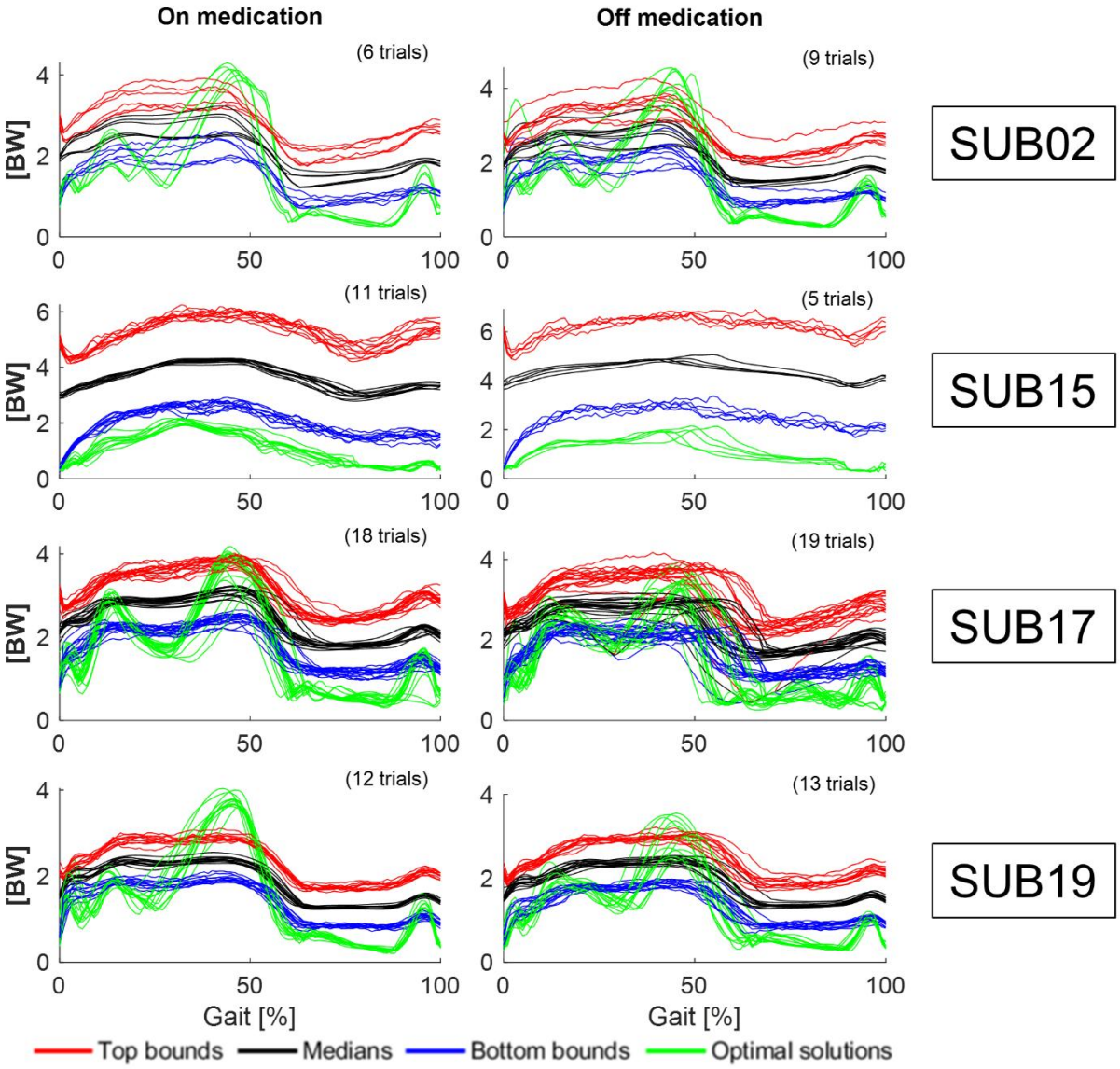

Figure 26. A comparison of all analysed trials was clustered into "on" and "off" medication for all subjects. Red lines are the upper bounds, blue lines are the lower bounds, and black lines are the median solutions of the performed stochastic simulations. The optimal solutions for each analysed trial - estimated via static optimisation - are reported in green. In brackets, the number of simulated trials is mentioned.

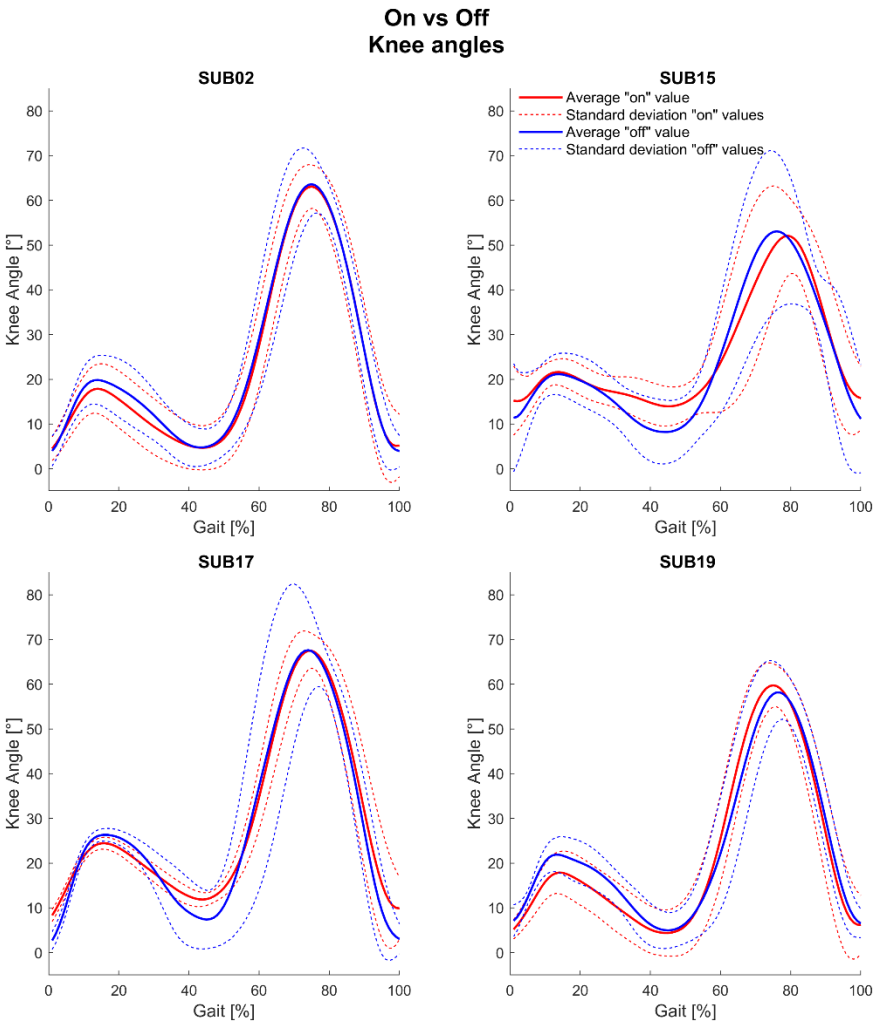

Figure 27. Comparison between predicted knee flexion angles among the on (red lines) and off (blue lines) medication clusters for all analysed subjects. The average values among trials (solid line) and the standard deviation (dashed line) are shown.

Discussion

The aim of this work was to assess the impact of impaired kinematics on the loading pattern of the knee joint in subjects with PD; this was conducted by adopting a stochastic approach (i.e., Myobolica tool) to compute feasible muscle activation patterns and by using the predicted muscle forces to estimate the knee JCFs. In this work, the first to use a stochastic approach in subjects with PD, two main hypotheses were investigated regarding the possibility of leveraging the stochastic approach to dig up differences in the on and off medication phases, and to detect gait asymmetry. Adopting the stochastic approach revealed moderate differences between medication conditions in both the width of the solution bands and the regularity of the solution profiles. These differences likely scaled with the severity of the pathology and were not captured as convincingly by the optimal solution. In contrast, the optimal solution showed a weak correlation with the stochastic solution, suggesting poorer performance in modelling the suboptimal motor control.

To the authors' knowledge, no studies regarding non-invasive estimation of knee JCF in patients with PD are available; so, no direct qualitative comparison with similar works has been possible. Values estimated in this work for subjects with lower H&Y scores – excluding SUB15 – align with ranges available in the literature for older adults with instrumented knee implants (about 1.8 – 3 BW)[214], [273]. Stochastic simulations across all subjects markedly deviated from the predicted optimal solutions, consistently lacking the "M" shaped knee load profile typically observed during overground gait (in healthy individuals); this deviation underlines the impact of impaired kinematics on the knee joint loads. Higher scores in the H&Y scale were associated with worse metrics between the stochastic and optimal solutions, consistent with theoretical expectations; it is worth noticing that, as widely documented in the scientific literature [253], higher scores in the H&Y scale are correlated with older age of the subjects of this analysis. While clustering outcomes were inconsistent, they could successfully distinguish between medication phases in the subject with the worst H&Y score (SUB15, Table 8). For the remaining subjects, the prediction performance was superior when adopting the stochastic approach compared to when leveraging only the optimal solution, yet further investigations are required.

Off medication the subjects exhibited a higher variability in the kinematics (Figure 27), which propagated to predicted JCF profiles. Notably, the two subjects with the highest variability in the knee kinematics (Figure 27, SUB15 and SUB17) were the subjects taking the highest doses of medicaments (600 and 1200 mg/day, respectively; Table 6). This variability impacted the joint loading patterns differently: SUB15, who was classified as severely affected by PD (H&Y 4), showed a slight decrease in the variability and a substantial decrease (about 1 BW) in the magnitude of the knee JCF while on medication. SUB17, with the highest medicament dose, showed a marked increases in the knee joint load variability with shifts in the peak positions and in the magnitude of the joint load while in the off condition.

This work, first in its genre, has few limitations. A generic musculoskeletal model was employed, limiting the accuracy with which subjects' anatomy and muscle properties can be modelled. This limitation, common to studies lacking medical imaging, likely resulted in stronger models' muscles than the actual subjects' and reduces the accuracy of the kinematic chain. Nonetheless, the generic models were rigorously scaled to match each subject's anthropometry following established guidelines [251]. Future access to medical imaging could allow the personalisation of the bone geometries and muscle properties, improving the model fidelity. Beyond this, Myobolica was configured to control muscle forces between zero and each muscle's tetanic force. Ideally, if

electromyography (EMG) data were available, the plausible range of muscle forces could have been constrained, and the muscle force profiles could have been informed by the EMG signal, as in [274]. Conversely, the absence of those might have resulted into solution spaces where the most dysfunctional muscle activations are not predicted by Myobolica; whether this limitation is present cannot be verified without experimental muscle activations. Unfortunately, EMG data are rarely collected in PD populations due to concerns related to the frailty of these individuals.

Simulating together left and right steps may represent a limitation in the conclusions reached, due to the assumption that PD impacted equally both legs and results were not altered by the comprehensive assessment; however, it has been done to make the most of the available dataset. Future applications of Myobolica will aim to expand the work sketched out in Appendix II and evaluate whether the stochastic approach can successfully quantify gait asymmetry, typical of PD.

More work is required to expand the assessment of Myobolica, especially when used to investigate clinical conditions and populations. Future work will be aimed to incorporate relevant clinical information (such as clinical scores of bradykinesia) into the simulations, towards the prediction of quantities and parameters of clinical interest and the identification of clinically meaningful differences. This can be observed in Appendix I, where the occurrence of rigidity could be speculated in subjects' movements in the off condition and it was likely sorted out after the assumption of the medicament. Such a speculation is not particularly replicable with the showed joint load results.

In the authors' opinion, even if it is not currently possible, it should be possible to upgrade Myobolica to leverage motion capture data, IMU, and other inertial sensors; this would allow us to expand the pool of available experimental data.

Despite certain limitations, this work is the first investigation of its kind within this domain. It lays an initial foundation for evaluating the impact of Parkinson's disease on joint loading patterns, thereby paving the way for future research. It is well documented that individuals with Parkinson's disease exhibit altered muscle activation strategies; however, the ability to quantitatively model their neuromuscular control may offer deeper insights into disease mechanisms and provide valuable information for predicting disease progression and severity.

Appendix I. Comparison of kinematics and kinetics

The following Appendix expands the qualitative comparison among subjects' kinematics and kinetics. In particular, hip flexion, abduction and rotation, knee flexion, and ankle flexion angles and torques are shown for the cluster introduced in the Materials and Methods chapter. A quantitative analysis may be redundant, since the solutions predicted with Myobolica already hinge on the subject's kinematics and kinetics (in particular, in the dynamic equilibrium equation, the joint torques and the muscle lever arms – a result of the kinematics – compare). Marked differences emerged between the on and off conditions for all subjects, proportionally to the PD severity. In general terms, the value ranges, both for joint angles and torques, appeared reduced in the off condition; this might suggest a general rigidity (typical of PD) partially sorted out with the assumption of the medicament.

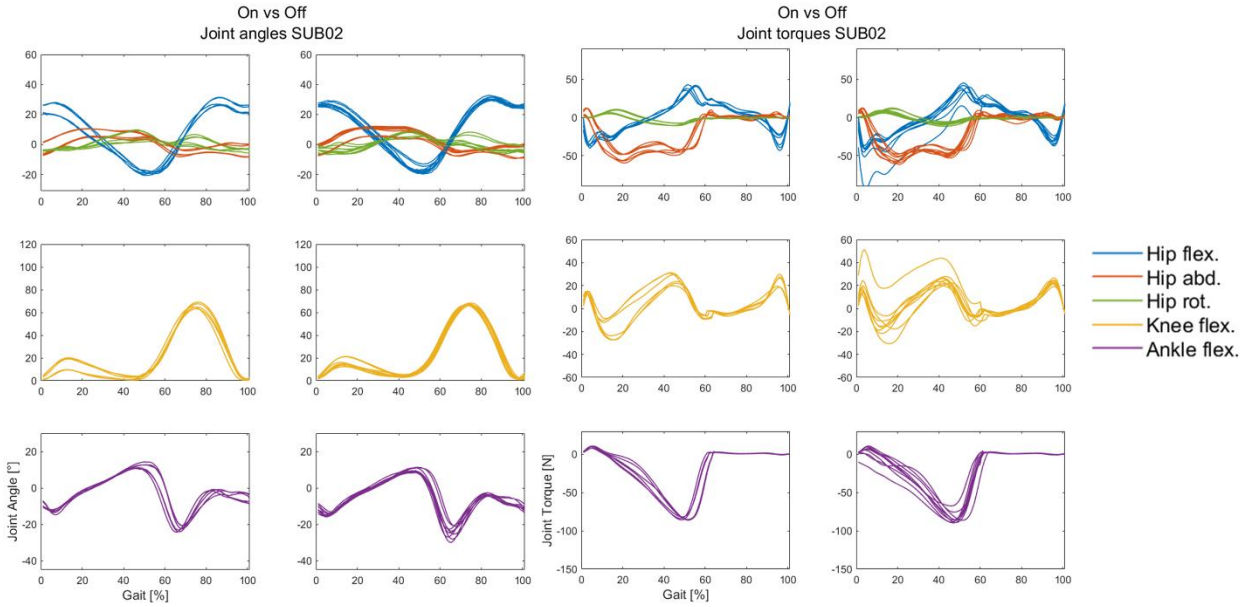

A.Fig. 6. Comparison between predicted hip flexion, abduction, and rotation, knee flexion, and ankle flexion angles (left) and torques (right) among the on and off medication clusters. Graphics for SUB02.

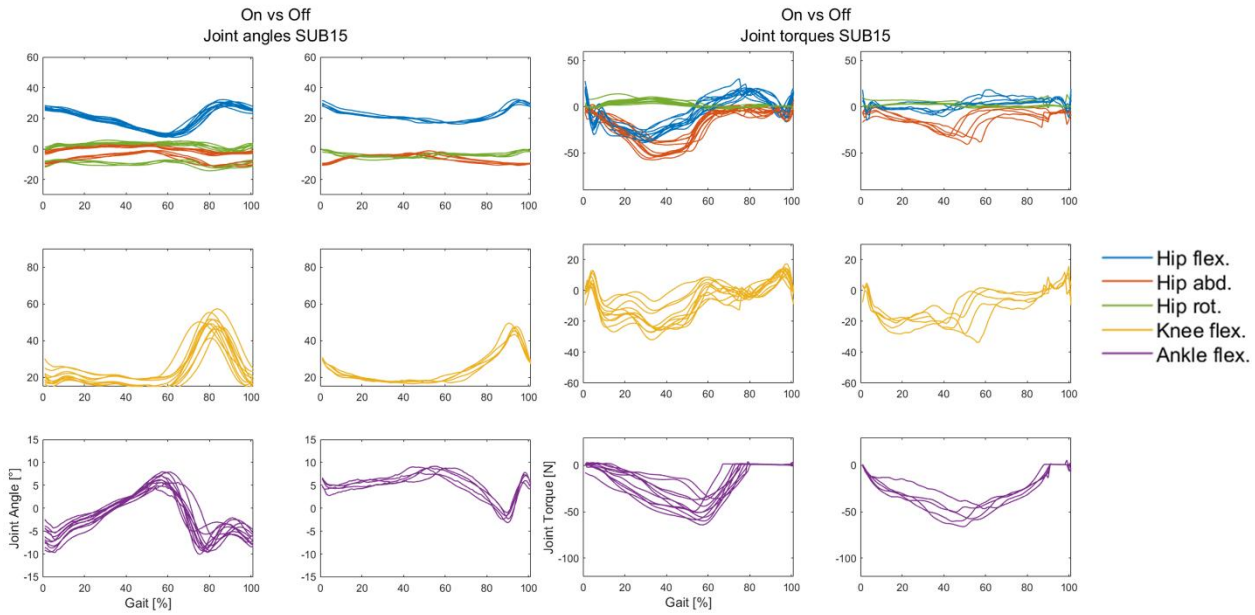

A.Fig. 7. Comparison between predicted hip flexion, abduction, and rotation, knee flexion, and ankle flexion angles (left) and torques (right) among the on and off medication clusters. Graphics for SUB15.

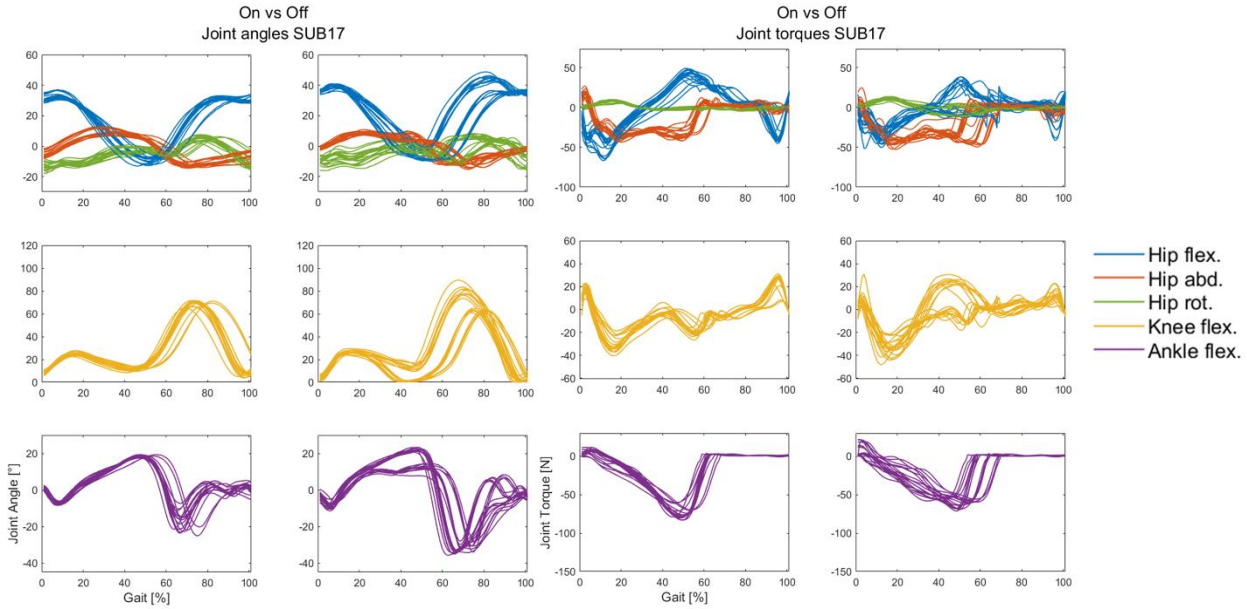

A.Fig. 8. Comparison between predicted hip flexion, abduction, and rotation, knee flexion, and ankle flexion angles (left) and torques (right) among the on and off medication clusters. Graphics for SUB17.

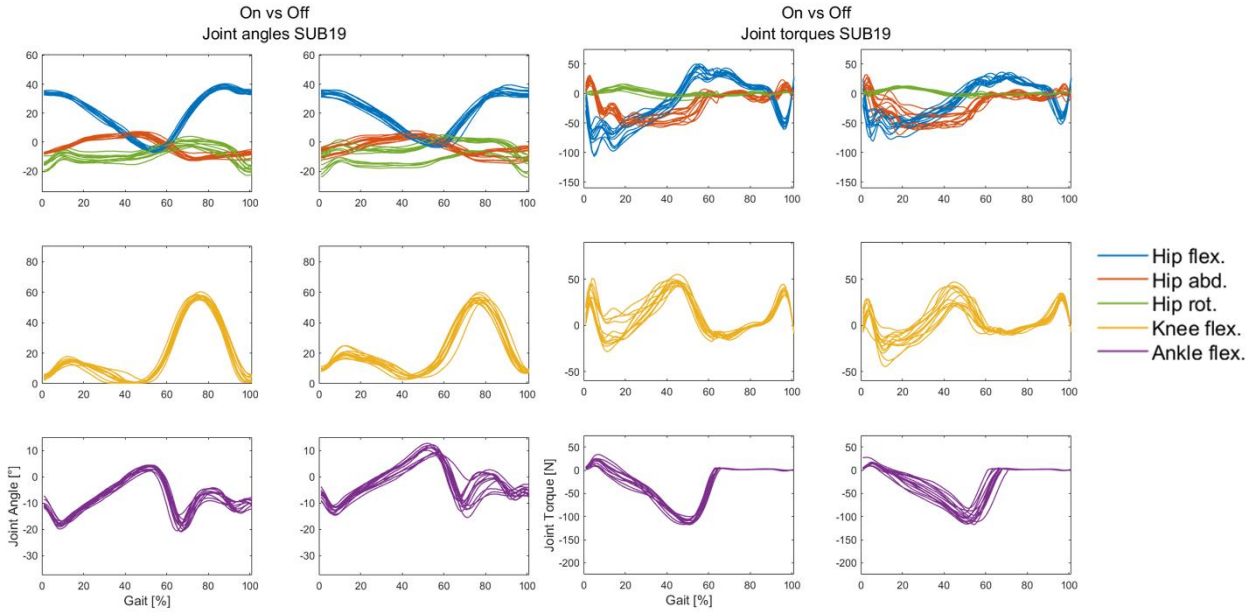

A.Fig. 9. Comparison between predicted hip flexion, abduction, and rotation, knee flexion, and ankle flexion angles (left) and torques (right) among the on and off medication clusters. Graphics for SUB19

Appendix II. Comparison of the left vs the right leg

In the following Appendix, a comparison between the hip flexion, abduction, and rotation, the knee flexion, and the ankle flexion kinematics and dynamics predicted in left and right step trials is reported for each subject. As shown in Appendix figure 14, non-negligible differences emerged between the knee JCFs predicted for the left and right legs. More pronounced differences, in the variability of the solution profiles and in the width of the solution bands, emerged for SUB02 and for SUB15; while

the latter was the most severely affected subject, the first was classified as H&Y 1 thus presenting unilateral symptoms. Because results obtained in the on and off medication conditions were assessed together, no firm conclusions can be drawn regarding potential gait asymmetry in these subjects. Nonetheless, it is reasonable to speculate that Myobolica could be used to predict or quantify gait asymmetry in individuals with PD.

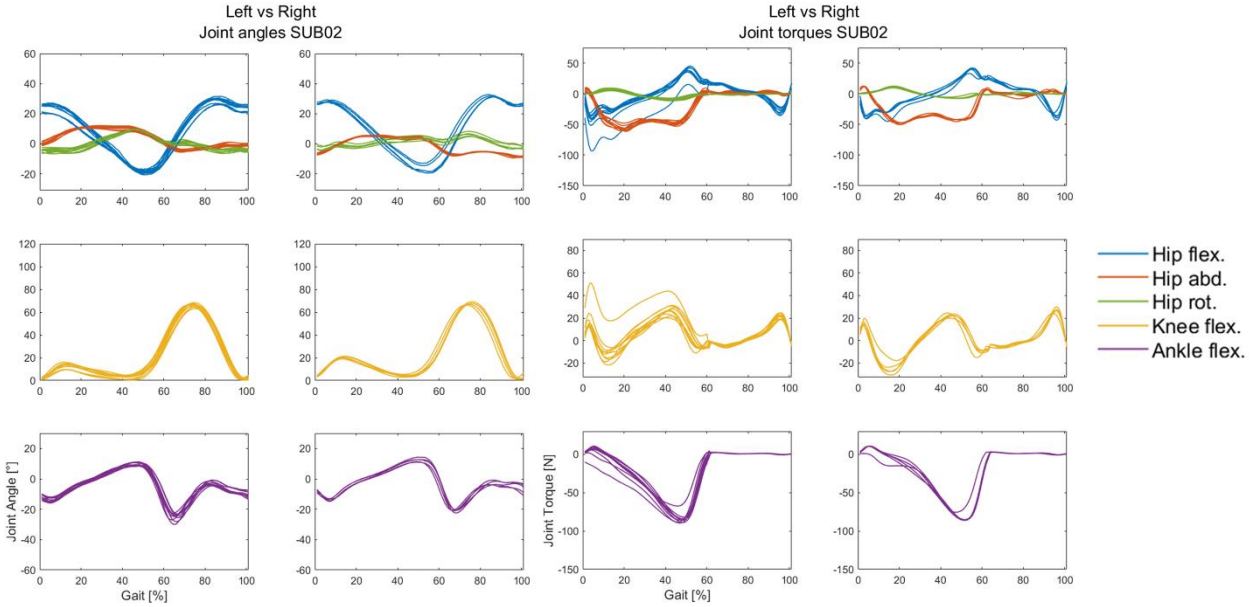

A.Fig. 10. Comparison between predicted hip flexion, abduction, and rotation, knee flexion, and ankle flexion angles (left) and torques (right) among the left and right step trials. Graphics for SUB02.

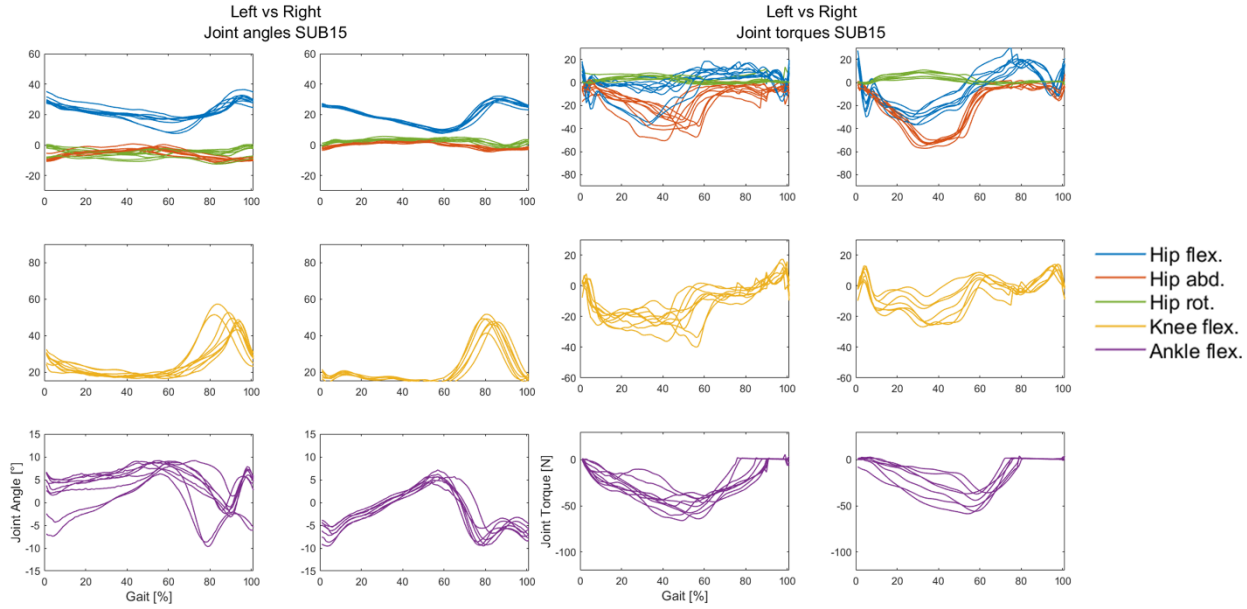

A.Fig. 11. Comparison between predicted hip flexion, abduction, and rotation, knee flexion, and ankle flexion angles (left) and torques (right) among the left and right step trials. Graphics for SUB15.

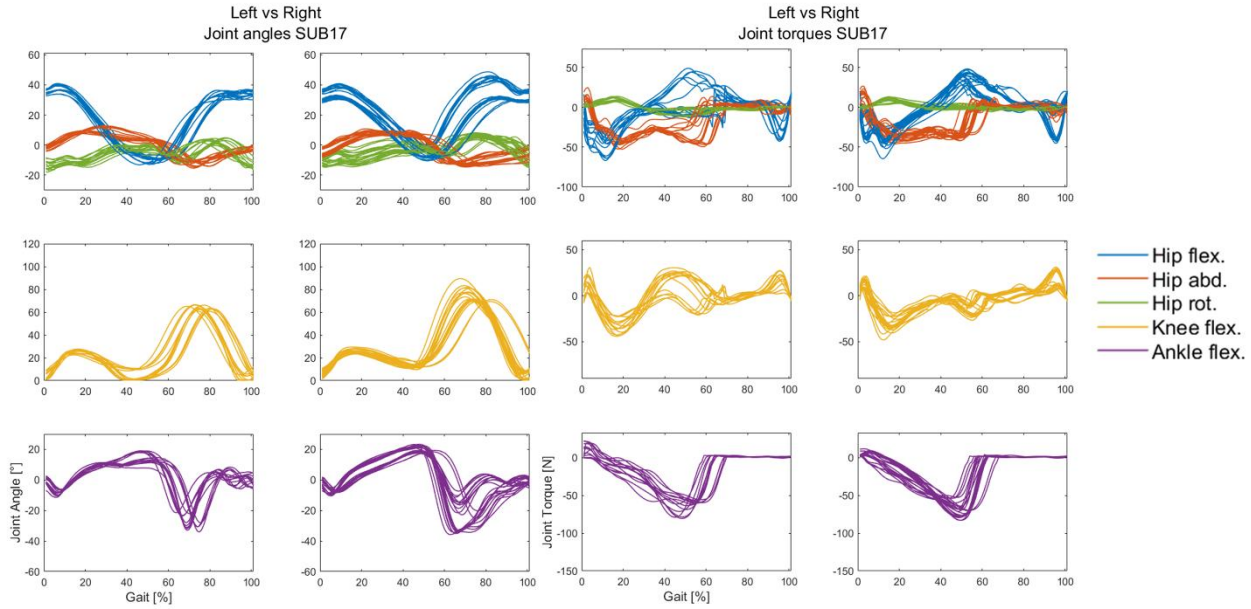

A.Fig. 12. Comparison between predicted hip flexion, abduction, and rotation, knee flexion, and ankle flexion angles (left) and torques (right) among the left and right step trials. Graphics for SUB17.

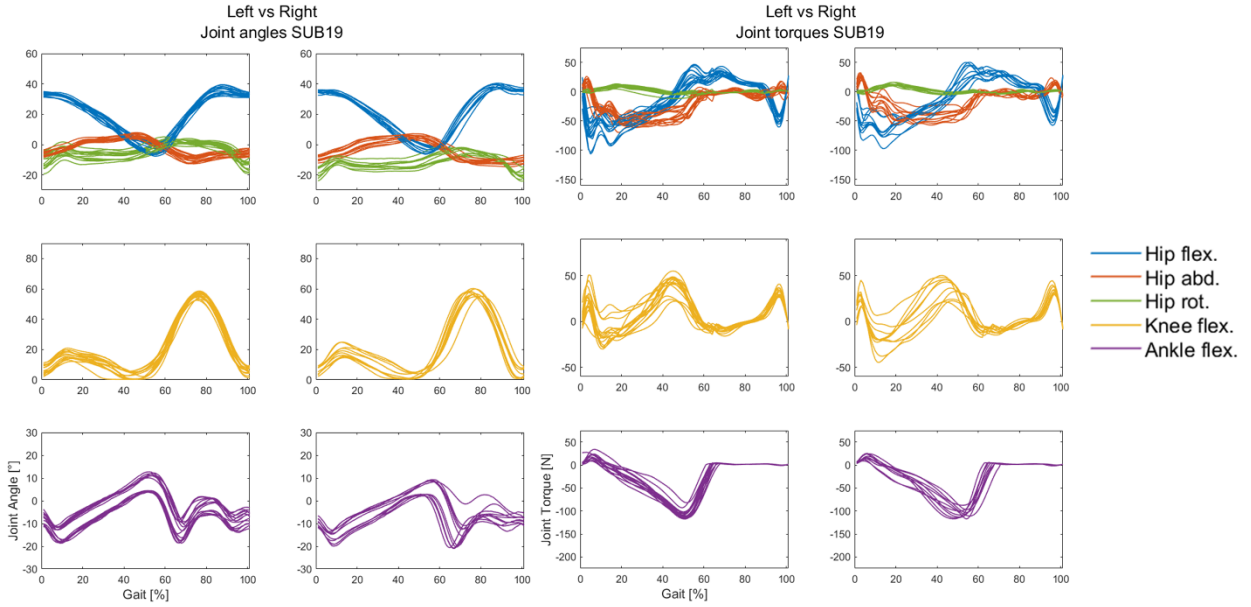

A.Fig. 13. Comparison between predicted hip flexion, abduction, and rotation, knee flexion, and ankle flexion angles (left) and torques (right) among the left and right step trials. Graphics for SUB19.

A.Table.1 Comparison of R^2 and root mean square error (RMSE) between knee JCF solutions estimated with Myobolica and the optimal solution estimated with OpenSim in the left and right leg simulations. The average width of the solution bands is reported for both clusters.

	Left leg			Right leg		
	r^2	RMSE [BW]	Bandwidth [BW]	r^2	RMSE [BW]	Bandwidth [BW]
SUB02	0.717±0.065	1.014±0.073	1.346±0.181	0.656±0.078	0.83±0.051	1.227±0.169
SUB15	0.551±0.221	2.968±0.259	3.556±0.406	0.660±0.195	2.567±0.254	3.352±0.321
SUB17	0.786±0.064	0.951±0.080	1.378±0.238	0.793±0.054	1.005±0.086	1.371±0.218
SUB19	0.722±0.058	0.809±0.059	1.055±0.138	0.751±0.052	0.754±0.053	0.996±0.159

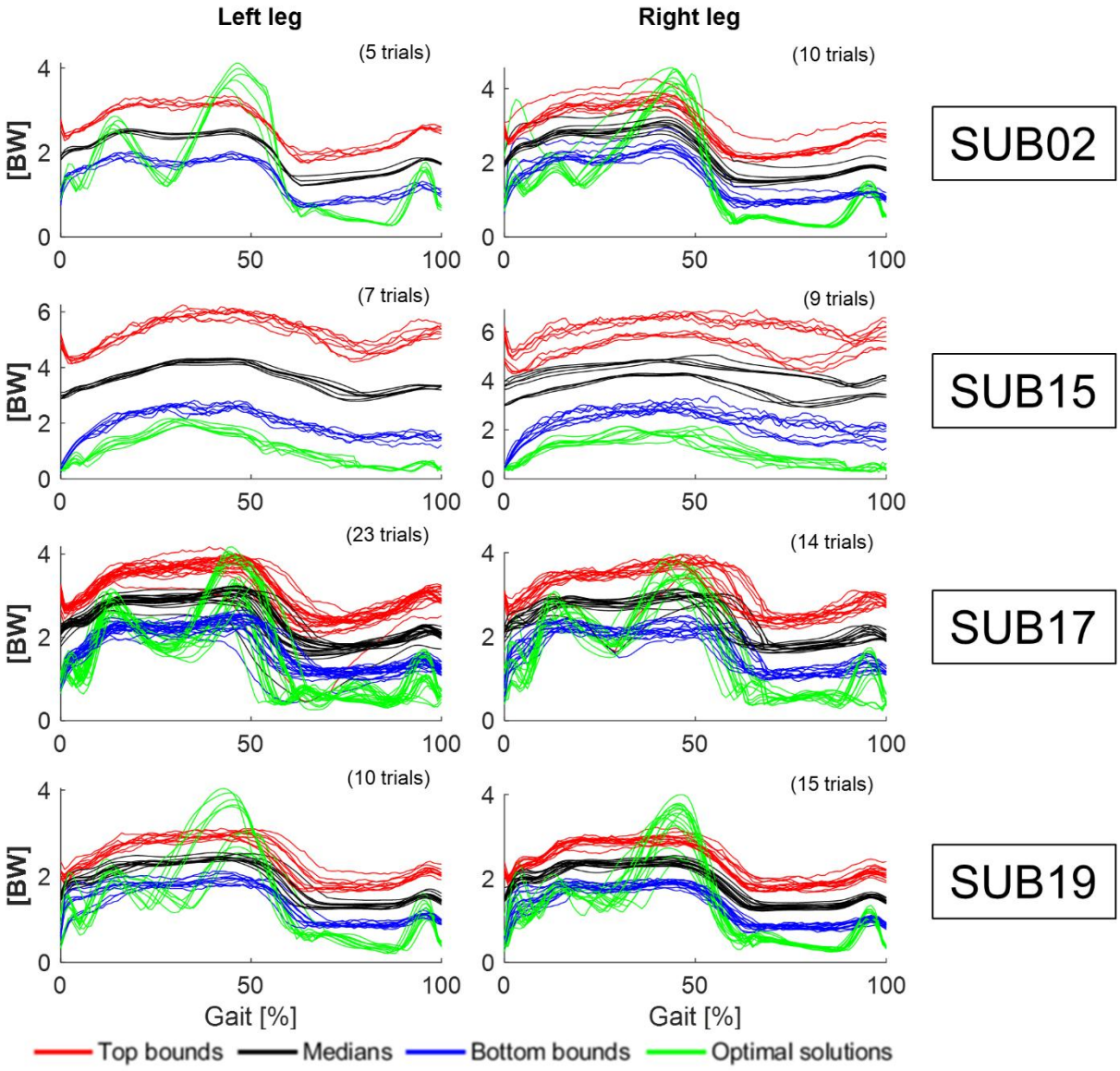

A.Fig. 14. A comparison of all analysed trials was clustered into "left" and "right" leg simulations for all subjects. Red lines are the upper bounds, blue lines are the lower bounds, and black lines are the median solutions of the performed stochastic simulations. The optimal solutions for each analysed trial - estimated with OpenSim - are reported in green. In brackets, the number of simulated trials is mentioned.

Toward future developments of Myobolica

In this final chapter, we discuss potential future directions for developing, testing, and using Myobolica to support the assessment of motor control in different populations and/or research contexts.

To date, the tool has been successfully used to study both lower and upper limb biomechanics and to preliminarily explore how a stochastic approach can be used to gain insights into how Parkinson's disease affects one's motor control. However, before the proposed approach can be used to address specific clinical needs, it is paramount that we perform a thorough sensitivity analysis on the constitutive parameters (gamma and sigma) and a robust validation using available datasets (e.g., the Grand Challenge Competition and the Orthoload datasets [214], [231]). The process of "Validating" a computer model or a simulation framework consists of demonstrating that the model can correctly simulate the reality it is trying to model [275]. Despite a validation step might appear as a logical procedure, it has been formalised as a fundamental step of the model credibility evaluation process just recently by the ASME VV-40-2018 standard [276], [277]. This is an enormous endeavour, the extent of which requires considerable resources, time, and effort, far beyond what remains for the completion of my PhD. To address this challenge, I started exploring two solutions: i) a collaboration with a high-performance computing (HPC) infrastructure to speed up the simulations and ii) unravelling the core aspects of conducting a sensitivity analysis to start gathering expertise.

Regarding the first initiative, a collaboration with the "Istituto Nazionale di Fisica Nucleare" (INFN, the Italian Institute for Nuclear Physics) has been drafted. Still, it will not be discussed further since much of the work was focused on administrative procedures rather than technical development. Regarding the second sought route, some preparatory activities have been done to plan an optimal strategy for conducting the sensitivity analysis, a key part of the validation process. In parallel, effective approaches were evaluated to assess and communicate the obtained results. In fact, the high dimensionality of the outputs produced by Myobolica represents a hurdle to the effective communication of predicted results and the definition of meaningful evaluation metrics.

After completing a rigorous verification and validation of the computational tool, necessary to ensure the underlying mathematics is correct, additional evaluations will be required to ensure the reliability of Myobolica in predicting or detecting clinically relevant metrics. To support its translation into the clinical practice, Myobolica could be further assessed using the V3 framework proposed by the Digital Medicine Society (DiMe), recently expanded into the V3+ version [278]. This framework integrates a clinical validation to assess whether the tool's outcomes acceptably identify or predicts meaningful clinical and biological states (within the intended patient population). Additionally, the V3+ version further introduce a usability component to evaluate the acceptability and burden of Myobolica when implemented into a clinical workflow [278]. This last assessment would evaluate that Myobolica could be used with efficiency and user-satisfaction. For clarity, these assessments have not been performed at this stage and will not be further detailed in this document.

Preliminary Uncertainty Quantification of the Myobolica Toolbox

To assess the robustness and reliability of the proposed computational toolbox, a preliminary Uncertainty Quantification (UQ) analysis was conducted. UQ is a methodological framework used to evaluate the uncertainties in the outputs of a computational model by propagating the input parameter uncertainties. Its importance is acknowledged in numerous fields that leverage computational simulations [279], [280], [281]. The analysis focused on two key input parameters (gamma and sigma); each parameter was specifically defined, grounded in direct data acquisition from subjects, or derived from related experimental studies. Therefore, the variability introduced in the analysis reflects plausible measurement errors of different magnitudes, rather than arbitrary assumptions. The adopted approach resembled the Design of Experiment (DoE) methods to generate random samples to propagate the uncertainties to the outputs, with the Latin Hypercube Sampling (LHS) method for the experimental design.

This evaluation is crucial for understanding how such uncertainties propagate through the model and influence its outputs. By quantifying these effects, this work may enhance confidence in the toolbox's predictive capabilities and provide a foundation for future refinements and broader clinical applicability.

Tested parameters

The tested parameters are gamma (γ) and sigma (σ). The first models the physiological constraint on how fast each muscle can produce force; the second models the presence of noise and uncertainties in the dynamic equilibrium equation. Both have been introduced and explained in Chapter 3 and Chapter "Myobolica: a stochastic approach to estimate physiological muscle control variability" (Appendix I).

Methods

To preliminarily explore the impact of input variability, each parameter range was discretised into multiple intervals, though not uniformly spaced. Central values were selected based on accurate estimates per Chapter "Myobolica: a stochastic approach to estimate physiological muscle control variability" (γ=0.002; σ=0.12). Additional sampling points were placed strategically around these reference values to assess local and broader sensitivity. Values within ±10 % (rounded) and more distant values (e.g., approximately one order of magnitude above and below) were selected to assess sigma behaviour. For gamma, values were chosen to plausibly represent young adults and trained individuals, along with more distant values (e.g., approximately one order of magnitude above and below). The closer the parameters' values are to zero, the less the Myobolica predicted solutions can deviate from the tentative solution provided as input to the toolbox; for this reason, this preliminary analysis prioritised parameter combinations higher than the reference combination; however, the prediction for smaller values was also assessed. The adopted approach did not strictly follow the LHS method but reflects a structured and informed sampling strategy designed to balance realism and efficiency. As a result, a total amount of 48 simulations was performed exploring 48 combinations of the two analysed parameters; a summary of the analysed parameter combinations is reported in Figure 28.

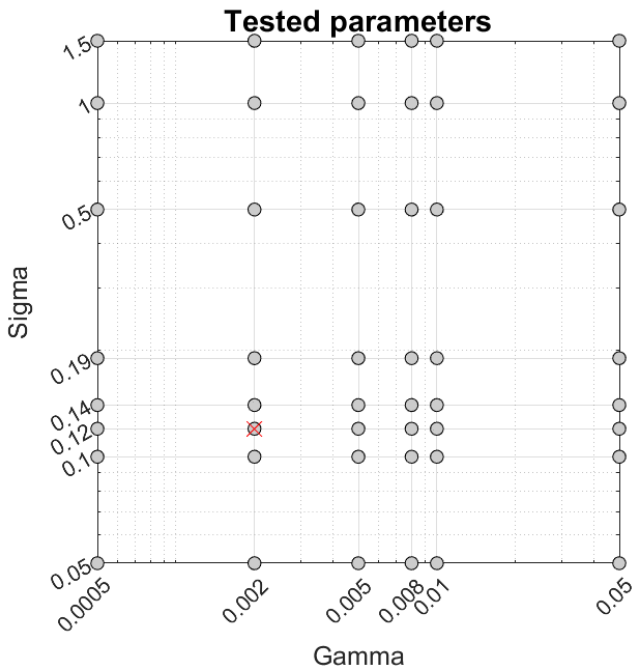

Figure 28. Parameter combinations tested in the UQ. Axes are in logarithmic scale. The red cross represents the parameter combination adopted in Chapter "Myobolica: a stochastic approach to estimate physiological muscle control variability".

This preliminary analysis was performed on the same model and data used in the study presented in Chapter "Myobolica: a stochastic approach to estimate physiological muscle control variability". For each combination of parameters, Myobolica identified 600k solutions. Two consecutive steps were simulated. However, to minimise time expenditure, the resulting joint contact forces have not been calculated yet. The analysis focused on the muscle forces and activations that represent the actual output of the tool. Notably, when the time and obtained expertise will allow us to assess the joint contact forces, it will be possible to validate the experimental joint forces from existing databases. However, since Myobolica generates not a single but a range of solutions, the scope will be to evaluate the position of the "real value" relative to Myobolica's solution band; ideally, a successful validation would demonstrate that the real value is placed within Myobolica's predicted band.

As the goal is to assess the impact of the constitutive parameters on the output from Myobolica, the solutions were compared (1) to the "optimal" solution from static optimisation (SO) obtained by minimising the sum of squared muscle activations and (2) to the solution identified via an EMG-assisted approach (CEINMS) [223]. For the latter, the model was first calibrated using the available experimental data. During the calibration process, the maximal isometric force of all muscles was allowed to vary between 70 % and 130 %, while the optimal fibre length and the tendon slack length were between 95 % and 105 % of their initial value. The EMG-assisted simulations were performed by setting the terms α, β and γ to 1, 1, and 50, respectively.

Data analysis – qualitative report of results

The first straightforward method to assess the results was to present them through graphical representations. Figures 29A and B show the Myobolica results for two parameter combinations.

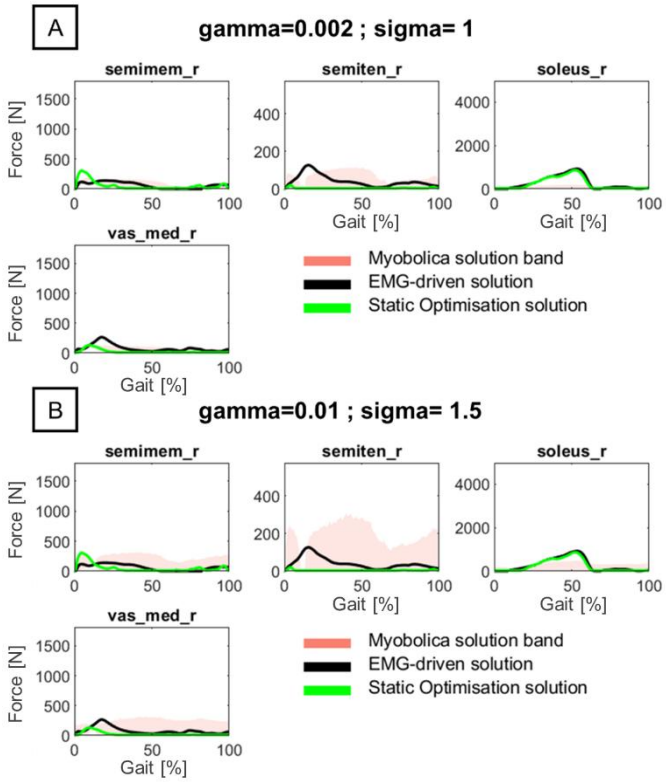

Figure 29. Comparison of muscle force solutions bands predicted with Myobolica (light red areas), the SO solution (green curve) and the CEINMS solution (black curve) for a subset of selected muscles and two parameter combinations.

Despite being intuitive, it lacks quantitative information, which is fundamental in assessing how variations in the parameters impact the predicted outputs of Myobolica. More measurable outcomes are required to perform the assessment.

Data analysis – r^2, RMSE and solutions bandwidth analysis

Frequently adopted methods to assess time-varying variables are the coefficient of determination (r^2) and the root mean square error (RMSE); their adoption represents a fast and intuitive way to perform a quantitative assessment. In addition, computing the width of the Myobolica's solution spaces (calculated as top solution minus bottom solution for each timeframe) has provided meaningful information, specifically in the context of such a toolbox aiming to explore sub-optimal motor control solution spaces.

For this assessment, a subsample of 6000 solutions for each muscle (1 every 100 Myobolica solutions) was compared to the two reference solutions (SO and CEINMS) by computing r^2 and RMSE between each muscle Myobolica solution and the two reference solutions. In addition, each muscle solution band area has been computed to assess the solution bandwidth. Results were reported through heatmaps, with the gamma parameter on the x-axis and the sigma parameter on the y-axis; the tested values are shown in the heatmaps, normalised to the maximum value found in each heatmap for consistency.

The results suggest that changing the parameters' values leads to variations in the solution profiles. As it can be seen from the reported heatmaps (Figures 30 and 31 reports results for two muscles with different involvement in the analysed motor task), larger values of the parameters correspond to larger deviations from the reference solutions (lower r^2 and higher RMSE), with gamma being more impactful; in particular, the more remarkable deviations from the reference solutions emerge for the highest value of gamma, with less noteworthy deviations emerge for remaining values (it is worth

noting that the highest gamma value is 22.7 times the value estimated from experimental value as per Chapter "Myobolica: a stochastic approach to estimate physiological muscle control variability").

Comparing Myobolica's solutions to the two references allows for assessing disparities in solution profiles. However, no straightforward conclusions about differences in the solution space structures can be stated. For this reason, linking the previous analysis with analysing the solutions' bandwidths may refine the assessment. Figure 32 shows heatmaps for the solution's bandwidths of selected muscles. Similarly to the previous analysis, significant deviations emerge when increasing the parameters, with gamma being more impactful than sigma; the predicted solutions band areas tend to increase, as expected, when bigger parameters are used. Adding the information on the bandwidth variations makes it possible to note deviations even locally; those local deviations do not emerge as significantly in the r^2 and RMSE analysis.

Analysing variations in the outputs through the r^2, RMSE, and the solution bandwidths allows for an assessment that is comprehensible and intuitive, due to the adoption of commonly accepted metrics. However, a large number of graphs is required to communicate the findings fully. In addition, this analysis may be valid when a reliable reference is available, such as an experimental measure, while it loses impact if a valuable reference solution is missing.

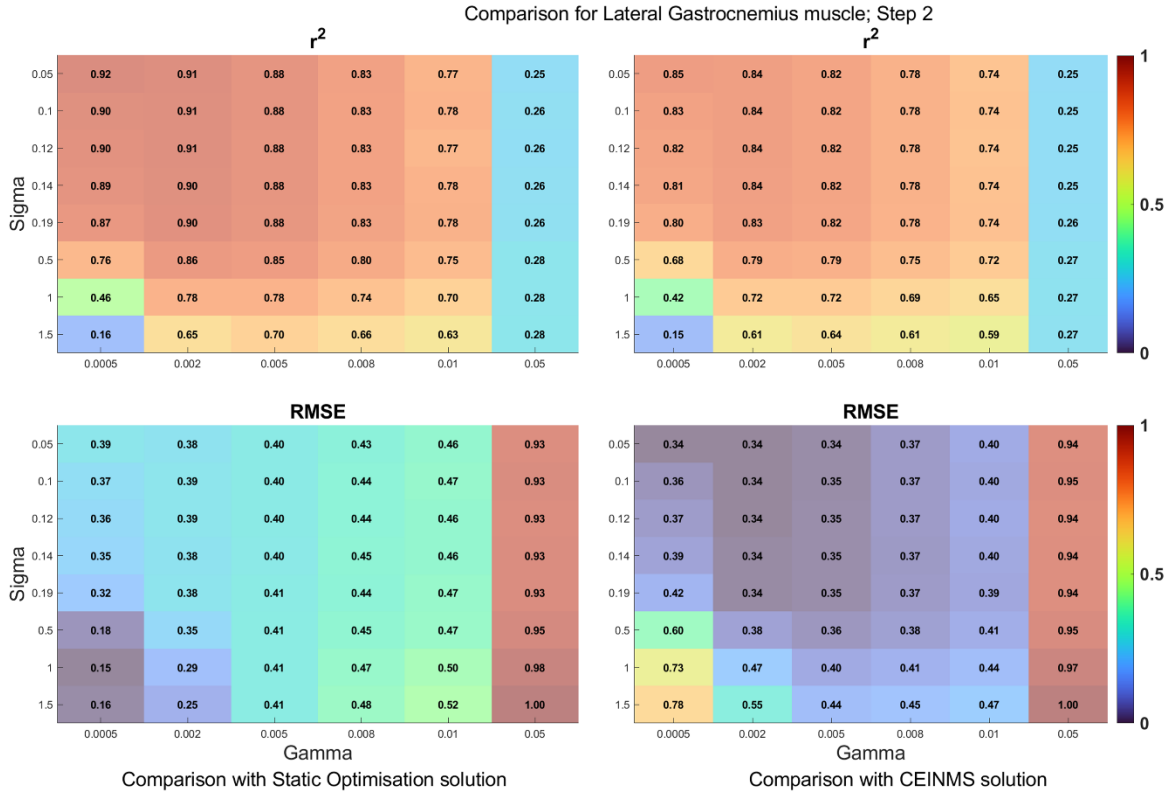

Figure 30. Heatmaps of the compared r^2 and RMSE for the lateral gastrocnemius muscle with the SO (left column) and CEINMs (right column). Each graph shows the gamma on the x-axis and the sigma values on the y-axis. All heatmaps are normalised to their respective maximum value.

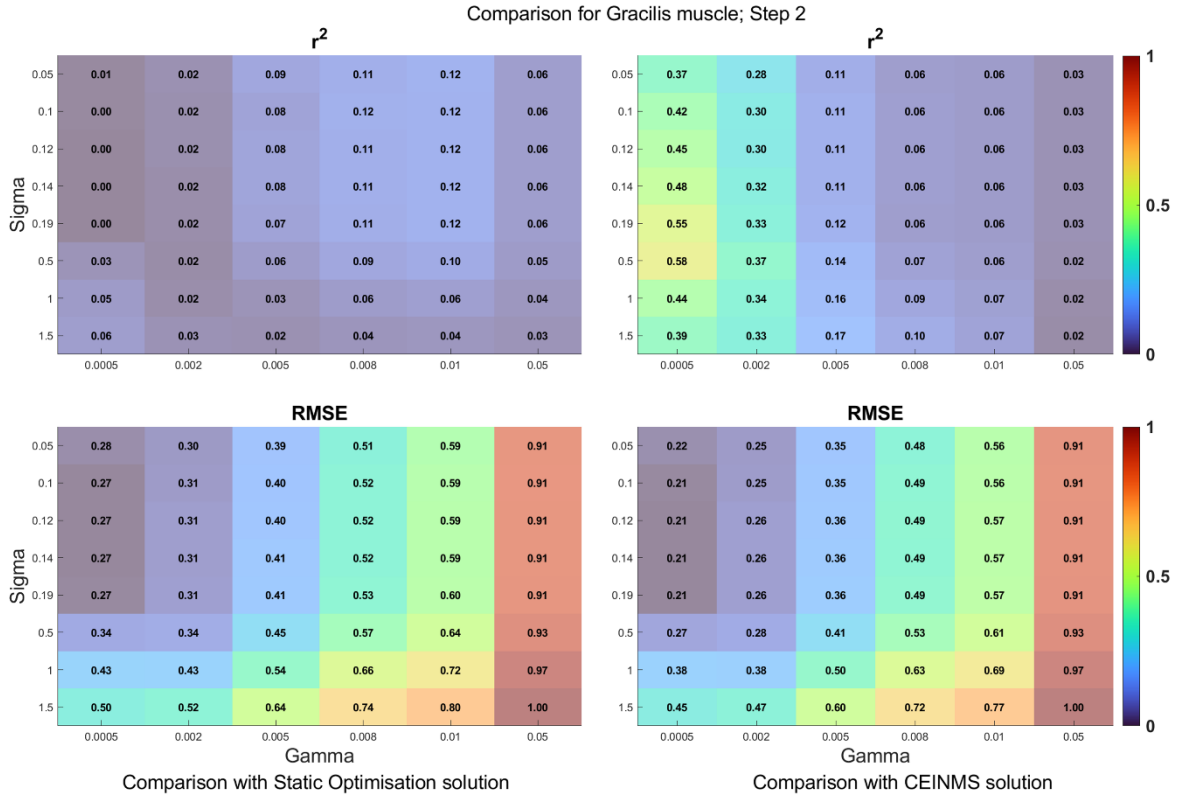

Figure 31. Heatmaps of the compared r2 and RMSE for the lateral gastrocnemius muscle with the SO (left column) and CEINMs (right column). Each graph shows the gamma on the x-axis and the sigma values on the y-axis. All heatmaps are normalised to their respective maximum value.

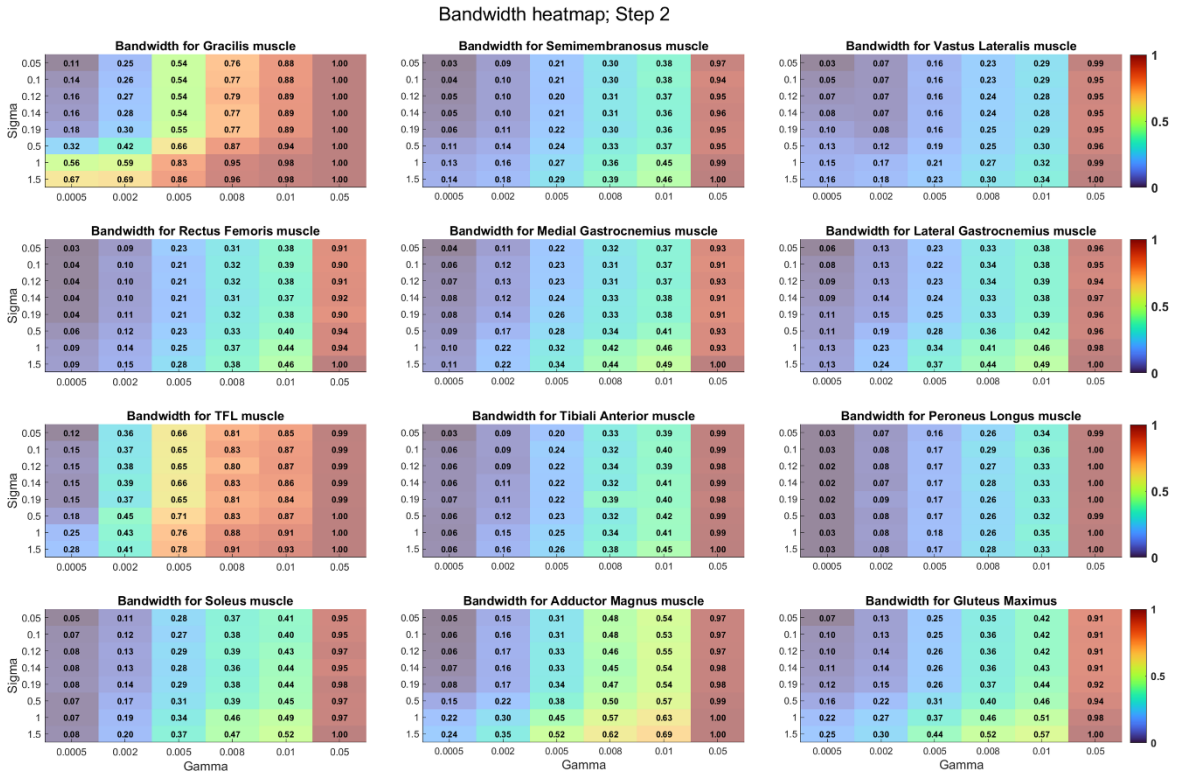

Figure 32. Heatmaps of the selected muscles' average bandwidth. Each graph shows the gamma on the x-axis and the sigma values on the y-axis. All heatmaps are normalised to their respective maximum value.

Data analysis – Procrustes analysis

Performing a validation that relies only on r^2 and RMSE might not be an up-to-mark analysis; statistical tests are required to determine if statistically significant differences are caused by the parameters' variations. Unfortunately, most statistical tests that are generally adopted seem to have issues when comparing big datasets. Often, little differences that appear negligible from a biomechanical standpoint (e.g., a few Newton differences in the predicted muscle forces) are marked as statistically significant. Alternative approaches, such as the Procrustes analysis, which is used primarily in psychometrics to compare survey responses or biology contexts to perform shape analysis of biological structures [282], may allow us to overcome this issue. It applies translation, rotation, and scaling (e.g., normalisation) to one of the sets of points to minimise the distance from the second, offering a quantitative measure of changes in the solution band structure.

To perform this analysis, one simulation has been selected as reference against which to compare every other one; in particular, the results obtained using the same combination of parameters adopted in the paper [246], reported in Chapter "Myobolica: a stochastic approach to estimate physiological muscle control variability", were set as reference (γ=0.002; σ=0.12). Each muscle force solution band was sorted in ascending order, and the maximum, minimum, median, and the 25^{th} and 75^{th} quantile solutions were extracted. The Procrustes analysis was performed using the *procrustes* function in the SciPy library of Python. The heatmaps for the lateral gastrocnemius and the gracilis muscles are reported in Figures 33 and 34.

The Procrustes analysis showed promising results, from which conclusions similar to those of the previous section may be stated. For the selected muscles, the distance of the predicted solution space from the reference one consistently increases when parameter values are increased, with gamma being more impactful than sigma in changing the shape of the solution space. Notably, for low gamma values, the impact of sigma is more significant.

This approach allows an intuitive comparison that does not require a reference solution; it is sufficient to select one of the predicted solutions as a reference. Moreover, the comparison is based on shape differences of the solution bands, so extracting only the quantiles is unlikely to result in a loss of information. Nonetheless, further investigation on this approach is required to deepen understanding and evaluate whether more efficient ways to employ it may be pursued.

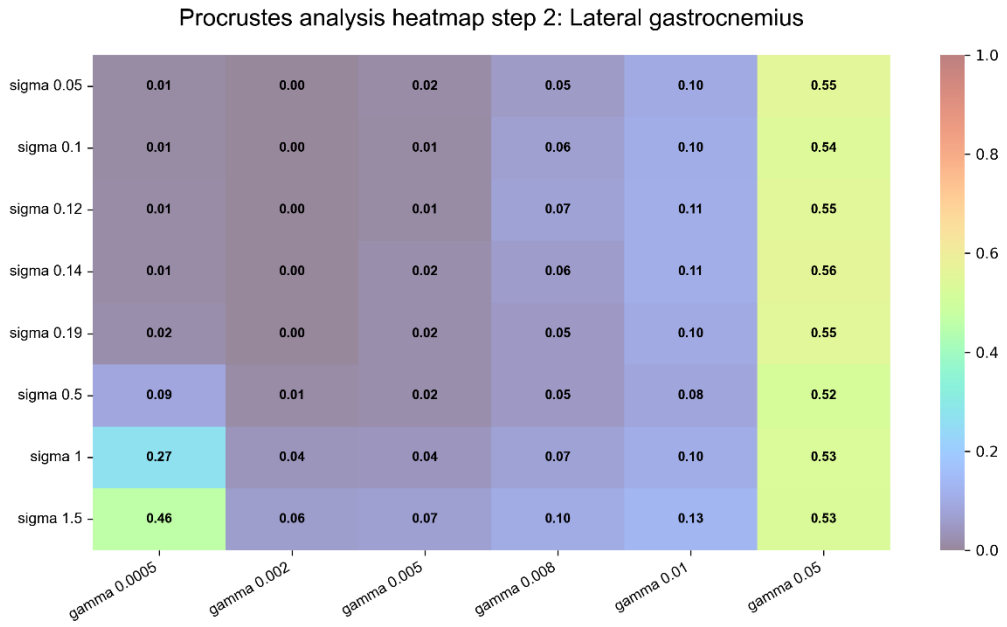

Figure 33. Heatmaps of the Procrustes analysis distance metrics between all simulations and the reference simulation for the lateral gastrocnemius. The graph has the gamma on the x-axis and the sigma values on the y-axis.

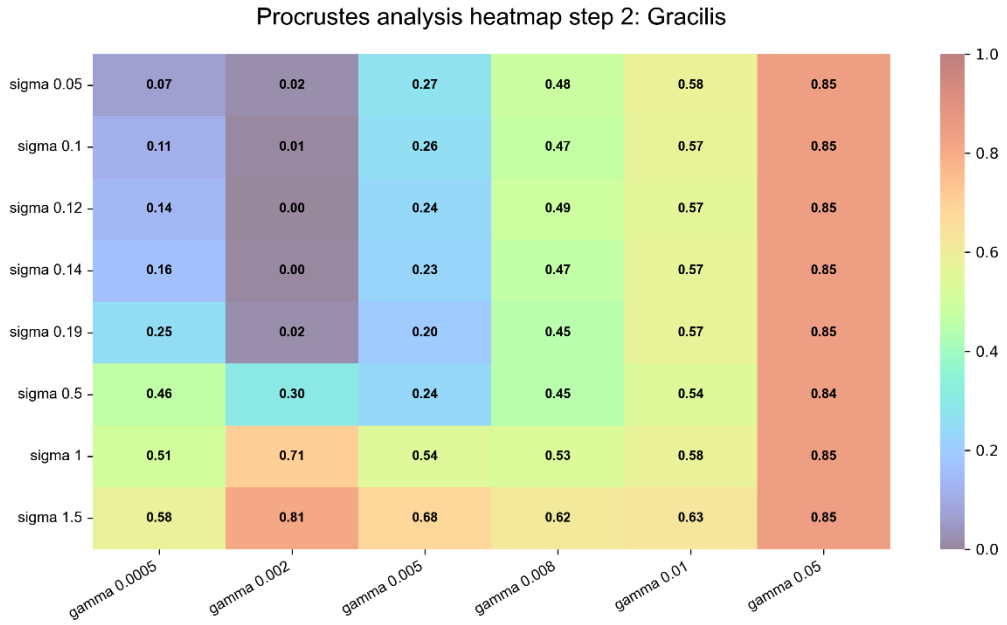

Figure 34. Heatmaps of the Procrustes analysis distance metrics between all simulations and the reference simulation for the gracilis. The graph has the gamma on the x-axis and the sigma values on the y-axis.

Data analysis – Kolmogorov-Smirnov and Energy distance tests

The last tested methods were the Kolmogorov-Smirnov and the Energy distance test. While the first is a non-parametric statistical test used to compare probability distributions, the Energy distance is a statistical distance between two distributions. However, both are employed to state whether the analysed distributions are statistically different. Those two tests may be considered part of the group showing issues described in the section dedicated to the Procrustes analysis; both were inferred with a p-value close to zero. As for the Procrustes analysis, the Chapter "Myobolica: a stochastic approach to estimate physiological muscle control variability" parameter combination was selected as a reference. Then, for each combination, each muscle was systematically compared (no quantiles were

extracted). The Kolmogorov-Smirnov test was performed using the *ks_2samp* function in the SciPy library, and the Energy distance metric was calculated using the *Energy()* function in the hyppo library of Python.

An example is shown in Figures 35 and 36, respectively, the Kolmogorov-Smirnov test results and the Energy distance metric for the lateral gastrocnemius. The p-value was below the threshold for both tests, always about 0 for the Kolmogorov-Smirnov and always <0.03 for the Energy distance measure. The results, *per se,* seem to suggest findings similar to those of the previously presented approaches. Still, it may be premature to state conclusions before delving into the causes of such low p-values for all comparisons. More investigation is required to investigate other statistical tools further and evaluate if better uses of these two methods may be developed.

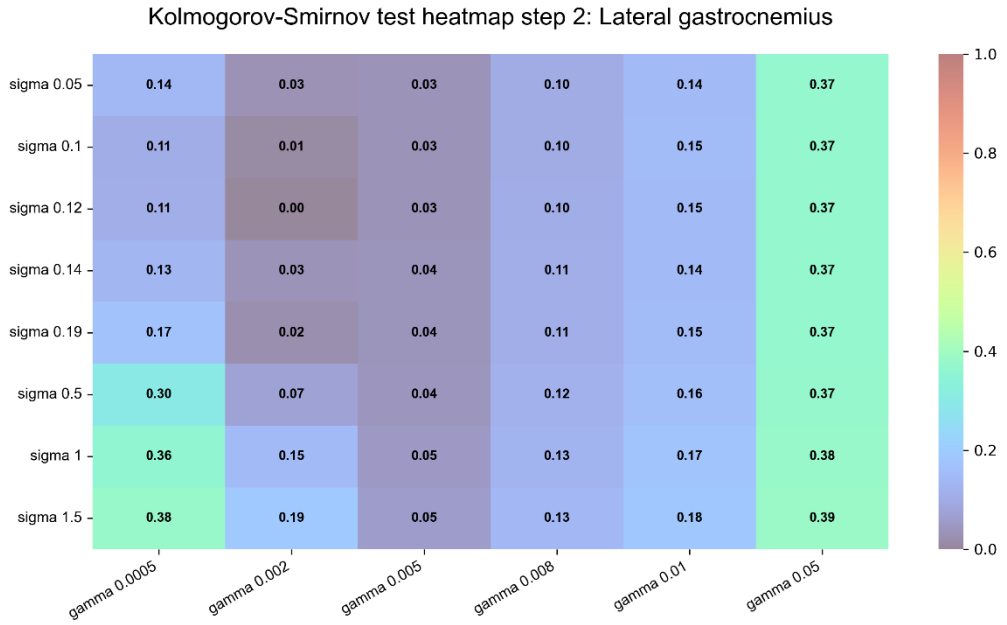

Figure 35. Heatmaps of the Kolmogorov-Smirnov test between all simulations and the reference simulation for the lateral gastrocnemius. The graph has the gamma on the x-axis and the sigma values on the y-axis.

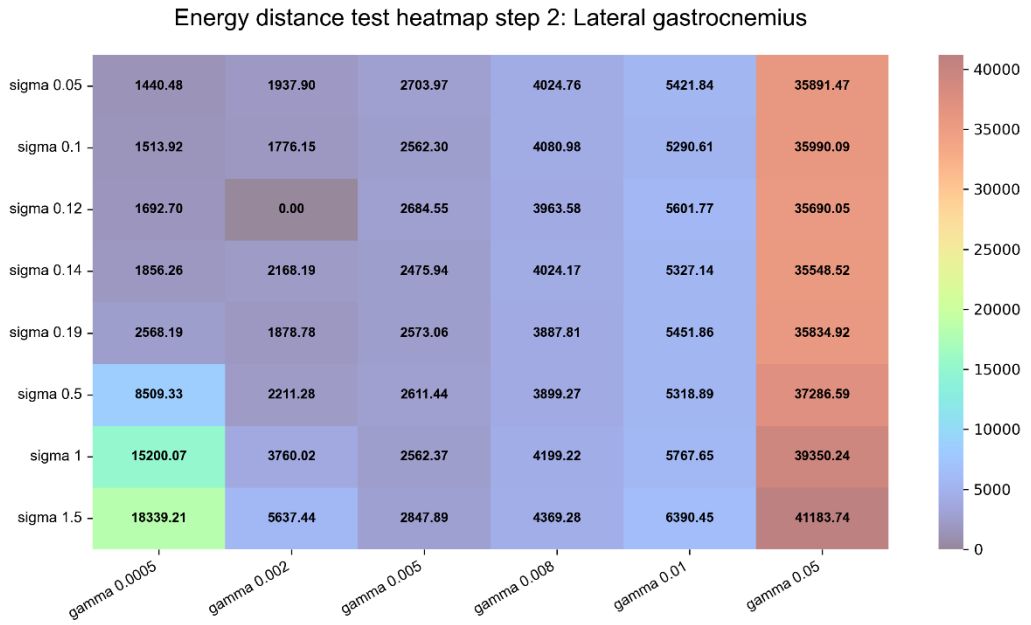

Figure 36. Heatmaps of the Energy distance metric between all simulations and the reference simulation for the lateral gastrocnemius. The graph has the gamma on the x-axis and the sigma values on the y-axis.

A context of use for Myobolica

Myobolica has been used to study upper and lower limb biomechanics in subjects who underwent a joint replacement. However, this is not the only application of the tool. Contrarily, Myobolica may and should be employed to investigate suboptimal motor control in various clinical populations characterised by suboptimal motor control. A first example was provided in Chapter "Explorative assessment of the knee joint load variability in four patients with Parkinson's disease", where the bands of solutions identified by Myobolica were analysed to understand how disease severity may affect the ability of a person with Parkinson's disease to adopt different neural strategies to perform a given task. The last section of this document will be dedicated to future developments of Myobolica, including some applications for the tool that we hypothesise. To begin with, as discussed in the previous chapter a validation of the tool is required in the near future. Subsequently, in the medium-term development of Myobolica, its expansion will focus on integrating additional modelling approaches and kinematics acquisition systems into the simulations. This will include a more rigorous incorporation of EMG signals to inform the simulations, the implementation of more physiologically realistic muscle dynamics, and the development of pipelines enabling the use of kinematics measured with wearable sensors. The expansion of Myobolica will continue with the introduction of a stochastic formulation for the inverse dynamics model that estimate joint torques, which are then used to predict the muscle forces. Lastly, a broader adoption of Myobolica in pathological populations will be pursued, with the aim of deepening the investigation of motor control and facilitating Myobolica's integration into clinical settings.

We are currently developing Myobolica to be as flexible as possible, to enhance it or engage with every innovative application that may emerge in the future. This allows the tool to be suitable for integration with other modelling approaches, such as those described in Chapter "Modeling human suboptimal control: a review". An improvement of the combination of Myobolica and EMG-informed approaches, aligned with the approach presented in Chapter "Stochastic modelling of muscle control

during shoulder abduction", may be implemented by employing the EMG information in the prior component of the Bayesian framework; analogous information may be employed to set muscle-specific gamma parameters. Similarly, it might be combined with optimal control methods, using Myobolica after the predictive simulations to explore the solution space around the predicted solution. Such a development could be complemented by the introduction of more realistic muscle dynamics, enabling the incorporation of the physiological force-length-velocity relationship of muscle. An impactful upcoming development stage to enhance Myobolica may be the integration of kinematics measured with motion capture technologies other than stereophotogrammetry. A tool capable of operating not only with the traditional stereophotogrammetry but also with wearable sensors or markerless motion capture systems would be applicable in in a much wider range of contexts. These systems enable more flexible and less expensive data acquisition compared to stereophotogrammetry, but with the frequently discussed downside of a loss of accuracy.

The outlined improvements may help reduce the dependency of Myobolica's results from the underlying musculoskeletal model, which is an impactful limitation emerged in the study on the shoulder abduction "Stochastic modelling of muscle control during shoulder abduction". To further address this issue, a long-term enhancement of Myobolica will involve replacing the deterministic inverse dynamics model, which is used to estimate joint torques, with a stochastic formulation, analogous to the stochastic approach already implemented for predicting muscle forces; this will enable the model to account not only for uncertainties in the muscle force estimation but also in the preceding analysis.

Other applications of Myobolica may be more straightforward and dedicated to non-healthy individuals. Firstly, it can be a valid tool to deepen the motor control, enabling testing of "what if" situations. For example, how the weakening of individual muscles or their hyperactivation (i.e., spasticity) may impact the adopted motor control strategy when performing a given task. It might be used to explore the capabilities of analysed subjects to reduce or better exploit the experimental data to be acquired, or to produce more results to predict adverse scenarios or potential risks. As exposed in Chapter "Explorative assessment of the knee joint load variability in four patients with Parkinson's disease", Myobolica might cluster between two medication phases, so plausibly, it may be able to track disease progression.

Depending on the performance and reliability of Myobolica in the mentioned future developments, its integration into a clinical setting may be hypothesised. The integration of modelling approaches, experimental measures (i.e., EMG), and clinical scores (i.e., bradykinesia scores in patients with PD), could improve the quality and accuracy of Myobolica's outcomes; the accessibility to the tool (thinking about a clinical setting) could be improved by an increase of the typologies of kinematics acquisition systems that could pair with Myobolica, making it possible to have an alternative to the expensive stereophotogrammetry. Those improvements could lead to clinicians prescribing a gait analysis to a patient and obtain, in a short time, an assessment of potential risks (as an example, overloaded joints or high risk of falling) together with a quantitative evaluation of disease severity. The outcomes could also include evaluations of specific symptoms, such as rigidity or gait asymmetry for patients with PD, allowing for a quantitative prediction of disability associated with various pathologies. Other than this screening-like adoption of Myobolica, another example of clinical application could involve its use throughout different follow-up of the patient; across the assessments, both the clinician and the patient could benefit from reliable and reproducible outcomes that quantitatively describe the progression and severity of the pathology the patient is affected by.

The applications that may suit Myobolica are various and may help many branches of scientific research. Its path is still long, but this project surely increased the knowledge about the stochastic modelling approach and secured a fundamental milestone to improve Myobolica and exploit this tool.

Bibliography

[1] D. Domkin, J. Laczko, S. Jaric, H. Johansson, e M. L. Latash, «Structure of joint variability in bimanual pointing tasks», *Exp. Brain Res.*, vol. 143, fasc. 1, pp. 11–23, mar. 2002, doi: 10.1007/s00221-001-0944-1.

[2] D. S. Reisman, J. P. Scholz, e G. Schöner, «Coordination underlying the control of whole body momentum during sit-to-stand», *Gait & Posture*, vol. 15, fasc. 1, pp. 45–55, feb. 2002, doi: 10.1016/S0966-6362(01)00158-8.

[3] J. P. Scholz, F. Danion, M. L. Latash, e G. Schöner, «Understanding finger coordination through analysis of the structure of force variability», *Biol. Cybern.*, vol. 86, fasc. 1, pp. 29–39, gen. 2002, doi: 10.1007/s004220100279.

[4] V. Firouzi, A. Seyfarth, S. Song, O. von Stryk, e M. Ahmad Sharbafi, «Biomechanical models in the lower-limb exoskeletons development: a review», *J. NeuroEng. Rehabil.*, vol. 22, fasc. 1, p. 12, gen. 2025, doi: 10.1186/s12984-025-01556-5.

[5] J. Rasmussen, M. Boocock, e G. Paul, «Advanced musculoskeletal simulation as an ergonomic design method», *WORK*, vol. 41, fasc. S1, pp. 6107–6111, mar. 2012, doi: 10.3233/WOR-2012-1069-6107.

[6] R. Ramirez-Campillo, F. Garcia-Pinillos, H. Chaabene, J. Moran, D. G. Behm, e U. Granacher, «Effects of Plyometric Jump Training on Electromyographic Activity and Its Relationship to Strength and Jump Performance in Healthy Trained and Untrained Populations: A Systematic Review of Randomized Controlled Trials», *J. Strength Cond. Res.*, vol. 35, fasc. 7, p. 2053, lug. 2021, doi: 10.1519/JSC.0000000000004056.

[7] J. Willer, S. J. Allen, R. J. Burden, e J. P. Folland, «How Humans Run Faster: The Neuromechanical Contributions of Functional Muscle Groups to Running at Different Speeds», *Scand. J. Med. Sci. Sports*, vol. 34, fasc. 8, p. e14690, 2024, doi: 10.1111/sms.14690.

[8] M. Wilson e Y.-H. Kwon, «The role of biomechanics in understanding dance movement: a review», *J Dance Med Sci*, vol. 12, fasc. 3, pp. 109–116, 2008.

[9] L. S. DeBolt e J. A. McCubbin, «The effects of home-based resistance exercise on balance, power, and mobility in adults with multiple sclerosis1», *ACRM*, vol. 85, fasc. 2, pp. 290–297, feb. 2004, doi: 10.1016/j.apmr.2003.06.003.

[10] P. Duncan *et al.*, «A Randomized, Controlled Pilot Study of a Home-Based Exercise Program for Individuals With Mild and Moderate Stroke», *Stroke*, vol. 29, fasc. 10, pp. 2055–2060, ott. 1998, doi: 10.1161/01.STR.29.10.2055.

[11] R. Cano-de-la-Cuerda *et al.*, «Theories and control models and motor learning: Clinical applications in neurorehabilitation», *Neurología (English Edition)*, vol. 30, fasc. 1, pp. 32–41, gen. 2015, doi: 10.1016/j.nrleng.2011.12.012.

[12] A. G. Fel'dman, «[On the functional tuning of the nervous system in movement control or preservation of stationary pose. II. Adjustable parameters in muscles]», *Biofizika*, vol. 11, fasc. 3, pp. 498–508, 1966.

[13] R. A. Schmidt, «A schema theory of discrete motor skill learning», *Psychological Review*, vol. 82, fasc. 4, pp. 225–260, 1975, doi: 10.1037/h0076770.

[14] C. S. Sherrington, *The integrative action of the nervous system*. in The integrative action of the nervous system. New Haven, CT, US: Yale University Press, 1906, pp. xvi, 411. doi: 10.1037/13798-000.

[15] J. P. Scholz e G. Schöner, «The uncontrolled manifold concept: identifying control variables for a functional task», *Exp. Brain Res.*, vol. 126, fasc. 3, pp. 289–306, mag. 1999, doi: 10.1007/s002210050738.

[16] N. Bernstein, *The Co-ordination and Regulation of Movements*. Pergamon Press, 1967.

[17] M. Latash, «There is no motor redundancy in human movements. There is motor abundance», *Motor Control*, vol. 4, fasc. 3, pp. 259–260, lug. 2000, doi: 10.1123/mcj.4.3.259.

[18] A. Roda-Sales, N. J. Jarque-Bou, V. Bayarri-Porcar, V. Gracia-Ibáñez, J. L. Sancho-Bru, e M. Vergara, «Electromyography and kinematics data of the hand in activities of daily living with special interest for ergonomics», *Sci. Data*, vol. 10, fasc. 1, p. 814, nov. 2023, doi: 10.1038/s41597-023-02723-w.

[19] V. T. Inman, J. B. deC. M. Saunders, e L. C. Abbott, «Observation on the function of the shoulder joint», *JBJS*, vol. 26, fasc. 1, p. 1, gen. 1944.

[20] R. Gross *et al.*, «The influence of gait speed on co-activation in unilateral spastic cerebral palsy children», *Clin. Biomech.*, vol. 28, fasc. 3, pp. 312–317, mar. 2013, doi: 10.1016/j.clinbiomech.2013.01.002.

[21] M. L. Latash e J. G. Anson, «What are "normal movements" in atypical populations?», *Behav. Brain Sci.*, vol. 19, fasc. 1, pp. 55–68, mar. 1996, doi: 10.1017/S0140525X00041467.

[22] G. Albani *et al.*, «Differences in the EMG pattern of leg muscle activation during locomotion in Parkinson's disease», *Funct. Neurol.*, vol. 18, fasc. 3, pp. 165–170, 2003.

[23] J. P. P. van Vugt, M. Stijl, R. a. C. Roos, e J. G. van Dijk, «Impaired antagonist inhibition may contribute to akinesia and bradykinesia in Huntington's disease», *Clin. Neurophysiol.*, vol. 114, fasc. 2, pp. 295–305, feb. 2003, doi: 10.1016/s1388-2457(02)00371-1.

[24] J. K. Carlyle e G. Mochizuki, «Influence of post-stroke spasticity on EMG-force coupling and force steadiness in biceps brachii», *J. Electromyogr. Kinesiol.*, vol. 38, pp. 49–55, feb. 2018, doi: 10.1016/j.jelekin.2017.11.005.

[25] S. K. Stackhouse, S. A. Binder-Macleod, e S. C. K. Lee, «Voluntary muscle activation, contractile properties, and fatigability in children with and without cerebral palsy», *Muscle Nerve*, vol. 31, fasc. 5, pp. 594–601, mag. 2005, doi: 10.1002/mus.20302.

[26] K. G. Hammond, R. F. Pfeiffer, M. S. LeDoux, e B. K. Schilling, «Neuromuscular rate of force development deficit in Parkinson disease», *Clin. Biomech.*, vol. 45, pp. 14–18, giu. 2017, doi: 10.1016/j.clinbiomech.2017.04.003.

[27] R. Shimose *et al.*, «Decreased rate of leg extensor force development in independently ambulant patients with acute stroke with mild paresis», *J. Biomech.*, vol. 96, p. 109345, nov. 2019, doi: 10.1016/j.jbiomech.2019.109345.

[28] J. Stevens-Lapsley, B. M. Kluger, e M. Schenkman, «Quadriceps Muscle Weakness, Activation Deficits, and Fatigue With Parkinson Disease», *Neurorehabil. Neural Repair*, vol. 26, fasc. 5, pp. 533–541, giu. 2012, doi: 10.1177/1545968311425925.

[29] M. E. Busse, C. M. Wiles, e R. W. van Deursen, «Co-activation: its association with weakness and specific neurological pathology», *J. NeuroEngineering Rehabil.*, vol. 3, fasc. 1, p. 26, nov. 2006, doi: 10.1186/1743-0003-3-26.

[30] E. Godaux, D. Koulischer, e J. Jacquy, «Parkinsonian bradykinesia is due to depression in the rate of rise of muscle activity», *Ann. Neurol.*, vol. 31, fasc. 1, pp. 93–100, 1992, doi: 10.1002/ana.410310117.

[31] M. J. Armstrong e M. S. Okun, «Diagnosis and Treatment of Parkinson Disease: A Review», *JAMA*, vol. 323, fasc. 6, pp. 548–560, feb. 2020, doi: 10.1001/jama.2019.22360.

[32] C. G. Goetz *et al.*, «Movement Disorder Society-sponsored revision of the Unified Parkinson's Disease Rating Scale (MDS-UPDRS): scale presentation and clinimetric testing results», *Mov. Disord.*, vol. 23, fasc. 15, pp. 2129–2170, nov. 2008, doi: 10.1002/mds.22340.

[33] S. Clael *et al.*, «Association of Strength and Physical Functions in People with Parkinson's Disease», *Neurosci J*, vol. 2018, p. 8507018, dic. 2018, doi: 10.1155/2018/8507018.

[34] A. Mirelman *et al.*, «Gait impairments in Parkinson's disease», *Lancet Neurol.*, vol. 18, fasc. 7, pp. 697–708, lug. 2019, doi: 10.1016/S1474-4422(19)30044-4.

[35] J. C. M. Schlachetzki *et al.*, «Wearable sensors objectively measure gait parameters in Parkinson's disease», *PLOS ONE*, vol. 12, fasc. 10, p. e0183989, ott. 2017, doi: 10.1371/journal.pone.0183989.

[36] V. Sidoroff *et al.*, «Characterization of gait variability in multiple system atrophy and Parkinson's disease», *J. Neurol.*, vol. 268, fasc. 5, pp. 1770–1779, mag. 2021, doi: 10.1007/s00415-020-10355-y.

[37] H. Gaßner *et al.*, «Gait variability as digital biomarker of disease severity in Huntington's disease», *J. Neurol.*, vol. 267, fasc. 6, pp. 1594–1601, giu. 2020, doi: 10.1007/s00415-020-09725-3.

[38] C. G. Kohn, W. L. Baker, M. F. Sidovar, e C. I. Coleman, «Walking speed and health-related quality of life in multiple sclerosis», *Patient*, vol. 7, fasc. 1, pp. 55–61, 2014, doi: 10.1007/s40271-013-0028-x.

[39] L. Delgado-Ortiz *et al.*, «How do people with COPD walk? A European study on digitally measured real-world gait», *Eur. Respir. J.*, vol. 66, fasc. 1, p. 2402303, lug. 2025, doi: 10.1183/13993003.02303-2024.

[40] L. Delgado-Ortiz *et al.*, «Real-world walking cadence in people with COPD», *ERJ Open Res.*, vol. 10, fasc. 2, pp. 00673–02023, mar. 2024, doi: 10.1183/23120541.00673-2023.

[41] L. Angelini *et al.*, «Wearable sensors can reliably quantify gait alterations associated with disability in people with progressive multiple sclerosis in a clinical setting», *J. Neurol.*, vol. 267, fasc. 10, pp. 2897–2909, ott. 2020, doi: 10.1007/s00415-020-09928-8.

[42] A. Polhemus *et al.*, «Walking on common ground: a cross-disciplinary scoping review on the clinical utility of digital mobility outcomes», *npj Digit. Med.*, vol. 4, fasc. 1, p. 149, ott. 2021, doi: 10.1038/s41746-021-00513-5.

[43] A. Bergland, L. Jørgensen, N. Emaus, e B. H. Strand, «Mobility as a predictor of all-cause mortality in older men and women: 11.8 year follow-up in the Tromsø study», *BMC Health Serv. Res.*, vol. 17, p. 22, gen. 2017, doi: 10.1186/s12913-016-1950-0.

[44] M. Cesari *et al.*, «Prognostic Value of Usual Gait Speed in Well-Functioning Older People—Results from the Health, Aging and Body Composition Study», *J. Am. Geriatr. Soc.*, vol. 53, fasc. 10, pp. 1675–1680, 2005, doi: 10.1111/j.1532-5415.2005.53501.x.

[45] J. Shafrin, J. Sullivan, D. P. Goldman, e T. M. Gill, «The association between observed mobility and quality of life in the near elderly», *PLoS ONE*, vol. 12, fasc. 8, p. e0182920, ago. 2017, doi: 10.1371/journal.pone.0182920.

[46] M. F. Levin e D. Piscitelli, «Motor Control: A Conceptual Framework for Rehabilitation», *Motor Control*, vol. 1, fasc. aop, pp. 1–21, lug. 2022, doi: 10.1123/mc.2022-0026.

[47] M. E. P. Stoykov, M. Stojakovich, e J. A. Stevens, «Beneficial effects of postural intervention on prehensile action for an individual with ataxia resulting from brainstem stroke», *NeuroRehabilitation*, vol. 20, fasc. 2, pp. 85–89, mag. 2005, doi: 10.3233/NRE-2005-20204.

[48] B. Rosén e G. Lundborg, «Early use of artificial sensibility to improve sensory recovery after repair of the median and ulnar nerve», *Scand. J. Plast. Reconstr. Surg. Hand. Surg.*, vol. 37, fasc. 1, pp. 54–57, 2003, doi: 10.1080/alp.37.1.54.57.

[49] S.-I. Lin e M. Woollacott, «Association between sensorimotor function and functional and reactive balance control in the elderly», *Age Ageing*, vol. 34, fasc. 4, pp. 358–363, lug. 2005, doi: 10.1093/ageing/afi089.

[50] A. R. Lindquist, C. L. Prado, R. M. Barros, R. Mattioli, P. H. L. da Costa, e T. F. Salvini, «Gait Training Combining Partial Body-Weight Support, a Treadmill, and Functional Electrical Stimulation: Effects on Poststroke Gait», *Phys. Ther.*, vol. 87, fasc. 9, pp. 1144–1154, set. 2007, doi: 10.2522/ptj.20050384.

[51] S. V. Duff e A. M. Gordon, «Learning of grasp control in children with hemiplegic cerebral palsy», *Dev. Med. Child Neurol.*, vol. 45, fasc. 11, pp. 746–757, nov. 2003, doi: 10.1017/S0012162203001397.

[52] M. F. Levin, S. M. Michaelsen, C. M. Cirstea, e A. Roby-Brami, «Use of the trunk for reaching targets placed within and beyond the reach in adult hemiparesis», *Exp. Brain Res.*, vol. 143, fasc. 2, pp. 171–180, mar. 2002, doi: 10.1007/s00221-001-0976-6.

[53] A. Asadi Nikooyan, H. E. J. Veeger, E. K. J. Chadwick, M. Praagman, e F. C. T. van der Helm, «Development of a comprehensive musculoskeletal model of the shoulder and elbow», *Med. Biol. Eng. Comput.*, vol. 49, fasc. 12, pp. 1425–1435, 2011, doi: 10.1007/s11517-011-0839-7.

[54] T. S. Buchanan, D. G. Lloyd, K. Manal, e T. F. Besier, «Neuromusculoskeletal Modeling: Estimation of Muscle Forces and Joint Moments and Movements From Measurements of Neural Command», *J. Appl. Biomech.*, vol. 20, fasc. 4, pp. 367–395, nov. 2004, doi: 10.1123/jab.20.4.367.

[55] S. L. Delp, J. P. Loan, M. G. Hoy, F. E. Zajac, E. L. Topp, e J. M. Rosen, «An interactive graphics-based model of the lower extremity to study orthopaedic surgical procedures», *IEEE Trans Biomed Eng*, vol. 37, fasc. 8, pp. 757–767, ago. 1990, doi: 10.1109/10.102791.

[56] K. J. Bennett *et al.*, «EMG-informed neuromusculoskeletal models accurately predict knee loading measured using instrumented implants», *IEEE Transactions on Biomedical Engineering*, pp. 1–1, 2022, doi: 10.1109/TBME.2022.3141067.

[57] M. A. Marra *et al.*, «A subject-specific musculoskeletal modeling framework to predict in vivo mechanics of total knee arthroplasty», *J Biomech Eng*, vol. 137, fasc. 2, p. 020904, feb. 2015, doi: 10.1115/1.4029258.

[58] M. F. Rabbi, L. E. Diamond, C. P. Carty, D. G. Lloyd, G. Davico, e C. Pizzolato, «A muscle synergy-based method to estimate muscle activation patterns of children with cerebral palsy using data collected from typically developing children», *Sci. Rep.*, vol. 12, fasc. 1, p. 3599, mar. 2022, doi: 10.1038/s41598-022-07541-5.

[59] H. Röhrle, R. Scholten, C. Sigolotto, W. Sollbach, e H. Kellner, «Joint forces in the human pelvis-leg skeleton during walking», *J. Biomech.*, vol. 17, fasc. 6, pp. 409–424, 1984, doi: 10.1016/0021-9290(84)90033-2.

[60] K. Veerkamp *et al.*, «The effects of electromyography-assisted modelling in estimating musculotendon forces during gait in children with cerebral palsy», *J. Biomech.*, vol. 92, pp. 45–53, lug. 2019, doi: 10.1016/j.jbiomech.2019.05.026.

[61] M. Bourgain, S. Hybois, P. Thoreux, O. Rouillon, P. Rouch, e C. Sauret, «Effect of shoulder model complexity in upper-body kinematics analysis of the golf swing», *J. Biomech.*, vol. 75, pp. 154–158, giu. 2018, doi: 10.1016/j.jbiomech.2018.04.025.

[62] K. M. Steele, M. S. DeMers, M. H. Schwartz, e S. L. Delp, «Compressive tibiofemoral force during crouch gait», *Gait & Posture*, vol. 35, fasc. 4, pp. 556–560, apr. 2012, doi: 10.1016/j.gaitpost.2011.11.023.

[63] M. Lavaill, S. Martelli, K. Cutbush, A. Gupta, G. K. Kerr, e P. Pivonka, «Latarjet's muscular alterations increase glenohumeral joint stability: A theoretical study», *J. Biomech.*, vol. 155, p. 111639, giu. 2023, doi: 10.1016/j.jbiomech.2023.111639.

[64] M. Viceconti, C. Curreli, F. Bottin, e G. Davico, «Effect of Suboptimal Neuromuscular Control on the Risk of Massive Wear in Total Knee Replacement», *Ann Biomed Eng*, vol. 49, fasc. 12, pp. 3349–3355, dic. 2021, doi: 10.1007/s10439-021-02795-y.

[65] R. Beckett e K. Chang, «An evaluation of the kinematics of gait by minimum energy», *J. Biomech.*, vol. 1, fasc. 2, pp. 147–159, lug. 1968, doi: 10.1016/0021-9290(68)90017-1.

[66] R. L. Waters e S. Mulroy, «The energy expenditure of normal and pathologic gait», *Gait & Posture*, vol. 9, fasc. 3, pp. 207–231, lug. 1999, doi: 10.1016/S0966-6362(99)00009-0.

[67] F. De Groote, A. L. Kinney, A. V. Rao, e B. J. Fregly, «Evaluation of Direct Collocation Optimal Control Problem Formulations for Solving the Muscle Redundancy Problem», *Annals of Biomedical Engineering*, vol. 44, fasc. 10, pp. 2922–2936, 2016, doi: 10.1007/s10439-016-1591-9.

[68] R. R. Neptune e M. L. Hull, «Evaluation of performance criteria for simulation of submaximal steady-state cycling using a forward dynamic model», *J Biomech Eng*, vol. 120, fasc. 3, pp. 334–341, giu. 1998, doi: 10.1115/1.2797999.

[69] F. E. Zajac, «Muscle coordination of movement: A perspective», *J. Biomech.*, vol. 26, pp. 109–124, gen. 1993, doi: 10.1016/0021-9290(93)90083-Q.

[70] B. R. Umberger e R. H. Miller, «Optimal Control Modeling of Human Movement», in *Handbook of Human Motion*, B. Müller, S. I. Wolf, G.-P. Brueggemann, Z. Deng, A. McIntosh, F. Miller, e W. S. Selbie, A c. di, Cham: Springer International Publishing, 2017, pp. 1–22. doi: 10.1007/978-3-319-30808-1_177-1.

[71] A. Seireg e R. J. Arvikar, «A mathematical model for evaluation of forces in lower extremeties of the musculo-skeletal system», *Journal of Biomechanics*, vol. 6, fasc. 3, pp. 313–326, mag. 1973, doi: 10.1016/0021-9290(73)90053-5.

[72] B. I. Prilutsky, W. Herzog, e T. L. Allinger, «Forces of individual cat ankle extensor muscles during locomotion predicted using static optimization», *J. Biomech.*, vol. 30, fasc. 10, pp. 1025–1033, ott. 1997, doi: 10.1016/S0021-9290(97)00068-7.

[73] P. G. S. Trainor, K. R. McLachlan, e W. D. McCall, «Modelling of forces in the human masticatory system with optimization of the angulations of the joint loads», *J. Biomech.*, vol. 28, fasc. 7, pp. 829–843, lug. 1995, doi: 10.1016/0021-9290(94)00128-Q.

[74] K. N. An, B. M. Kwak, E. Y. Chao, e B. F. Morrey, «Determination of muscle and joint forces: a new technique to solve the indeterminate problem», *J Biomech Eng*, vol. 106, fasc. 4, pp. 364–367, nov. 1984, doi: 10.1115/1.3138507.

[75] N. Brook, J. Mizrahi, M. Shoham, e J. Dayan, «A biomechanical model of index finger dynamics», *Med. Eng. Phys.*, vol. 17, fasc. 1, pp. 54–63, gen. 1995, doi: 10.1016/1350-4533(95)90378-O.

[76] J. H. Challis e D. G. Kerwin, «An Analytical Examination of Muscle Force Estimations Using Optimization Techniques», *Proc Inst Mech Eng H*, vol. 207, fasc. 3, pp. 139–148, set. 1993, doi: 10.1243/PIME_PROC_1993_207_286_02.

[77] R. Happee, «Inverse dynamic optimization including muscular dynamics, a new simulation method applied to goal directed movements», *Journal of Biomechanics*, vol. 27, fasc. 7, pp. 953–960, lug. 1994, doi: 10.1016/0021-9290(94)90267-4.

[78] D. Karlsson e B. Peterson, «Towards a model for force predictions in the human shoulder», *J. Biomech.*, vol. 25, fasc. 2, pp. 189–199, feb. 1992, doi: 10.1016/0021-9290(92)90275-6.

[79] D. D. Penrod, D. T. Davy, e D. P. Singh, «An optimization approach to tendon force analysis», *J. Biomech.*, vol. 7, fasc. 2, pp. 123–129, mar. 1974, doi: 10.1016/0021-9290(74)90050-5.

[80] J. E. Pierce e G. Li, «Muscle forces predicted using optimization methods are coordinate system dependent», *J. Biomech.*, vol. 38, fasc. 4, pp. 695–702, apr. 2005, doi: 10.1016/j.jbiomech.2004.05.016.

[81] R. Raikova, «A model of the flexion — Extension motion in the elbow joint — Some problems concerning muscle forces modelling and computation», *J. Biomech.*, vol. 29, fasc. 6, pp. 763–772, giu. 1996, doi: 10.1016/0021-9290(95)00072-0.

[82] R. Raikova, «A general approach for modelling and mathematical investigation of the human upper limb», *J. Biomech.*, vol. 25, fasc. 8, pp. 857–867, ago. 1992, doi: 10.1016/0021-9290(92)90226-Q.

[83] B. P. Yeo, «Investigations concerning the principle of minimal total muscular force», *J. Biomech.*, vol. 9, fasc. 6, pp. 413–416, gen. 1976, doi: 10.1016/0021-9290(76)90119-6.

[84] S. H. M. Brown e J. R. Potvin, «Constraining spine stability levels in an optimization model leads to the prediction of trunk muscle cocontraction and improved spine compression force estimates», *J. Biomech.*, vol. 38, fasc. 4, pp. 745–754, apr. 2005, doi: 10.1016/j.jbiomech.2004.05.011.

[85] V. K. Goel, W. Kong, J. S. Han, J. N. Weinstein, e L. G. Gilbertson, «A combined finite element and optimization investigation of lumbar spine mechanics with and without muscles», *Spine (Phila Pa 1976)*, vol. 18, fasc. 11, pp. 1531–1541, set. 1993.

[86] M. A. Nussbaum, D. B. Chaffin, e C. J. Rechtien, «Muscle lines-of-action affect predicted forces in optimization-based spine muscle modeling», *J. Biomech.*, vol. 28, fasc. 4, pp. 401–409, apr. 1995, doi: 10.1016/0021-9290(94)00078-I.

[87] A. Schultz, K. Haderspeck, D. Warwick, e D. Portillo, «Use of lumbar trunk muscles in isometric performance of mechanically complex standing tasks», *J. Orthop. Res.*, vol. 1, fasc. 1, pp. 77–91, 1983, doi: 10.1002/jor.1100010111.

[88] R. A. Brand, D. R. Pedersen, e J. A. Friederich, «The sensitivity of muscle force predictions to changes in physiologic cross-sectional area», *J. Biomech.*, vol. 19, fasc. 8, pp. 589–596, gen. 1986, doi: 10.1016/0021-9290(86)90164-8.

[89] R. D. Crowninshield, R. C. Johnston, J. G. Andrews, e R. A. Brand, «A biomechanical investigation of the human hip», *Journal of Biomechanics*, vol. 11, fasc. 1, pp. 75–85, gen. 1978, doi: 10.1016/0021-9290(78)90045-3.

[90] R. D. Crowninshield e R. A. Brand, «A physiologically based criterion of muscle force prediction in locomotion», *Journal of Biomechanics*, vol. 14, fasc. 11, pp. 793–801, gen. 1981, doi: 10.1016/0021-9290(81)90035-X.

[91] D. E. Hardt, «Determining Muscle Forces in the Leg During Normal Human Walking—An Application and Evaluation of Optimization Methods», *J. Biomech. Eng.*, vol. 100, fasc. 2, pp. 72–78, mag. 1978, doi: 10.1115/1.3426195.

[92] G. Li, K. R. Kaufman, E. Y. Chao, e H. E. Rubash, «Prediction of antagonistic muscle forces using inverse dynamic optimization during flexion/extension of the knee», *J. Biomech. Eng.*, vol. 121, fasc. 3, pp. 316–322, giu. 1999, doi: 10.1115/1.2798327.

[93] A. G. Patriarco, R. W. Mann, S. R. Simon, e J. M. Mansour, «An evaluation of the approaches of optimization models in the prediction of muscle forces during human gait», *Journal of Biomechanics*, vol. 14, fasc. 8, pp. 513–525, gen. 1981, doi: 10.1016/0021-9290(81)90001-4.

[94] D. R. Pedersen, R. A. Brand, e D. T. Davy, «Pelvic muscle and acetabular contact forces during gait», *J Biomech*, vol. 30, fasc. 9, pp. 959–965, set. 1997, doi: 10.1016/s0021-9290(97)00041-9.

[95] A. Pedotti, V. V. Krishnan, e L. Stark, «Optimization of muscle-force sequencing in human locomotion», *Math. Biosci.*, vol. 38, fasc. 1, pp. 57–76, gen. 1978, doi: 10.1016/0025-5564(78)90018-4.

[96] J. Dul, M. A. Townsend, R. Shiavi, e G. E. Johnson, «Muscular synergism—I. On criteria for load sharing between synergistic muscles», *J. Biomech.*, vol. 17, fasc. 9, pp. 663–673, gen. 1984, doi: 10.1016/0021-9290(84)90120-9.

[97] J. Rasmussen, M. Damsgaard, e M. Voigt, «Muscle recruitment by the min/max criterion — a comparative numerical study», *Journal of Biomechanics*, vol. 34, fasc. 3, pp. 409–415, mar. 2001, doi: 10.1016/S0021-9290(00)00191-3.

[98] W. L. Nelson, «Physical principles for economies of skilled movements», *Biol. Cybern.*, vol. 46, fasc. 2, pp. 135–147, feb. 1983, doi: 10.1007/BF00339982.

[99] B. I. Prilutsky e V. M. Zatsiorsky, «Optimization-Based Models of Muscle Coordination», *Exerc. Sport Sci. Rev.*, vol. 30, fasc. 1, p. 32, gen. 2002, doi: 10.1097/00003677-200201000-00007.

[100] W. Herzog, «Individual muscle force estimations using a non-linear optimal design», *Journal of Neuroscience Methods*, vol. 21, fasc. 2, pp. 167–179, ott. 1987, doi: 10.1016/0165-0270(87)90114-2.

[101] M. Praagman, E. K. J. Chadwick, F. C. T. van der Helm, e H. E. J. Veeger, «The relationship between two different mechanical cost functions and muscle oxygen consumption», *Journal of Biomechanics*, vol. 39, fasc. 4, pp. 758–765, gen. 2006, doi: 10.1016/j.jbiomech.2004.11.034.

[102] E. Forster, U. Simon, P. Augat, e L. Claes, «Extension of a state-of-the-art optimization criterion to predict co-contraction», *Journal of Biomechanics*, vol. 37, fasc. 4, pp. 577–581, apr. 2004, doi: 10.1016/j.jbiomech.2003.09.003.

[103] B. van Veen, E. Montefiori, L. Modenese, C. Mazzà, e M. Viceconti, «Muscle recruitment strategies can reduce joint loading during level walking», *Journal of Biomechanics*, vol. 97, p. 109368, dic. 2019, doi: 10.1016/j.jbiomech.2019.109368.

[104] B. C. van Veen, C. Mazzà, e M. Viceconti, «The Uncontrolled Manifold Theory Could Explain Part of the Inter-Trial Variability of Knee Contact Force During Level Walking», *IEEE*

Transactions on Neural Systems and Rehabilitation Engineering, vol. 28, fasc. 8, pp. 1800–1807, ago. 2020, doi: 10.1109/TNSRE.2020.3003559.

[105] D. Tsirakos, V. Baltzopoulos, e R. Bartlett, «Inverse optimization: functional and physiological considerations related to the force-sharing problem», *Crit. Rev. Biomed. Eng.*, vol. 25, fasc. 4–5, pp. 371–407, 1997, doi: 10.1615/critrevbiomedeng.v25.i4-5.20.

[106] Y.-C. Lin, T. W. Dorn, A. G. Schache, e M. G. Pandy, «Comparison of different methods for estimating muscle forces in human movement», *Proc Inst Mech Eng H*, vol. 226, fasc. 2, pp. 103–112, feb. 2012, doi: 10.1177/0954411911429401.

[107] F. De Groote *et al.*, «A physiology based inverse dynamic analysis of human gait: potential and perspectives», *Comput Methods Biomech Biomed Engin*, vol. 12, fasc. 5, pp. 563–574, ott. 2009, doi: 10.1080/10255840902788587.

[108] D. G. Thelen e F. C. Anderson, «Using computed muscle control to generate forward dynamic simulations of human walking from experimental data», *Journal of Biomechanics*, vol. 39, fasc. 6, pp. 1107–1115, gen. 2006, doi: 10.1016/j.jbiomech.2005.02.010.

[109] D. G. Thelen, F. C. Anderson, e S. L. Delp, «Generating dynamic simulations of movement using computed muscle control», *Journal of Biomechanics*, vol. 36, fasc. 3, pp. 321–328, mar. 2003, doi: 10.1016/S0021-9290(02)00432-3.

[110] M. Wesseling *et al.*, «Muscle optimization techniques impact the magnitude of calculated hip joint contact forces», *J Orthop Res*, vol. 33, fasc. 3, pp. 430–438, mar. 2015, doi: 10.1002/jor.22769.

[111] F. C. Anderson, J. M. Ziegler, M. G. Pandy, e R. T. Whalen, «Application of high-performance computing to numerical simulation of human movement», *J Biomech Eng*, vol. 117, fasc. 1, pp. 155–157, feb. 1995, doi: 10.1115/1.2792264.

[112] F. C. Anderson e M. G. Pandy, «Static and dynamic optimization solutions for gait are practically equivalent», *Journal of Biomechanics*, vol. 34, fasc. 2, pp. 153–161, feb. 2001.

[113] S. M. McGill, «A myoelectrically based dynamic three-dimensional model to predict loads on lumbar spine tissues during lateral bending», *J. Biomech.*, vol. 25, fasc. 4, pp. 395–414, apr. 1992, doi: 10.1016/0021-9290(92)90259-4.

[114] S. M. McGill e R. W. Norman, «Partitioning of the L4-L5 dynamic moment into disc, ligamentous, and muscular components during lifting», *Spine (Phila Pa 1976)*, vol. 11, fasc. 7, pp. 666–678, set. 1986, doi: 10.1097/00007632-198609000-00004.

[115] G. Davico, D. G. Lloyd, C. P. Carty, B. A. Killen, D. Devaprakash, e C. Pizzolato, «Multi-level personalization of neuromusculoskeletal models to estimate physiologically plausible knee joint contact forces in children», *Biomech Model Mechanobiol*, vol. 21, fasc. 6, pp. 1873–1886, dic. 2022, doi: 10.1007/s10237-022-01626-w.

[116] Q. Shao, D. N. Bassett, K. Manal, e T. S. Buchanan, «An EMG-driven model to estimate muscle forces and joint moments in stroke patients», *Computers in Biology and Medicine*, vol. 39, fasc. 12, pp. 1083–1088, dic. 2009, doi: 10.1016/j.compbiomed.2009.09.002.

[117] T. S. Buchanan, D. G. Lloyd, K. Manal, e T. F. Besier, «Estimation of muscle forces and joint moments using a forward-inverse dynamics model», *Med Sci Sports Exerc*, vol. 37, fasc. 11, pp. 1911–1916, nov. 2005, doi: 10.1249/01.mss.0000176684.24008.6f.

[118] D. G. Lloyd e T. S. Buchanan, «A model of load sharing between muscles and soft tissues at the human knee during static tasks», *J Biomech Eng*, vol. 118, fasc. 3, pp. 367–376, ago. 1996, doi: 10.1115/1.2796019.

[119] D. G. Thelen, A. B. Schultz, S. D. Fassois, e J. A. Ashton-Miller, «Identification of dynamic myoelectric signal-to-force models during isometric lumbar muscle contractions», *J Biomech*, vol. 27, fasc. 7, pp. 907–919, lug. 1994, doi: 10.1016/0021-9290(94)90263-1.

[120] H. Hatze, «Estimation of myodynamic parameter values from observations on isometrically contracting muscle groups», *Europ. J. Appl. Physiol.*, vol. 46, fasc. 4, pp. 325–338, lug. 1981, doi: 10.1007/BF00422120.

[121] D. G. Lloyd e T. F. Besier, «An EMG-driven musculoskeletal model to estimate muscle forces and knee joint moments in vivo», *Journal of Biomechanics*, vol. 36, fasc. 6, pp. 765–776, giu. 2003, doi: 10.1016/S0021-9290(03)00010-1.

[122] M. Sartori, D. Farina, e D. G. Lloyd, «Hybrid neuromusculoskeletal modeling to best track joint moments using a balance between muscle excitations derived from electromyograms and optimization», *Journal of Biomechanics*, vol. 47, fasc. 15, pp. 3613–3621, nov. 2014, doi: 10.1016/j.jbiomech.2014.10.009.

[123] N. Assila, C. Pizzolato, R. Martinez, D. G. Lloyd, e M. Begon, «EMG-Assisted Algorithm to Account for Shoulder Muscles Co-Contraction in Overhead Manual Handling», *Applied Sciences*, vol. 10, fasc. 10, Art. fasc. 10, gen. 2020, doi: 10.3390/app10103522.

[124] H. Kainz *et al.*, «Selective dorsal rhizotomy improves muscle forces during walking in children with spastic cerebral palsy», *Clinical Biomechanics*, vol. 65, pp. 26–33, mag. 2019, doi: 10.1016/j.clinbiomech.2019.03.014.

[125] A. J. Meyer, C. Patten, e B. J. Fregly, «Lower extremity EMG-driven modeling of walking with automated adjustment of musculoskeletal geometry», *PLOS ONE*, vol. 12, fasc. 7, p. e0179698, lug. 2017, doi: 10.1371/journal.pone.0179698.

[126] P. Silvestros, E. Preatoni, H. S. Gill, e D. Cazzola, «Hyperflexion is unlikely to be the primary cervical spine injury mechanism in accidental head-on rugby tackling», 20 febbraio 2022, *bioRxiv*. doi: 10.1101/2022.02.18.481008.

[127] M. Sartori, L. Gizzi, D. G. Lloyd, e D. Farina, «A musculoskeletal model of human locomotion driven by a low dimensional set of impulsive excitation primitives», *Front. Comput. Neurosci.*, vol. 7, p. 79, 2013, doi: 10.3389/fncom.2013.00079.

[128] D. Ao, M. S. Shourijeh, C. Patten, e B. J. Fregly, «Evaluation of Synergy Extrapolation for Predicting Unmeasured Muscle Excitations from Measured Muscle Synergies», *Front Comput Neurosci*, vol. 14, p. 588943, dic. 2020, doi: 10.3389/fncom.2020.588943.

[129] J. Taborri *et al.*, «Feasibility of Muscle Synergy Outcomes in Clinics, Robotics, and Sports: A Systematic Review», *Appl Bionics Biomech*, vol. 2018, p. 3934698, apr. 2018, doi: 10.1155/2018/3934698.

[130] M. Sartori, «Modelling and Simulating Human Movement Neuromechanics», in *Novel Bioinspired Actuator Designs for Robotics*, P. Beckerle, M. A. Sharbafi, T. Verstraten, P. P. Pott, e A. Seyfarth, A c. di, in Studies in Computational Intelligence. , Cham: Springer International Publishing, 2021, pp. 13–20. doi: 10.1007/978-3-030-40886-2_2.

[131] A. H. Caillet, A. T. M. Phillips, D. Farina, e L. Modenese, «Estimation of the firing behaviour of a complete motoneuron pool by combining electromyography signal decomposition and realistic motoneuron modelling», *PLOS Computational Biology*, vol. 18, fasc. 9, p. e1010556, set. 2022, doi: 10.1371/journal.pcbi.1010556.

[132] Y. Wen, S. Avrillon, J. C. Hernandez-Pavon, S. J. Kim, F. Hug, e J. L. Pons, «A convolutional neural network to identify motor units from high-density surface electromyography signals in

real time», *J. Neural Eng.*, vol. 18, fasc. 5, p. 056003, apr. 2021, doi: 10.1088/1741-2552/abeead.

[133] T. Kapelner, M. Sartori, F. Negro, e D. Farina, «Neuro-Musculoskeletal Mapping for Man-Machine Interfacing», *Sci Rep*, vol. 10, fasc. 1, Art. fasc. 1, apr. 2020, doi: 10.1038/s41598-020-62773-7.

[134] M. Sartori, U. Ş. Yavuz, e D. Farina, «In Vivo Neuromechanics: Decoding Causal Motor Neuron Behavior with Resulting Musculoskeletal Function», *Sci Rep*, vol. 7, fasc. 1, Art. fasc. 1, ott. 2017, doi: 10.1038/s41598-017-13766-6.

[135] M. L. Latash, «The Bliss of Motor Abundance», *Exp Brain Res*, vol. 217, fasc. 1, pp. 1–5, mar. 2012, doi: 10.1007/s00221-012-3000-4.

[136] J. P. Scholz, G. Schöner, e M. L. Latash, «Identifying the control structure of multijoint coordination during pistol shooting», *Exp Brain Res*, vol. 135, fasc. 3, pp. 382–404, dic. 2000, doi: 10.1007/s002210000540.

[137] M. L. Latash, J. P. Scholz, e G. Schöner, «Motor Control Strategies Revealed in the Structure of Motor Variability», *Exercise and Sport Sciences Reviews*, vol. 30, fasc. 1, p. 26, gen. 2002.

[138] D. E. Hurwitz, K. C. Foucher, e T. P. Andriacchi, «A new parametric approach for modeling hip forces during gait», *Journal of Biomechanics*, vol. 36, fasc. 1, pp. 113–119, gen. 2003, doi: 10.1016/S0021-9290(02)00328-7.

[139] H. J. Lundberg, K. C. Foucher, e M. A. Wimmer, «A parametric approach to numerical modeling of TKR contact forces», *Journal of Biomechanics*, vol. 42, fasc. 4, pp. 541–545, mar. 2009, doi: 10.1016/j.jbiomech.2008.11.030.

[140] S. Martelli, F. Taddei, A. Cappello, S. van Sint Jan, A. Leardini, e M. Viceconti, «Effect of sub-optimal neuromotor control on the hip joint load during level walking», *Journal of Biomechanics*, vol. 44, fasc. 9, pp. 1716–1721, giu. 2011, doi: 10.1016/j.jbiomech.2011.03.039.

[141] S. Martelli, D. Calvetti, E. Somersalo, M. Viceconti, e F. Taddei, «Computational tools for calculating alternative muscle force patterns during motion: A comparison of possible solutions», *Journal of Biomechanics*, vol. 46, fasc. 12, pp. 2097–2100, ago. 2013, doi: 10.1016/j.jbiomech.2013.05.023.

[142] M. Viceconti, F. Taddei, L. Cristofolini, S. Martelli, C. Falcinelli, e E. Schileo, «Are spontaneous fractures possible? An example of clinical application for personalised, multiscale neuro-musculo-skeletal modelling», *J Biomech*, vol. 45, fasc. 3, pp. 421–426, feb. 2012, doi: 10.1016/j.jbiomech.2011.11.048.

[143] G. Maldonado, F. Bailly, P. Souères, e B. Watier, «On the coordination of highly dynamic human movements: an extension of the Uncontrolled Manifold approach applied to precision jump in parkour», *Sci Rep*, vol. 8, fasc. 1, Art. fasc. 1, ago. 2018, doi: 10.1038/s41598-018-30681-6.

[144] M. L. Latash, «3 - Features of the system for movement production», in *Fundamentals of Motor Control*, M. L. Latash, A c. di, San Diego: Academic Press, 2012, pp. 25–53. doi: 10.1016/B978-0-12-415956-3.00003-8.

[145] M. L. Latash, «10 - Neurophysiological structures», in *Fundamentals of Motor Control*, M. L. Latash, A c. di, San Diego: Academic Press, 2012, pp. 171–210. doi: 10.1016/B978-0-12-415956-3.00010-5.

[146] J. Duysens e H. W. A. A. Van de Crommert, «Neural control of locomotion; Part 1: The central pattern generator from cats to humans», *Gait & Posture*, vol. 7, fasc. 2, pp. 131–141, mar. 1998, doi: 10.1016/S0966-6362(97)00042-8.

[147] S. Grillner, «Locomotion in vertebrates: central mechanisms and reflex interaction», *Physiol Rev*, vol. 55, fasc. 2, pp. 247–304, apr. 1975, doi: 10.1152/physrev.1975.55.2.247.

[148] F. Dzeladini, J. van den Kieboom, e A. Ijspeert, «The contribution of a central pattern generator in a reflex-based neuromuscular model», *Frontiers in Human Neuroscience*, vol. 8, 2014, doi: https://doi.org/10.3389%2Ffnhum.2014.00371.

[149] P. Jiang, R. Chiba, K. Takakusaki, e J. Ota, «Generation of the Human Biped Stance by a Neural Controller Able to Compensate Neurological Time Delay», *PLOS ONE*, vol. 11, fasc. 9, p. e0163212, set. 2016, doi: 10.1371/journal.pone.0163212.

[150] K. Kaminishi, P. Jiang, R. Chiba, K. Takakusaki, e J. Ota, «Postural control of a musculoskeletal model against multidirectional support surface translations», *PLOS ONE*, vol. 14, fasc. 3, p. e0212613, mar. 2019, doi: 10.1371/journal.pone.0212613.

[151] D. A. Kistemaker, A. J. K. Van Soest, J. D. Wong, I. Kurtzer, e P. L. Gribble, «Control of position and movement is simplified by combined muscle spindle and Golgi tendon organ feedback», *J Neurophysiol*, vol. 109, fasc. 4, pp. 1126–1139, feb. 2013, doi: 10.1152/jn.00751.2012.

[152] N. Ogihara e N. Yamazaki, «Generation of human bipedal locomotion by a bio-mimetic neuro-musculo-skeletal model», *Biol Cybern*, vol. 84, fasc. 1, pp. 1–11, gen. 2001, doi: 10.1007/PL00007977.

[153] S. Song e H. Geyer, «A neural circuitry that emphasizes spinal feedback generates diverse behaviours of human locomotion», *The Journal of Physiology*, vol. 593, fasc. 16, pp. 3493–3511, 2015, doi: 10.1113/JP270228.

[154] C. F. Ong, T. Geijtenbeek, J. L. Hicks, e S. L. Delp, «Predicting gait adaptations due to ankle plantarflexor muscle weakness and contracture using physics-based musculoskeletal simulations», *PLOS Computational Biology*, vol. 15, fasc. 10, p. e1006993, ott. 2019, doi: 10.1371/journal.pcbi.1006993.

[155] H. Geyer e H. Herr, «A muscle-reflex model that encodes principles of legged mechanics produces human walking dynamics and muscle activities», *IEEE Trans Neural Syst Rehabil Eng*, vol. 18, fasc. 3, pp. 263–273, giu. 2010, doi: 10.1109/TNSRE.2010.2047592.

[156] A. Di Russo *et al.*, «Investigating the roles of reflexes and central pattern generators in the control and modulation of human locomotion using a physiologically plausible neuromechanical model», *J Neural Eng*, vol. 20, fasc. 6, nov. 2023, doi: 10.1088/1741-2552/acfdcc.

[157] J. M. Wang, S. R. Hamner, S. L. Delp, e V. Koltun, «Optimizing locomotion controllers using biologically-based actuators and objectives», *ACM Trans. Graph.*, vol. 31, fasc. 4, p. 25:1-25:11, lug. 2012, doi: 10.1145/2185520.2185521.

[158] N. F. J. Waterval *et al.*, «Validation of forward simulations to predict the effects of bilateral plantarflexor weakness on gait», *Gait & Posture*, vol. 87, pp. 33–42, giu. 2021, doi: 10.1016/j.gaitpost.2021.04.020.

[159] G. Taga, Y. Yamaguchi, e H. Shimizu, «Self-organized control of bipedal locomotion by neural oscillators in unpredictable environment», *Biol. Cybern.*, vol. 65, fasc. 3, pp. 147–159, lug. 1991, doi: 10.1007/BF00198086.

[160] K. Matsuoka, «Mechanisms of frequency and pattern control in the neural rhythm generators», *Biol. Cybernetics*, vol. 56, fasc. 5, pp. 345–353, lug. 1987, doi: 10.1007/BF00319514.

[161] G. Taga, «A model of the neuro-musculo-skeletal system for human locomotion», *Biol. Cybern.*, vol. 73, fasc. 2, pp. 97–111, lug. 1995, doi: 10.1007/BF00204048.

[162] S. A. Haghpanah, F. Farahmand, e H. Zohoor, «Modular neuromuscular control of human locomotion by central pattern generator», *J Biomech*, vol. 53, pp. 154–162, feb. 2017, doi: 10.1016/j.jbiomech.2017.01.020.

[163] M. M. van der Krogt, L. Bar-On, T. Kindt, K. Desloovere, e J. Harlaar, «Neuro-musculoskeletal simulation of instrumented contracture and spasticity assessment in children with cerebral palsy», *Journal of NeuroEngineering and Rehabilitation*, vol. 13, fasc. 1, p. 64, lug. 2016, doi: 10.1186/s12984-016-0170-5.

[164] A. Falisse, L. Bar-On, K. Desloovere, I. Jonkers, e F. D. Groote, «A spasticity model based on feedback from muscle force explains muscle activity during passive stretches and gait in children with cerebral palsy», *PLOS ONE*, vol. 13, fasc. 12, p. e0208811, dic. 2018, doi: 10.1371/journal.pone.0208811.

[165] S. Song e H. Geyer, «Predictive neuromechanical simulations indicate why walking performance declines with ageing», *The Journal of Physiology*, vol. 596, fasc. 7, pp. 1199–1210, 2018, doi: 10.1113/JP275166.

[166] S. Aoi, N. Ogihara, Y. Sugimoto, e K. Tsuchiya, «Simulating Adaptive Human Bipedal Locomotion Based on Phase Resetting Using Foot-Contact Information», *Advanced Robotics*, vol. 22, fasc. 15, pp. 1697–1713, gen. 2008, doi: 10.1163/156855308X3689785.

[167] K. Veerkamp *et al.*, «Evaluating cost function criteria in predicting healthy gait», *Journal of Biomechanics*, vol. 123, p. 110530, giu. 2021, doi: 10.1016/j.jbiomech.2021.110530.

[168] M. Mansouri, A. E. Clark, A. Seth, e J. A. Reinbolt, «Rectus femoris transfer surgery affects balance recovery in children with cerebral palsy: A computer simulation study», *Gait & Posture*, vol. 43, pp. 24–30, gen. 2016, doi: 10.1016/j.gaitpost.2015.08.016.

[169] T. Geijtenbeek, «SCONE: Open Source Software for Predictive Simulation of Biological Motion», *JOSS*, vol. 4, fasc. 38, p. 1421, giu. 2019, doi: 10.21105/joss.01421.

[170] T. Geijtenbeek, M. van de Panne, e A. F. van der Stappen, «Flexible muscle-based locomotion for bipedal creatures», *ACM Trans. Graph.*, vol. 32, fasc. 6, p. 206:1-206:11, nov. 2013, doi: 10.1145/2508363.2508399.

[171] D. Muñoz, C. D. Marchis, L. Gizzi, e G. Severini, «Predictive simulation of sit-to-stand based on reflexive-controllers», *PLOS ONE*, vol. 17, fasc. 12, p. e0279300, dic. 2022, doi: 10.1371/journal.pone.0279300.

[172] J. A. Sharp, K. Burrage, e M. J. Simpson, «Implementation and acceleration of optimal control for systems biology», *Journal of The Royal Society Interface*, vol. 18, fasc. 181, p. 20210241, ago. 2021, doi: 10.1098/rsif.2021.0241.

[173] M. L. Kaplan e J. H. Heegaard, «Predictive algorithms for neuromuscular control of human locomotion», *Journal of Biomechanics*, vol. 34, fasc. 8, pp. 1077–1083, ago. 2001, doi: 10.1016/S0021-9290(01)00057-4.

[174] A. Falisse, G. Serrancolí, C. L. Dembia, J. Gillis, I. Jonkers, e F. De Groote, «Rapid predictive simulations with complex musculoskeletal models suggest that diverse healthy and pathological human gaits can emerge from similar control strategies», *Journal of The Royal Society Interface*, vol. 16, fasc. 157, p. 20190402, ago. 2019, doi: 10.1098/rsif.2019.0402.

[175] C. K. Chow e D. H. Jacobson, «Studies of human locomotion via optimal programming», *Mathematical Biosciences*, vol. 10, fasc. 3, pp. 239–306, apr. 1971, doi: 10.1016/0025-5564(71)90062-9.

[176] H. Hatze, «The complete optimization of a human motion», *Mathematical Biosciences*, vol. 28, fasc. 1, pp. 99–135, gen. 1976, doi: 10.1016/0025-5564(76)90098-5.

[177] M. L. Audu e D. T. Davy, «A Comparison of optimal control algorithms for complex bioengineering studies», *Optimal Control Applications and Methods*, vol. 9, fasc. 1, pp. 101–106, 1988, doi: 10.1002/oca.4660090110.

[178] A. J. van Soest, A. L. Schwab, M. F. Bobbert, e G. J. van Ingen Schenau, «The influence of the biarticularity of the gastrocnemius muscle on vertical-jumping achievement», *Journal of Biomechanics*, vol. 26, fasc. 1, pp. 1–8, gen. 1993, doi: 10.1016/0021-9290(93)90608-H.

[179] M. Stelzer e O. von Stryk, «Efficient forward dynamics simulation and optimization of human body dynamics», *ZAMM - Journal of Applied Mathematics and Mechanics / Zeitschrift für Angewandte Mathematik und Mechanik*, vol. 86, fasc. 10, pp. 828–840, 2006, doi: 10.1002/zamm.200610290.

[180] M. Ackermann e A. J. van den Bogert, «Optimality principles for model-based prediction of human gait», *Journal of Biomechanics*, vol. 43, fasc. 6, pp. 1055–1060, apr. 2010, doi: 10.1016/j.jbiomech.2009.12.012.

[181] T. W. Dorn, J. M. Wang, J. L. Hicks, e S. L. Delp, «Predictive Simulation Generates Human Adaptations during Loaded and Inclined Walking», *PLOS ONE*, vol. 10, fasc. 4, p. e0121407, apr. 2015, doi: 10.1371/journal.pone.0121407.

[182] L.-F. Lee e B. R. Umberger, «Generating optimal control simulations of musculoskeletal movement using OpenSim and MATLAB», *PeerJ*, vol. 4, p. e1638, gen. 2016, doi: 10.7717/peerj.1638.

[183] A. J. van den Bogert, M. Hupperets, H. Schlarb, e B. Krabbe, «Predictive musculoskeletal simulation using optimal control: effects of added limb mass on energy cost and kinematics of walking and running», *Proceedings of the Institution of Mechanical Engineers, Part P: Journal of Sports Engineering and Technology*, vol. 226, fasc. 2, pp. 123–133, giu. 2012, doi: 10.1177/1754337112440644.

[184] A. Falisse *et al.*, «Physics-Based Simulations to Predict the Differential Effects of Motor Control and Musculoskeletal Deficits on Gait Dysfunction in Cerebral Palsy: A Retrospective Case Study», *Front Hum Neurosci*, vol. 14, p. 40, 2020, doi: 10.3389/fnhum.2020.00040.

[185] H. Hatze, «An efficient simulation method for discrete-value controled large-scale neuromyoskeletal system models», *Journal of Biomechanics*, vol. 34, fasc. 2, pp. 267–271, feb. 2001, doi: 10.1016/S0021-9290(00)00175-5.

[186] B. R. Umberger, K. G. M. Gerritsen, e P. E. Martin, «A model of human muscle energy expenditure», *Computer Methods in Biomechanics and Biomedical Engineering*, vol. 9, fasc. 5, pp. 342–342, ott. 2006, doi: 10.1080/10255840612331393266.

[187] S. H. Scott, «Optimal feedback control and the neural basis of volitional motor control», *Nat Rev Neurosci*, vol. 5, fasc. 7, Art. fasc. 7, lug. 2004, doi: 10.1038/nrn1427.

[188] E. Todorov, «Optimality principles in sensorimotor control», *Nat Neurosci*, vol. 7, fasc. 9, Art. fasc. 9, set. 2004, doi: 10.1038/nn1309.

[189] E. Todorov e M. I. Jordan, «Optimal feedback control as a theory of motor coordination», *Nat Neurosci*, vol. 5, fasc. 11, Art. fasc. 11, nov. 2002, doi: 10.1038/nn963.

[190] T. Van Wouwe, L. H. Ting, e F. De Groote, «An approximate stochastic optimal control framework to simulate nonlinear neuromusculoskeletal models in the presence of noise», *PLoS Computational Biology*, vol. 18, fasc. 6, 2022, doi: 10.1371/journal.pcbi.1009338.

[191] X. B. Peng, P. Abbeel, S. Levine, e M. van de Panne, «DeepMimic: example-guided deep reinforcement learning of physics-based character skills», *ACM Trans. Graph.*, vol. 37, fasc. 4, p. 143:1-143:14, lug. 2018, doi: 10.1145/3197517.3201311.

[192] B. Zhou, H. Zeng, F. Wang, Y. Li, e H. Tian, «Efficient and Robust Reinforcement Learning with Uncertainty-based Value Expansion», 10 dicembre 2019, *arXiv*: arXiv:1912.05328. doi: 10.48550/arXiv.1912.05328.

[193] S. Song *et al.*, «Deep reinforcement learning for modeling human locomotion control in neuromechanical simulation», *Journal of NeuroEngineering and Rehabilitation*, vol. 18, fasc. 1, p. 126, ago. 2021, doi: 10.1186/s12984-021-00919-y.

[194] S. Martelli, D. Calvetti, E. Somersalo, e M. Viceconti, «Stochastic modelling of muscle recruitment during activity», *Interface Focus*, vol. 5, fasc. 2, p. 20140094, apr. 2015, doi: 10.1098/rsfs.2014.0094.

[195] A. Bersani, G. Davico, e M. Viceconti, «Modeling Human Suboptimal Control: A Review», *J. Appl. Biomech.*, vol. 39, fasc. 5, pp. 294–303, ott. 2023, doi: 10.1123/jab.2023-0015.

[196] D. C. Lin, C. P. McGowan, K. P. Blum, e L. H. Ting, «Yank: the time derivative of force is an important biomechanical variable in sensorimotor systems», *J. Exp. Biol.*, vol. 222, fasc. 18, p. jeb180414, set. 2019, doi: 10.1242/jeb.180414.

[197] S. L. Delp *et al.*, «OpenSim: open-source software to create and analyze dynamic simulations of movement», *IEEE Trans Biomed Eng*, vol. 54, fasc. 11, pp. 1940–1950, nov. 2007, doi: 10.1109/TBME.2007.901024.

[198] L. D. Landau e E. M. Lifshitz, *Mechanics*.

[199] D. Calvetti e E. Somersalo, *Bayesian Scientific Computing*, vol. 215. in Applied Mathematical Sciences, vol. 215. Cham: Springer International Publishing, 2023. doi: 10.1007/978-3-031-23824-6.

[200] J. P. Kaipio e E. Somersalo, *Statistical and Computational Inverse Problems*, vol. 160. in Applied Mathematical Sciences, vol. 160. New York, NY: Springer, 2005. doi: 10.1007/b138659.

[201] D. Calvetti e E. Somersalo, «Inverse problems: From regularization to Bayesian inference», *WIREs Computational Statistics*, vol. 10, fasc. 3, p. e1427, 2018, doi: 10.1002/wics.1427.

[202] A. Kavounoudias, R. Roll, e J. P. Roll, «The plantar sole is a “dynamometric map” for human balance control», *Neuroreport*, vol. 9, fasc. 14, pp. 3247–3252, ott. 1998, doi: 10.1097/00001756-199810050-00021.

[203] P. M. Kennedy e J. T. Inglis, «Distribution and behaviour of glabrous cutaneous receptors in the human foot sole», *J. Physiol.*, vol. 538, fasc. Pt 3, pp. 995–1002, feb. 2002, doi: 10.1113/jphysiol.2001.013087.

[204] A. Mündermann, C. O. Dyrby, e T. P. Andriacchi, «Secondary gait changes in patients with medial compartment knee osteoarthritis: Increased load at the ankle, knee, and hip during walking», *Arthritis & Rheumatism*, vol. 52, fasc. 9, pp. 2835–2844, 2005, doi: 10.1002/art.21262.

[205] B. M. Nigg, «Biomechanics, load analysis and sports injuries in the lower extremities», *Sports. Med.*, vol. 2, fasc. 5, pp. 367–379, 1985, doi: 10.2165/00007256-198502050-00005.

[206] Z. H. He, R. Bottinelli, M. A. Pellegrino, M. A. Ferenczi, e C. Reggiani, «ATP consumption and efficiency of human single muscle fibers with different myosin isoform composition.», *Biophys. J.*, vol. 79, fasc. 2, pp. 945–961, ago. 2000, doi: 10.1016/S0006-3495(00)76349-1.

[207] C. T. Kelley, *Iterative Methods for Optimization*. in Frontiers in Applied Mathematics. Society for Industrial and Applied Mathematics, 1999. doi: 10.1137/1.9781611970920.

[208] J. Heino, D. Calvetti, e E. Somersalo, «Metabolica: a statistical research tool for analyzing metabolic networks», *Comput Methods Programs Biomed*, vol. 97, fasc. 2, pp. 151–167, feb. 2010, doi: 10.1016/j.cmpb.2009.07.007.

[209] J. Heino, K. Tunyan, D. Calvetti, e E. Somersalo, «Bayesian flux balance analysis applied to a skeletal muscle metabolic model», *J. Theor. Biol.*, vol. 248, fasc. 1, pp. 91–110, set. 2007, doi: 10.1016/j.jtbi.2007.04.002.

[210] M. Kac, «On distributions of certain Wiener functionals», *Trans. Amer. Math. Soc.*, vol. 65, fasc. 1, pp. 1–13, 1949, doi: 10.1090/S0002-9947-1949-0027960-X.

[211] P. Del Moral, «Feynman-Kac Formulae», in *Feynman-Kac Formulae: Genealogical and Interacting Particle Systems with Applications*, P. Del Moral, A c. di, New York, NY: Springer, 2004, pp. 47–93. doi: 10.1007/978-1-4684-9393-1_2.

[212] W. C. Chow, «Brownian bridge», *WIREs Computational Statistics*, vol. 1, fasc. 3, pp. 325–332, 2009, doi: 10.1002/wics.38.

[213] M. B. I. Raez, M. S. Hussain, e F. Mohd-Yasin, «Techniques of EMG signal analysis: detection, processing, classification and applications», *Biol. Proced. Online*, vol. 8, pp. 11–35, mar. 2006, doi: 10.1251/bpo115.

[214] B. J. Fregly *et al.*, «Grand challenge competition to predict in vivo knee loads», *J. Orthop. Res.*, vol. 30, fasc. 4, pp. 503–513, 2012, doi: 10.1002/jor.22023.

[215] K. Martinopoulou, O. Donti, W. A. Sands, G. Terzis, e G. C. Bogdanis, «Evaluation of The Isometric and Dynamic Rates of Force Development in Multi-Joint Muscle Actions», *J. Hum. Kinet.*, vol. 81, pp. 135–148, feb. 2022, doi: 10.2478/hukin-2021-0130.

[216] T. Kamo *et al.*, «Rate of torque development and the risk of falls among community dwelling older adults in Japan», *Gait & Posture*, vol. 72, pp. 28–33, lug. 2019, doi: 10.1016/j.gaitpost.2019.05.019.

[217] T. B. Palmer, R. M. Thiele, E. C. Conchola, D. B. Smith, e B. J. Thompson, «A Preliminary Study of the Utilization of Maximal and Rapid Strength Characteristics to Identify Chair-Rise Performance Abilities in Very Old Adults», *J. Geriatr. Phys. Ther.*, vol. 39, fasc. 3, p. 102, set. 2016, doi: 10.1519/JPT.0000000000000060.

[218] E. Sundstrup *et al.*, «Muscle function and postural balance in lifelong trained male footballers compared with sedentary elderly men and youngsters», *Scand. J. Med. Sci. Sports*, vol. 20, fasc. s1, pp. 90–97, 2010, doi: 10.1111/j.1600-0838.2010.01092.x.

[219] S. Sahrom, J. C. Wilkie, K. Nosaka, e A. J. Blazevich, «Comparison of methods of derivation of the yank-time signal from the vertical ground reaction force–time signal for identification of movement-related events», *J. Biomech.*, vol. 115, p. 110048, gen. 2021, doi: 10.1016/j.jbiomech.2020.110048.

[220] A. Péter *et al.*, «Comparing Surface and Fine-Wire Electromyography Activity of Lower Leg Muscles at Different Walking Speeds», *Front Physiol*, vol. 10, p. 1283, 2019, doi: 10.3389/fphys.2019.01283.

[221] J. Lo *et al.*, «Functional implications of muscle co-contraction during gait in advanced age», *Gait Posture*, vol. 53, pp. 110–114, mar. 2017, doi: 10.1016/j.gaitpost.2017.01.010.

[222] A. H. Caillet, A. T. M. Phillips, D. Farina, e L. Modenese, «Estimation of the firing behaviour of a complete motoneuron pool by combining electromyography signal decomposition and realistic motoneuron modelling», *PLOS Comput. Biol.*, vol. 18, fasc. 9, p. e1010556, set. 2022, doi: 10.1371/journal.pcbi.1010556.

[223] C. Pizzolato *et al.*, «CEINMS: A toolbox to investigate the influence of different neural control solutions on the prediction of muscle excitation and joint moments during dynamic motor tasks», *Journal of Biomechanics*, vol. 48, fasc. 14, pp. 3929–3936, nov. 2015, doi: 10.1016/j.jbiomech.2015.09.021.

[224] H. Geyer e H. Herr, «A Muscle-Reflex Model That Encodes Principles of Legged Mechanics Produces Human Walking Dynamics and Muscle Activities», *IEEE Trans. Neural Syst. Rehabil. Eng.*, vol. 18, fasc. 3, pp. 263–273, giu. 2010, doi: 10.1109/TNSRE.2010.2047592.

[225] M. Amankwah, A. Bersani, D. Calvetti, G. Davico, E. Somersalo, e M. Viceconti, «Exploring muscle recruitment by Bayesian methods during motion», *Chaos, Solitons & Fractals*, vol. 185, p. 115082, ago. 2024, doi: 10.1016/j.chaos.2024.115082.

[226] S. H. Collins e A. D. Kuo, «Two Independent Contributions to Step Variability during Over-Ground Human Walking», *PLOS ONE*, vol. 8, fasc. 8, p. e73597, ago. 2013, doi: 10.1371/journal.pone.0073597.

[227] G. Davico, L. Labanca, I. Gennarelli, M. G. Benedetti, e M. Viceconti, «Towards a comprehensive biomechanical assessment of the elderly combining in vivo data and in silico methods», *Front. Bioeng. Biotechnol.*, vol. 12, mag. 2024, doi: 10.3389/fbioe.2024.1356417.

[228] L. L. Andersen e P. Aagaard, «Influence of maximal muscle strength and intrinsic muscle contractile properties on contractile rate of force development», *Eur. J. Appl. Physiol.*, vol. 96, fasc. 1, pp. 46–52, gen. 2006, doi: 10.1007/s00421-005-0070-z.

[229] D. P. LaRoche, K. A. Cremin, B. Greenleaf, e R. V. Croce, «Rapid torque development in older female fallers and nonfallers: A comparison across lower-extremity muscles», *J. Electromyogr. Kinesiol.*, vol. 20, fasc. 3, pp. 482–488, giu. 2010, doi: 10.1016/j.jelekin.2009.08.004.

[230] B. Kirking, J. Krevolin, C. Townsend, C. W. Colwell, e D. D. D'Lima, «A multiaxial force-sensing implantable tibial prosthesis», *J Biomech*, vol. 39, fasc. 9, pp. 1744–1751, gen. 2006, doi: 10.1016/j.jbiomech.2005.05.023.

[231] G. Bergmann, F. Graichen, A. Bender, M. Kääb, A. Rohlmann, e P. Westerhoff, «In vivo glenohumeral contact forces—Measurements in the first patient 7 months postoperatively», *J. Biomech.*, vol. 40, fasc. 10, pp. 2139–2149, gen. 2007, doi: 10.1016/j.jbiomech.2006.10.037.

[232] C. Klemt *et al.*, «Analysis of shoulder compressive and shear forces during functional activities of daily life», *Clin Biomech (Bristol, Avon)*, vol. 54, pp. 34–41, mag. 2018, doi: 10.1016/j.clinbiomech.2018.03.006.

[233] H. Bruttel, D. M. Spranz, M. Bülhoff, N. Aljohani, S. I. Wolf, e M. W. Maier, «Comparison of glenohumeral and humerothoracical range of motion in healthy controls, osteoarthritic patients and patients after total shoulder arthroplasty performing different activities of daily living», *Gait & Posture*, vol. 71, pp. 20–25, giu. 2019, doi: 10.1016/j.gaitpost.2019.04.001.

[234] D. J. Magermans, E. K. J. Chadwick, H. E. J. Veeger, e F. C. T. van der Helm, «Requirements for upper extremity motions during activities of daily living», *Clin. Biomech.*, vol. 20, fasc. 6, pp. 591–599, lug. 2005, doi: 10.1016/j.clinbiomech.2005.02.006.

[235] I. Jonkers, E. Beaucage-Gauvreau, B. A. Killen, D. Gupta, L. Scheys, e F. D. Groote, «In Silico Biomarkers of Motor Function to Inform Musculoskeletal Rehabilitation and Orthopedic Treatment», *J. Appl. Biomech.*, vol. 39, fasc. 5, pp. 284–293, giu. 2023, doi: 10.1123/jab.2023-0029.

[236] B. A. Killen, A. Falisse, F. De Groote, e I. Jonkers, «In Silico-Enhanced Treatment and Rehabilitation Planning for Patients with Musculoskeletal Disorders: Can Musculoskeletal Modelling and Dynamic Simulations Really Impact Current Clinical Practice?», *Applied Sciences*, vol. 10, fasc. 20, Art. fasc. 20, gen. 2020, doi: 10.3390/app10207255.

[237] H. E. J. Veeger, D. J. Magermans, J. Nagels, E. K. J. Chadwick, e F. C. T. van der Helm, «A kinematical analysis of the shoulder after arthroplasty during a hair combing task», *Clin. Biomech.*, vol. 21, pp. S39–S44, gen. 2006, doi: 10.1016/j.clinbiomech.2005.09.012.

[238] A. A. Nikooyan, H. E. J. Veeger, P. Westerhoff, F. Graichen, G. Bergmann, e F. C. T. van der Helm, «Validation of the Delft Shoulder and Elbow Model using *in-vivo* glenohumeral joint contact forces», *J. Biomech.*, vol. 43, fasc. 15, pp. 3007–3014, nov. 2010, doi: 10.1016/j.jbiomech.2010.06.015.

[239] A. Kian *et al.*, «Static optimization underestimates antagonist muscle activity at the glenohumeral joint: A musculoskeletal modeling study», *J. Biomech.*, vol. 97, p. 109348, dic. 2019, doi: 10.1016/j.jbiomech.2019.109348.

[240] E. Croci *et al.*, «Load-induced increase in muscle activity during 30° abduction in patients with rotator cuff tears and control subjects», *J. Orthop. Traumatol.*, vol. 24, fasc. 1, p. 41, ago. 2023, doi: 10.1186/s10195-023-00720-8.

[241] J. Wickham, T. Pizzari, K. Stansfeld, A. Burnside, e L. Watson, «Quantifying 'normal' shoulder muscle activity during abduction», *J. Electromyogr. Kinesiol.*, vol. 20, fasc. 2, pp. 212–222, apr. 2010, doi: 10.1016/j.jelekin.2009.06.004.

[242] M. Besomi *et al.*, «Consensus for experimental design in electromyography (CEDE) project: Amplitude normalization matrix», *Journal of Electromyography and Kinesiology*, vol. 53, p. 102438, ago. 2020, doi: 10.1016/j.jelekin.2020.102438.

[243] M. Febrer-Nafría, A. Nasr, M. Ezati, P. Brown, J. M. Font-Llagunes, e J. McPhee, «Predictive multibody dynamic simulation of human neuromusculoskeletal systems: a review», *Multibody Syst. Dyn.*, vol. 58, fasc. 3, pp. 299–339, ago. 2023, doi: 10.1007/s11044-022-09852-x.

[244] P. Puchaud, F. Bailly, e M. Begon, «Direct multiple shooting and direct collocation perform similarly in biomechanical predictive simulations», *Comput. Methods Appl. Mech. Eng.*, vol. 414, p. 116162, set. 2023, doi: 10.1016/j.cma.2023.116162.

[245] R. T. Johnson, D. Lakeland, e J. M. Finley, «Using Bayesian inference to estimate plausible muscle forces in musculoskeletal models», *J. NeuroEng. Rehabil.*, vol. 19, fasc. 1, p. 34, mar. 2022, doi: 10.1186/s12984-022-01008-4.

[246] A. Bersani, M. Amankwah, D. Calvetti, E. Somersalo, M. Viceconti, e G. Davico, «Myobolica: a stochastic approach to estimate physiological muscle control variability», *IEEE Trans. Neural. Syst. Rehabil. Eng.*, vol. PP, ago. 2024, doi: 10.1109/TNSRE.2024.3447791.

[247] D. H. E. J. Veeger, F. C. T. van der Helm, e A. A. Nikooyan, «Kinematic and kinetic data recorded with an instrumented shoulder prosthesis». 4TU.ResearchData, 13 luglio 2023. doi: 10.4121/86DB1D7D-13D9-4631-9C6B-1E3134A1AB38.V1.

[248] A. A. Nikooyan *et al.*, «An EMG-driven musculoskeletal model of the shoulder», *Hum. Mov. Sci.*, vol. 31, fasc. 2, pp. 429–447, apr. 2012, doi: 10.1016/j.humov.2011.08.006.

[249] M. Lavaill, C. Pizzolato, B. Bolsterlee, S. Martelli, e P. Pivonka, «Benchmark and validation of state-of-the-art muscle recruitment strategies in shoulder modelling», *Multibody Syst. Dyn.*, vol. 64, fasc. 1, pp. 105–120, mag. 2025, doi: 10.1007/s11044-024-09997-x.

[250] M. Millard, T. Uchida, A. Seth, e S. L. Delp, «Flexing Computational Muscle: Modeling and Simulation of Musculotendon Dynamics», *J. Biomech. Eng.*, vol. 135, fasc. 021005, feb. 2013, doi: 10.1115/1.4023390.

[251] J. L. Hicks, T. K. Uchida, A. Seth, A. Rajagopal, e S. L. Delp, «Is My Model Good Enough? Best Practices for Verification and Validation of Musculoskeletal Models and Simulations of Movement», *Journal of Biomechanical Engineering*, vol. 137, fasc. 020905, feb. 2015, doi: 10.1115/1.4029304.

[252] G. Davico, L. Labanca, I. Gennarelli, M. G. Benedetti, e M. Viceconti, «Towards a comprehensive biomechanical assessment of the elderly combining in vivo data and in silico methods», *Front. Bioeng. Biotechnol.*, vol. 12, p. 1356417, 2024, doi: 10.3389/fbioe.2024.1356417.

[253] T. Capriotti e K. Terzakis, «Parkinson Disease», *Home Healthcare Now*, vol. 34, fasc. 6, p. 300, giu. 2016, doi: 10.1097/NHH.0000000000000398.

[254] F. Haddad, M. Sawalha, Y. Khawaja, A. Najjar, e R. Karaman, «Dopamine and Levodopa Prodrugs for the Treatment of Parkinson's Disease», *Molecules*, vol. 23, fasc. 1, p. 40, gen. 2018, doi: 10.3390/molecules23010040.

[255] H. R. Morris, M. G. Spillantini, C. M. Sue, e C. H. Williams-Gray, «The pathogenesis of Parkinson's disease», *The Lancet*, vol. 403, fasc. 10423, pp. 293–304, gen. 2024, doi: 10.1016/S0140-6736(23)01478-2.

[256] M. M. Hoehn e M. D. Yahr, «Parkinsonism: onset, progression and mortality», *Neurology*, vol. 17, fasc. 5, pp. 427–442, mag. 1967, doi: 10.1212/wnl.17.5.427.

[257] C. G. Goetz *et al.*, «Movement Disorder Society Task Force report on the Hoehn and Yahr staging scale: status and recommendations», *Mov. Disord.*, vol. 19, fasc. 9, pp. 1020–1028, set. 2004, doi: 10.1002/mds.20213.

[258] M. Pistacchi *et al.*, «Gait analysis and clinical correlations in early Parkinson's disease», *Funct. Neurol.*, vol. 32, fasc. 1, pp. 28–34, 2017, doi: 10.11138/fneur/2017.32.1.028.

[259] G. Albani, V. Cimolin, A. Fasano, C. Trotti, M. Galli, e A. Mauro, «"Masters and servants" in parkinsonian gait: a three-dimensional analysis of biomechanical changes sensitive to disease progression», *Funct. Neurol.*, vol. 29, fasc. 2, pp. 99–105, 2014.

[260] A. Islam, L. Alcock, K. Nazarpour, L. Rochester, e A. Pantall, «Effect of Parkinson's disease and two therapeutic interventions on muscle activity during walking: a systematic review», *npj Parkinsons Dis.*, vol. 6, fasc. 1, p. 22, set. 2020, doi: 10.1038/s41531-020-00119-w.

[261] P. Krack *et al.*, «Five-year follow-up of bilateral stimulation of the subthalamic nucleus in advanced Parkinson's disease», *N. Engl. J. Med.*, vol. 349, fasc. 20, pp. 1925–1934, nov. 2003, doi: 10.1056/NEJMoa035275.

[262] C. L. Tomlinson *et al.*, «Physiotherapy versus placebo or no intervention in Parkinson's disease», *Cochrane Database Syst. Rev.*, fasc. 7, p. CD002817, lug. 2012, doi: 10.1002/14651858.CD002817.pub2.

[263] J. W. Skinner, E. A. Christou, e C. J. Hass, «Lower Extremity Muscle Strength and Force Variability in Persons With Parkinson Disease», *JNPT*, vol. 43, fasc. 1, p. 56, gen. 2019, doi: 10.1097/NPT.0000000000000244.

[264] G. E. Stelmach e C. J. Worringham, «The preparation and production of isometric force in Parkinson's disease», *Neuropsychologia*, vol. 26, fasc. 1, pp. 93–103, gen. 1988, doi: 10.1016/0028-3932(88)90033-4.

[265] J. W. Skinner, H. K. Lee, R. T. Roemmich, S. Amano, e C. J. Hass, «Execution of Activities of Daily Living in Persons with Parkinson Disease», *Med. Sci. Sports Exerc.*, vol. 47, fasc. 9, pp. 1906–1912, set. 2015, doi: 10.1249/MSS.0000000000000598.

[266] M. Romanato, D. Volpe, A. Guiotto, F. Spolaor, M. Sartori, e Z. and Sawacha, «Electromyography-informed modeling for estimating muscle activation and force alterations in Parkinson's disease», *CMBBE*, vol. 25, fasc. 1, pp. 14–26, gen. 2022, doi: 10.1080/10255842.2021.1925887.

[267] G. Davico, C. Pizzolato, D. G. Lloyd, S. J. Obst, H. P. J. Walsh, e C. P. Carty, «Increasing level of neuromusculoskeletal model personalisation to investigate joint contact forces in cerebral palsy: A twin case study», *Clin. Biomech. (Bristol)*, vol. 72, pp. 141–149, feb. 2020, doi: 10.1016/j.clinbiomech.2019.12.011.

[268] M. F. Rabbi, C. Pizzolato, D. G. Lloyd, C. P. Carty, D. Devaprakash, e L. E. Diamond, «Non-negative matrix factorisation is the most appropriate method for extraction of muscle synergies in walking and running», *Sci. Rep.*, vol. 10, fasc. 1, p. 8266, mag. 2020, doi: 10.1038/s41598-020-65257-w.

[269] A. Falisse, G. Serrancolí, C. L. Dembia, J. Gillis, I. Jonkers, e F. De Groote, «Rapid predictive simulations with complex musculoskeletal models suggest that diverse healthy and pathological human gaits can emerge from similar control strategies», *J. R. Soc. Interface*, vol. 16, fasc. 157, p. 20190402, ago. 2019, doi: 10.1098/rsif.2019.0402.

[270] T. K. F. Shida *et al.*, «A public data set of walking full-body kinematics and kinetics in individuals with Parkinson's disease», *Front. Neurosci.*, vol. 17, feb. 2023, doi: 10.3389/fnins.2023.992585.

[271] A. Mantoan, M. Reggiani, M. Sartori, Z. Sawacha, C. Pizzolato, e C. Cobelli, «A Matlab generic tool to efficiently process C3D files for applications in OpenSim», ago. 2013.

[272] A. Rajagopal, C. L. Dembia, M. S. DeMers, D. D. Delp, J. L. Hicks, e S. L. Delp, «Full-Body Musculoskeletal Model for Muscle-Driven Simulation of Human Gait», *IEEE Trans Biomed Eng*, vol. 63, fasc. 10, pp. 2068–2079, ott. 2016, doi: 10.1109/TBME.2016.2586891.

[273] I. Kutzner *et al.*, «Loading of the knee joint during activities of daily living measured *in vivo* in five subjects», *J. Biomech.*, vol. 43, fasc. 11, pp. 2164–2173, ago. 2010, doi: 10.1016/j.jbiomech.2010.03.046.

[274] A. Bersani, S. Martelli, M. Lavaill, e G. Davico, «Stochastic modelling of muscle control during shoulder abduction», *J. Biomech.*, vol. 193, p. 112993, dic. 2025, doi: 10.1016/j.jbiomech.2025.112993.

[275] M. Viceconti, F. Pappalardo, B. Rodriguez, M. Horner, J. Bischoff, e F. Musuamba Tshinanu, «*In silico* trials: Verification, validation and uncertainty quantification of predictive models used in the regulatory evaluation of biomedical products», *Methods*, vol. 185, pp. 120–127, gen. 2021, doi: 10.1016/j.ymeth.2020.01.011.

[276] A. Aldieri, C. Curreli, J. A. Szyszko, A. A. La Mattina, e M. Viceconti, «Credibility assessment of computational models according to ASME V&V40: Application to the Bologna Biomechanical Computed Tomography solution», *Comput. Methods Programs Biomed.*, vol. 240, p. 107727, ott. 2023, doi: 10.1016/j.cmpb.2023.107727.

[277] The American Society of Mechanical Engineers (ASME), «Assessing Credibility of Computational Modeling Through Verification and Validation: Application to Medical Devices», *ASME V&V40-2018*, 2018.

[278] J. P. Bakker *et al.*, «V3+ extends the V3 framework to ensure user-centricity and scalability of sensor-based digital health technologies», *npj Digit. Med.*, vol. 8, fasc. 1, p. 51, gen. 2025, doi: 10.1038/s41746-024-01322-2.

[279] M. Bolic, «Chapter 1 - Concepts in performance evaluation and uncertainty analysis», in *Pervasive Cardiovascular and Respiratory Monitoring Devices*, M. Bolic, A c. di, Academic Press, 2023, pp. 1–35. doi: 10.1016/B978-0-12-820947-9.00008-8.

[280] L. Li, L. Zhang, B. Zhang, H. Liu, e Z. Zheng, «A review of uncertainty quantification and its applications in numerical simulation of scramjet combustor», *Int. J. Thermofluids*, vol. 18, p. 100351, mag. 2023, doi: 10.1016/j.ijft.2023.100351.

[281] X. Wu e T. Kozlowski, «Chapter 17 - Inverse uncertainty quantification based on the modular Bayesian approach», in *Risk-Informed Methods and Applications in Nuclear and Energy Engineering*, C. L. Smith, K. Le Blanc, e D. Mandelli, A c. di, Academic Press, 2024, pp. 319–331. doi: 10.1016/B978-0-323-91152-8.00006-5.

[282] A. Andreella e L. Finos, «Procrustes Analysis for High-Dimensional Data», *Psychometrika*, vol. 87, fasc. 4, pp. 1422–1438, dic. 2022, doi: 10.1007/s11336-022-09859-5.